Genomic Stress in Human Neurodevelopment: The Role of p53

Nadine Michel
Columbia, Maryland

B.S Neuroscience, Duke University, 2013
M.S Biological and Physical Sciences, University of Virginia, 2017

A Dissertation presented to the Graduate Faculty of the University of Virginia for the Degree of Doctor of Philosophy

Neuroscience Graduate Program

University of Virginia
March 2020

Abstract

The human cortex consists of upwards of 80-90 billion neurons. The vast majority of these neurons are born during early brain development during a short time frame in which progenitors rapidly proliferate, differentiate, and migrate to the appropriate cortical layer. Mouse models of cortical development have revealed that DNA damage occurs at high rates during this time period, and DNA damage repair is essential for normal development. One of the required repair pathways is non-homologous end joining (NHEJ) which repairs DNA double-strand breaks (DSBs) throughout the cell cycle. NHEJ deficient mice are embryonically lethal or develop small brains; however, concurrent *p53* knockout rescues this phenotype, indicating that p53 kills neural progenitor cells (NPCs) harboring DNA DSBs during early cortical development. It was previously unclear how genomic stress activated p53 during neurogenesis and how p53 altered the fate of neural cells in human cortical development. With the discovery of the Yamanaka factors, human-induced pluripotent stem cells (hiPSCs) were quickly generated, providing an *in vitro* model of human neurodevelopment to study models of normal and pathological cortical development. Combined with single-cell approaches, including single-cell RNA-seq and imaging cytometry, the temporal dynamics of DNA DSBs and cell fate during neuronal differentiation can be quantified and better understood. The goal of this study was to determine the role of p53 in response to genomic stress in hiPSC-derived NPCs and their progeny.

NPCs are a heterogeneous cell population and require single-cell approaches to best examine DNA DSB dynamics during development. In Chapter II we developed a technique to assess genomic stress through the quantification of DNA DSB regions using Imaging Flow Cytometry. We characterized DNA DSBs, cell cycle stage, and cell fate (death, proliferation, differentiation) during hiPSC-derived neurogenesis and observed fluctuating levels of DNA DSBs. NPCs and neurons contained comparable percentages of cells with breaks, but cell death was increased in the early differentiating NPCs compared to the progenitors. This

finding implicates a different response to transcription and replication stress in neural cells.

In Chapter III we examined the differences between transcription and replication stress in neural cells in more depth and discovered that p53 is activated in transcription but not replication stress. Furthermore, the activation of p53 during transcriptionally induced DNA DSBs often led to cell death. During hiPSC-derived neurogenesis, p53 eliminated NPCs with DNA DSBs by preventing them from proliferating and increasing cell death. Previous studies of DNA DSBs in NPCs have shown an enrichment in breaks in long neural genes due to a proposed collision between transcription and replication machinery. Using DNA DSB mapping, we located DNA DSBs in highly transcribed genes and observed no relationship in breaks between p53 and gene length. However, we observed DNA DSB enrichment at the transcription start sites of p53 deficient cells in high risk alleles for neurodevelopmental disorders.

We conducted additional experiments to examine how other isogenic cell types respond to genomic stress and assessed whether genomic stress led to neurons with neuroinflammatory phenotypes (Chapter IV, Appendix). hiPSC-derived astrocytes were more resistant to genomic stress; they exhibited fewer DNA DSBs, lower percentages of cells in cell cycle arrest, and less p53 activation compared to isogenic NPCs. Furthermore, genomic stress did not lead to neuroinflammatory phenotypes, but rather a deficiency in p53 increased levels of secreted VEGF and Fractalkine. We also observed different secretion patterns in astrocytes versus neurons and concluded that these differences in cytokine/chemokine secretion may be instrumental in future studies investigating the functional role of neuroinflammation during early brain development.

Overall, this work furthers our understanding of the role of p53 in human neurodevelopment by providing context for the parameters of activation of p53 in neural cells. p53 was previously known to induce cell death and cell cycle arrest in mammalian cells with DNA DSBs, and from the work presented here we show that p53 is activated in response to transcription and not replication stress in NPCs.

Acknowledgements and Dedication

The work presented in this dissertation would not have been possible without the support of mentors, family, friends, and colleagues. Their guidance and advice have been invaluable to my development as a scientist and individual over the past four years.

First, I would like to thank my advisor, Michael McConnell. Throughout my training he has given me freedom to explore scientific ideas, opportunities to experience different scientific communities through collaborations and conferences, and guidance during the inevitable times in research that are frustrating and difficult to navigate.

Several members of the McConnell Lab have played pivotal roles in my development as a scientist. Ian Burbulis has had a significant impact on my ability to problem solve as a scientist and work through obstacles. Thank you for supporting me in person and from a distance. I am thankful for the help I received from past lab members Lise Harbom, Matt Wolpert, Luke Oostdyk, and Usnish Majumdar for helping me build my foundation and skills as a scientist. Thank you to our lab technician Mark Haakenson. Special thanks to my undergrads, Umar Arshad and Reem Al-Humadi, for contributing significant time and effort to the experiments included in my dissertation and manuscript. I never could have finished analyzing my single-cell RNA-seq experiments without Chris Cowing-Zitron. Thank you for your hard work and dedication.

Thank you to the members of my committee: Jaideep Kapur, Todd Stukenberg, Noelle Dwyer, Yuh-Hwa Wang, and George Bloom. Your input on my research has been much appreciated. Special thanks to Jaideep Kapur for providing insight and direction throughout my time in graduate school, and Yuh-Hwa Wang, for being a second mentor to me and giving me her time, support, and expertise on a consistent basis.

I must also thank the members of the Wang lab: Naomi Atkin, Heather Raimer, Sandeep Singh, and Arkadi Manukyan. Your constant support, whether it be reagents, time, trouble-shooting, or eating cake have been deeply encouraging to me.

Fortunately, UVA is a very collaborative environment, due in part to the various core facilities available to scientists. The Flow Cytometry Core Facility, Stem Cell Core Facility, and Genome Analysis Technology Core have been immensely helpful throughout my training. Special thanks to Joanne Lannigan, who spent countless hours troubleshooting our approach for identifying neural cells using imaging flow cytometry, and Veronica Porterfield, for supporting me in cell culture when the experiments were particularly demanding.

I want to thank my friends in Charlottesville and from afar that have supported me along my journey. I have had the incredible opportunity to be a part of great communities in Charlottesville that have given me tremendous support throughout my training. The Perkin's House, the Farm House, Victory Church, and the Charlottesville Jazz Society kept me motivated. Thank you for the meals and emotional support. Special thanks to Hiruni Amarasekara, for proofreading my dissertation, you are the best college roommate of all time, and Sikoya Ashburn for being my accountability partner while I wrote my dissertation.

Finally, I would like to thank my family for the all the encouragement and support they have given me throughout my training. All of it has led to be accomplishing this goal and I would not be here without them. Nathan, thank you for checking in and making sure I was alive. Mom, I love you so much, thank you for the phone calls and threats to come to Charlottesville if I don't get enough sleep. Dad, thank you for making me believe I can be anything I put my mind to. This accomplishment is as much yours as it is mine.

Table of Contents

Publication Information

Chapter I contains excerpts from the following publication:

Harbom L.J*, Michel N*, and McConnell M.J. *Single-cell analysis of diversity in human stem cell-derived neurons.* Cell Tissue Res. (2018) PMID: 29185070
*Co-authorship

The basis of Chapter II is the following publication:

Michel N, Majumdar U.B, Lannigan J, and McConnell M.J. *Quantifying Neural Genome Dynamics Using Imaging Flow Cytometry.* Cytometry Part A. (2019) PMID: 31063256

The basis of Chapter III is the following submitted manuscript:

Nadine Michel, Umar Arshad, Reem Al-Humadi, Sandeep Singh, Arkadi Manukyan, Lana Gore, Ian E Burbulis, Yuh-Hwa Wang, Michael J McConnell. *p53 mediates transcription associated DNA DSBs during hiPSC-based neurogenesis.* Stem Cell Reports. (under review)

List of Abbreviations and Acronyms

Aβ	Amyloid Beta
AD	Alzheimer's Disease
A-EJ	Alternative end-joining
ALS	Amyotrophic Lateral Sclerosis
aNSCs	Active Neural Stem Cells
APH	Aphidicolin
AQP4	Aquaporin 4
ATM	Ataxia-Telangiectasia Mutated
ATR	Ataxia-telangiectasia and Rad3-related protein
BF	Brightfield
BrdU	Bromodeoxyuridine/ 5-bromo-2'-deoxyuridine
BSM	Brain Somatic Mosaicism
CFS	Common Fragile Site
CHK1	Checkpoint Kinase 1
CHK2	Checkpoint Kinase 2
.cif	Compensated Image File
CNV	Copy Number Variant
CPT	Camptothecin
CX3CL1	Chemokine ligand 3 (Fractalkine)
DAPI	4′,6-diamidino-2-phenylindole
DDR	DNA Damage Response
DMSO	Dimethyl sulfoxide
DNA DSB	DNA Double-Strand Break
DNA-PKcs	DNA-Dependent Protein Kinase
EDF	Enhanced Depth of Field
FACS	Fluorescent-Activated Cell Sorting
FISH	Fluorescence In-Situ Hybridization
FKN	Fractalkine
FMO	Fluorescence Minus One
GO	Gene Ontology
iPSC	Induced Pluripotent Stem Cells (mouse or human)
hESC	Human Embryonic Stem Cell
hiPSC	Human Induced Pluripotent Stem Cells
HR	Homologous Recombination
HTGTS	High Throughput Genome Wide Translocation Sequencing
H2AX	Histone Family Member X
IFC	Imaging Flow Cytometry
IKNM	Interkinetic Nuclear Migration
IFNα2	Interferon Alpha 2
LIG4	Ligase IV
LINE1	Long Interspersed Nuclear Element One
MMEJ	Microhomology Mediated End Joining
NHEJ	Non-Homologous End Joining
NPC	Neural Progenitor Cell
pATM	Phosphorylated Ataxia-Telangiectasia Mutated

PD	Parkinson’s Disease
PE	Phycoerythrin
PerCP	Peridinin Chlorophyll Protein Complex
PFA	Paraformaldehyde
PI	Propidium Iodide
pLKO.1	Control shRNA plasmid
PTM	Post Translational Modification
$p53^{KD}$	p53 shRNA knock down
QC	Quality Control
qNSCs	Quiescent Neural Stem Cells
RGC	Radial Glial Cell
sAPPα	Soluble Amyloid Precursor Protein-Alpha
SKY	Spectral Karyotype
SNV	Single Nucleotide Variant
TSS	Transcriptional Start Site
VEGF	Vascular Endothelial Growth Factor

Chapter I

Introduction

Cortical Development

The human cortex is a unique and irreplaceable organ in the body. From the beginning of embryogenesis, the development of the nervous system is a highly coordinated and intricate process. The cerebral cortex consists of six layers that all function together to allow for the highest level of cognitive, emotional, sensory, and motor function (Kwan, Sestan, & Anton, 2012). All of the capabilities of the cortex come from the precise placement of neurons and neural connections (e.g. synapses) in the brain (Manzini & Walsh, 2011). If the organization of the cortex is incorrect or altered in any way there is an increased outcome of cognitive impairment, intellectual disability, and neuropsychiatric and neurologic disorders (Casanova, Buxhoeveden, & Gomez, 2003; Flaherty *et al.*, 2017; Marchetto *et al.*, 2017; Marchetto *et al.*, 2010).

Unique Features of Neuroepithelium

The cortex develops in a stereotyped “inside out” manner, with the deepest layers of the cortex being formed before the superficial layers (Agirman, Broix, & Nguyen, 2017; Haubensak, Attardo, Denk, & Huttner, 2004). A key feature of neuroepithelium is apical-basal polarity that ultimately defines the behavior of neural stem cells and progenitors (Farkas & Huttner, 2008). Apical progenitors, which include neuroepithelial cells and radial glial cells (RGCs) divide while simultaneously remaining attached by adherens junctions at the ventricular surface (Noctor, Martinez-Cerdeno, & Kriegstein, 2008). Basal progenitors comprise neural progenitors that undergo mitosis away from the ventricular surface (i.e. ventricular zone, sub-ventricular zone). These progenitors are not attached to the ventricular surface and migrate to the next layer of the cortex (Miyata *et al.*, 2004). Initially, RGCs expand the progenitor pool and divide symmetrically; producing two progenitors. Later in development, RGCs divide asymmetrically and produce intermediate progenitors and post-mitotic neurons. The intermediate progenitors have symmetric divisions into two post-mitotic neurons (Noctor, Martinez-Cerdeno, Ivic, & Kriegstein, 2004). The newborn neurons migrate to the next layer above by traveling on the radial processes of the RGCs (Noctor, Flint,

Weissman, Dammerman, & Kriegstein, 2001). Transcription factors and signaling cues also shape the organization and migration pattern of neurons to form different cortical layers (Kwan *et al.*, 2012).

Genomic Stress During Cortical Development

The adult cortex is projected to have as many as 80-90 billion neurons (Williams & Herrup, 1988) and given the short timeframe for neurodevelopment; neural progenitor cells undergo a rapid succession of cell divisions before ultimately differentiating into neurons (Blaschke, Staley, & Chun, 1996; F. K. Wong & Marin, 2019). The high rate of proliferation and transcription in progenitors creates a challenging environment to maintain a stable genome (Abyzov *et al.*, 2017). Unlike other cells and tissues in the body, neurons are post-mitotic and cannot be replaced (Bhardwaj *et al.*, 2006; Rakic, 2006). Therefore, the genomic changes incurred during neurodevelopment can have consequences ranging from normal phenotypes to neuropsychiatric disorders (McConnell *et al.*, 2017). A common read-out of genomic stress and instability is the presence of DNA damage. The consequent studies in this dissertation focus specifically on DNA Double-Strand Breaks (DNA DSBs) as they are the most pathological form of DNA Damage (Hastings, Lupski, Rosenberg, & Ira, 2009).

DNA DSB Repair

After a DSB occurs there are multiple options for repair that can be initiated depending on the stage of the cell cycle and cell type (So, Le Guen, Lopez, & Guirouilh-Barbat, 2017). Homologous recombination (HR) is typically initiated shortly before and after DNA replication during S phase or G2, while non-homologous end joining (NHEJ) occurs predominately during G1. HR was originally considered an error-free form of DNA repair because it uses sister chromatids as a template, while NHEJ was considered more error prone because it ligates two ends of complimentary DNA without a homologous template (Sung & Klein, 2006). However, advances in live imaging of the repair of DNA DSBs have demonstrated that HR can generate genomic instability and that NHEJ has a high

rate of fidelity (Guirouilh-Barbat, Lambert, Bertrand, & Lopez, 2014). Furthermore, an alternative NHEJ pathway called alternative end-joining (A-EJ) or microhomology mediated end-joining (MMEJ), that is mediated by different proteins has been discovered and linked to genomic instability (Chang, Pannunzio, Adachi, & Lieber, 2017; McVey & Lee, 2008).

NHEJ can take place at any point during the cell cycle and has actually been shown to be a primarily error-free process that is both conservative and adaptable (Betermier, Bertrand, & Lopez, 2014). The heterodimer Ku80-Ku70 recruit DNA-dependent protein kinase (DNA-PKcs) to come to the site of a DNA DSB. The two broken ends are ligated back together by Ligase 4 (LIG4). Ku80 and Ku70 are instrumental in stabilizing the broken ends of DNA by maintaining their location positionally and protecting them from further degradation (Soutoglou *et al.*, 2007).

A-EJ is highly mutagenic because it is initiated by a resection of a single-strand and the resolution of the two breaks often leads to a deletion. Therefore, it is possible that CNVs may arise from A-EJ repair (Arlt, Wilson, & Glover, 2012). In a study by Arlt et. al in mouse embryonic stem cells, the frequency and location of *de novo* CNVs did not change in LIG4 knock-out mice, showing that canonical NHEJ is not responsible for CNV formation. The authors conclude that alternative end joining may be the mechanism instead (Arlt, Rajendran, Birkeland, Wilson, & Glover, 2012).

NHEJ in Mouse Cortical Development

Notably, deficits in DNA DSB repair pathways (specifically NHEJ) lead to phenotypes of cancer, sterility, immunological deficits, and neurological disorders (Altmann & Gennery, 2016). While the first three phenotypes are mechanistically clear (i.e., mutagenesis, meiosis, V(D)J recombination), the mechanism behind the neurological effects of the accumulation of DNA DSBs was more ambiguous. Over the past twenty years, more studies have shed light on the significance of DNA damage in the nervous system and the impact it has on aging and early neurodevelopment.

NHEJ is one of the most important forms of DNA repair in nervous system development. Since neurons are post-mitotic they rely heavily on NHEJ as a primary form of DNA DSB repair (McKinnon, 2017). Four proteins in NHEJ (Ku80, Ku70, LIG4, and Xrcc4) are all necessary for proper neurodevelopment to occur. *LIG4* and X*rcc4* knock-out mice are embryonically lethal and *Ku80* and *Ku70* knock outs have massive neuronal apoptosis (Chun & Schatz, 1999; Gu *et al.*, 2000). Further examination of *Ku80* knock out mice through in situ end labeling showed high levels of apoptosis in the ventricular zone of the cortex (McConnell *et al.*, 2004). The ventricular zone is where neural progenitors are beginning to differentiate into neurons and migrate to the appropriate layers of the cortex (Kageyama, Ohtsuka, Shimojo, & Imayoshi, 2008; Rash, Lim, Breunig, & Vaccarino, 2011). Death of neural progenitor cells (NPC) at this layer of the cortex indicates that massive cell death occurs during early neurogenesis (Chun & Schatz, 1999). However, if the tumor suppressor gene *p53* is also knocked out in addition to *Lig4* or *Xrcc4,* mice develop normal brains and the embryonic lethality is rescued (Bunting & Nussenzweig, 2013; Frank *et al.*, 2000; Gao *et al.*, 2000). This suggests that p53 is inducing death of NPCs undergoing neurogenesis with unrepaired DNA DSBs.

p53 and DNA DSBs

Since the discovery of p53 in 1979 by six independent investigators and the subsequent discovery that it is a tumor suppressor gene ten years later, p53 has been at the forefront of cancer research (Levine, 1997; Levine & Oren, 2009). However, the role of p53 extends beyond tumor suppression due to its broad effects as a transcription factor. Studies have shown that p53 has thousands of potential binding sites in the genome (Kaneshiro, Tsutsumi, Tsuji, Shirahige, & Aburatani, 2007), suggesting that it has a vast network of influence that remains to be discovered. p53 has been shown to play an active role in apoptosis, cell cycle regulation, senescence, cell differentiation, motility and migration, and cell-cell communication (Bieging, Mello, & Attardi, 2014)**.**

After the discovery of *p53*, knockout and knock-in mutant mice studies were commonly used to examine the mechanism by which p53 prevented tumor formation. In normal cell conditions, p53 is present at low levels because it is quickly degraded in the proteasome due to ubiquitinoylation by mouse double-minute-2 (MDM2) (Haupt, Maya, Kazaz, & Oren, 1997). In times of genomic stress where DNA damage increases such as replication stress, transcriptional stress, or oxidative stress, DNA damage proteins stabilize *p53* through post-translational modifications (PTMs). The PTMs stabilize *p53* by preventing it from being degraded, this allows p53 protein levels to accumulate. p53 then activates target genes that activate cell cycle arrest, DNA repair, apoptosis, or senescence (Bieging *et al.*, 2014).

Initially when a DNA DSB occurs, ataxia telangiectasia mutated kinase (ATM) and ataxia telangiectasia RAD3-related kinase (ATR) are activated and phosphorylate p53. ATM and ATR then activate checkpoint kinase-2 (Chk2) and checkpoint kinase-1 (Chk1) respectively, which also stabilize p53 by phosphorylating serine 15 and 20 (Helton & Chen, 2007). One of the first studies that led to the description of p53 as the “guardian of the genome” was the discovery that p53 induces G1 cell cycle arrest following DNA damage signals (Levine, 1997). p53 triggers the arrest by activating Cdkn1a or p21, but it can also inhibit progression past the G2 checkpoint by upregulating Gadd45 and 14-3-3α which inhibit Cdc2, a kinase required for entry into mitosis (Taylor & Stark, 2001).

p53 also plays a role in maintaining fidelity of DNA DSB repair. In HR-mediated repair if a homologous sequence is used instead of a sister chromatid then there is potential for gene conversion, duplication or deletion. p53 has been shown to regulate HR by binding with single-stranded DNA to prevent inappropriate HR initiation (Romanova, Willers, Blagosklonny, & Powell, 2004). It also directly binds Rad41 to prevent exchange between sister chromatids (Sturzbecher, Donzelmann, Henning, Knippschild, & Buchhop, 1996), and prevents recombination by promoting the clearance of Rad51 foci (Orre *et al.*, 2006).

p53 Activation and Cell Fate

When DNA damage levels are high, p53 can trigger apoptosis, senescence, or differentiation. p53 can initiate apoptosis by activating the extrinsic or intrinsic apoptotic pathway. In the extrinsic pathway, p53 can upregulate FAS receptor, death receptor-4, and death receptor-5 which all eventually lead to activation of caspases (Jin & El-Deiry, 2005). p53 can also activate multiple parts of the intrinsic pathway including BAX, BAK, PUMA, and NOXA (Chipuk & Green, 2006). p53 can also induce senescence by activating CDKN1a, Pai1, and Pml not only in response to DNA damage but also hyperproliferation signals like ARF (Bieging *et al.*, 2014).

A few significant studies have emerged revealing that p53 plays an active role in differentiation. After DNA damage in mouse embryonic stem cells, p53 promotes differentiation by suppressing expression of Nanog, a pluripotency factor. p53 binds to the promoter region of Nanog and recruits other suppression factors (Lin *et al.*, 2005). p53 is also a known barrier to stem cell pluripotency such that when p53 or one of its target genes, *p21*, is knocked down, somatic cells can be reprogrammed intro stem cells more efficiently (Kawamura *et al.*, 2009). In 2017 Wang and colleagues examined how the p53 family (p53, 63, and 73) mediates mesendodermal differentiation of ESCs in embryonic mouse development. By investigating ESCs in culture and in the developing embryo, Wang et. al discovered that the p53 family binds to a promoter region of Wnt3 and upregulates transcription leading to βeta-catenin signaling and expression of genes specific to a mesendodermal cell fate. Triple knock-outs of the *p53* family led to defects in early embryo development (Q. Wang *et al.*, 2017).

The vast majority of studies studying the role of p53 in mammalian cells and development have focused on the post-translational modifications of the protein and the upregulation of genes associated with various cell fates (i.e., cell arrest, death, senescence). The Lahav group has produced a significant body of work looking at the temporal dynamics of p53 activity and how that can ultimately mediate cell fate using mathematical modeling and *in vitro* studies (Lahav, 2004;

Reyes *et al.*, 2018). Through live-cell imaging and tracking of p53 protein levels their experiments demonstrate that sustained p53 activation leads to an irreversible cell fate (i.e. death, senescence), but pulses of p53 activity activate DNA damage repair pathways that maintain the proliferative capacity of the cell (Hafner *et al.*, 2017). Their experimental approach has also allowed them to examine single cell divisions in response to DNA damage and determine which cells get arrested in response to DNA damage and which remain proliferative. Interestingly, they observed that despite the level of DNA damage, the most important factor in reliably predicting cell fate in response to p53 was actually the half-life of the target mRNA being upregulated in response to p53 binding. CDKN1A for instance, has a short half-life and therefore would not remain stable when the p53 oscillatory pattern is pulsing; however when the level of p53 is sustained the levels of CDKN1A also stabilize and more mRNA is translated into functional protein (Hafner *et al.*, 2017).

All of these studies highlight the crucial roles that p53 plays in cell fate, particularly in response to DNA damage. But this still leaves several questions unanswered. If the role of p53 in mammalian cells is to induce the proper repair of DNA DSBs or induce apoptosis in cells with unrepaired DNA DSBs, why are somatic mutations so prevalent in neurons?

Brain Somatic Mosaicism

Somatic mosaicism refers to the observation of somatic cells from one monozygotic individual containing different genomes. While somatic mutations are linked to mutagenesis, cancer, and various diseases, many somatic mutations are observed in normal tissue from healthy individuals. Surprisingly, the brain is no exception. Despite cortical neurons being long-lived cells that lack the ability to regenerate, somatic mosaicism is present in the brain in many forms (McConnell *et al.*, 2017). The genomic mosaicism in the brain includes: aneuploidies and aneusomies, long interspersed nuclear element type I (LINE1) repeat elements, single nucleotide variations (SNVs), and copy number variants (CNVs) (Rohrback, Siddoway, Liu, & Chun, 2018).

Initially, the first studies analyzing brain somatic mosaicism (BSM) quantified aneuploidy in NPCs using spectral karyotyping (SKY) and revealed that around 30% of NPCs contained aneuploidy in the developing mouse cerebral cortex (Rehen *et al.*, 2001). Eventually human and mouse post-mitotic neurons were assessed and had an average of 18% aneuploidy using SKY and fluorescence in-situ hybridization (FISH) (Rehen *et al.*, 2005; Rohrback, Siddoway, *et al.*, 2018; Yurov *et al.*, 2005; Yurov, Iourov, *et al.*, 2007; Yurov, Vorsanova, *et al.*, 2007). The mechanism behind these aneuploidies was revealed by histology and real-time imaging to arise from nondisjunction, micronuclei, multiple nuclei, lagging chromosomes, and supernumerary centrosomes leading to multipolar cell division (Yang *et al.*, 2003).

Another source of BSM is LINE1 elements. Retrotransposable elements make up 17% of the human genome within the germline (Viollet, Monot, & Cristofari, 2014). LINE1 RNA contains two components: ORF1 which is RNA binding protein and ORF2 which is a reverse transcriptase and endonuclease. Together these elements promote LINE1 DNA insertion into different genomic locations (Hancks & Kazazian, 2012). In 2005, Muotri and colleagues discovered somatic retrotransposition in NPCs from the rat hippocampus (Muotri *et al.*, 2005). In 2009, these elements were discovered to be present in human neural stem cell lines at a higher level than other tissues (Muotri, Zhao, Marchetto, & Gage, 2009).

The most prevalent form of BSM is SNVs. In a study that isolated single neurons from a neurotypical human brain, ~1000-1500 SNVs were observed per neuronal genome (M. A. Lodato *et al.*, 2015). SNVs accumulate with age and increase dramatically during neurogenesis (Abyzov *et al.*, 2017; Bae *et al.*, 2018; M. A. Lodato *et al.*, 2018). CNVs are also present in human neurons. The first single-cell study of human cortical neurons revealed that at least one megabase-scale de novo CNV was present in up to 41% of neurons (McConnell *et al.*, 2013). Subsequent studies found similar CNVs in at least 10% of neurons (Cai *et al.*, 2014; Knouse, Wu, & Amon, 2016). CNVs also increase during neurogenesis but unlike SNVs, diminish with age (W. D. Chronister *et al.*, 2019; McConnell *et al.*, 2013).

Connecting DNA DSBs, Neural Genes, and CNVs

CNVs are an intriguing form of BSM because they arise from DNA DSBs which are abundant in cortical development (Arlt, Wilson, *et al.*, 2012), and they are associated with a growing list of brain disorders; from neurodevelopmental to neurodegenerative (McConnell *et al.*, 2017). In 2015, a study revealed that common fragile sites (CFS) and CNV hotspots localize to the same genomic locations. To further understand the mechanism behind this co-localization of two different forms of genomic instability, Glover et. al used Bru-seq nascent RNA sequencing and discovered that the factor unifying CNVs and CFSs was large actively transcribed genes (Wilson *et al.*, 2015). Large transcriptional units are late-replicating and by exposing human and mouse fibroblasts to mild replicative stress, Wilson and colleagues observed increased replication fork failure and organized deletion and duplication CNVs in the transcribed and flanking regions of these large genes. They observed the same phenomenon in different cell lines with unique sets of highly transcribed genes and concluded that the mechanism is a collision between replication and transcription machinery leading to genomic instability (e.g. CNVs and CFS) as others had previously hypothesized (Aguilera & Garcia-Muse, 2012, 2013). Although this study was conducted in human fibroblasts, a majority of the large transcriptional units identified were neural genes associated with neuropsychiatric and neurodevelopmental disorders.

A few years later, recurrent DNA DSBs were observed in a similar subset of genes from mildly stressed *Lig4*$^{-/-}$ *p53*$^{-/-}$ mouse NPCs using high-throughput, genome-wide, translocation sequencing (HTGTS) (Wei *et al.*, 2016). These genes were also shown to be transcriptionally active and late-replicating in the mouse progenitor cells. The majority of genes identified are involved in a variety of key neural functions such as synaptogenesis and neural cell adhesion. Many of the genomic locations observed are high risk alleles associated with neuropsychiatric disorders such as autism and schizophrenia which further validated the work done earlier by Wilson et. al using different approaches. These studies reveal that the

combination of replication stress and the transcription of long neural genes in NPCs is a source of DNA DSBs, CFSs, and de novo CNVs.

Transcriptional stress has also been examined in cortical neurons in relation to autism (King *et al.*, 2013). Neurons exposed to transcriptional stress via TOP1 inhibition have impaired expression of long genes (>200kb), many of which overlap with the long genes with DNA DSBs from the aforementioned studies. Taken together these findings indicate that NPCs go through replicative and transcriptional stress during development which predisposes them to genomic instability, and ultimately somatic mosaicism in the brain.

p53 and Neuronal Differentiation

Given the role p53 plays in determining cell fate in response to DNA damage and the immense genomic stress occurring during cortical development, a likely model is that p53 plays an active role in preventing the differentiation of NPCs with DNA DSBs. As mentioned previously, mice that lack NHEJ components are embryonically lethal or have small brains due to excessive cell death in the ventricular zone. Those phenotypes are rescued in dual *p53*$^{-\backslash-}$ mice (Frank *et al.*, 2000). This would indicate that p53 surveys DNA DSBs during early cortical development and induces cell death, however, there are several studies indicating that p53 actually promotes a neuronal cell fate.

p53 mRNA levels are at their highest during differentiation of several tissues, including the brain (Rogel, Popliker, Webb, & Oren, 1985; Schmid, Lorenz, Hameister, & Montenarh, 1991). Interestingly, p53 null mice have increased neuronal apoptosis in the spinal cord and a buildup of neural precursor cells in the neural tube (Armstrong, Kaufman, Harrison, & Clarke, 1995). Some studies have demonstrated that knocking down p53 in neural progenitor cells leads to a significant reduction in neurons during neuronal differentiation (Aranha, Sola, Low, Steer, & Rodrigues, 2009) and that p53 is required for neurite outgrowth of primary neurons and axonal regeneration in mice (Di Giovanni *et al.*, 2006). Yet, others have shown that p53 expression is highest in proliferating cells and goes down to

minimal levels in terminal differentiation (Gottlieb *et al.*, 1997). A recent study revealed that the loss of p53 causes transdifferentiation of tumor-associated sensory nerves; leading to head and neck cancer (Amit *et al.*, 2020).

The range and somewhat contradictory functions attributed to p53 during neural differentiation is most likely due to several factors: (1) other members of the p53 protein family have been shown to compensate when one family member is downregulated (F. D. Miller & Kaplan, 2007) (2) PTMs of p53 greatly influence where it binds (Meek & Anderson, 2009), and (3) protein-protein interactions alter the function of p53 (Budhram-Mahadeo *et al.*, 2006). Studies have demonstrated that PTMs impact the function of p53. Certain PTMs, such as phosphorylation of serine 15 on the N-terminus, favor neuronal death (Culmsee & Mattson, 2005), while others, such as acetylation of regions of the c-terminus, promote G1/S arrest and neuronal differentiation (K. Wong *et al.*, 2004).

Another crucial element that is theorized to alter the decision-making of p53 is the amount of DNA damage. In 2006, Helton and Chen wrote a review on how p53 modulates the DNA damage response and designed a model for the different functions of p53 based on DNA damage levels (Helton & Chen, 2007). In summary, their model shows that normally p53 protein levels are kept low by ubiquitin-mediated protein degradation, however, phosphorylation of p53 by DNA damage-sensing proteins stabilizes and activates p53. At low levels of DNA damage, p53 promotes cell survival by activating cell cycle arrest, regulating DNA repair, and inducing other pro-survival pathways. At high levels of DNA damage, p53 pro-apoptotic function is activated leading to apoptosis, senescence, and differentiation which Helton and Chen hypothesize is an alternative mechanism to eliminate damaged cells. While this model is based on a significant amount of experimental data, the authors are not incorporating the development of the nervous system, in which differentiating cells with DNA damage would have irreversible and life-long effects. Furthermore, others have shown that the level of DNA damage is not a consistent predictor of p53 activation and consequent cell fate (Hafner *et al.*, 2017).

Discovering the role of p53 in human-based cortical development

Currently it is unclear how p53 activation impacts human neural stem cells during development. Mouse knock out studies have shown that the brain develops normally (i.e. size and basic function) and that in the context of unresolved DNA DSBs in early brain development, p53 is most likely killing progenitors and newborn neurons. Earlier it was discussed that mechanisms of somatic mosaicism include replication stress, oxidative damage, and error-prone DNA repair. These sources of mosaicism also coincide with inducers of p53 (e.g. DNA DSBs) and they are stressors that are present during cortical development. All of these factors combine to make p53 a major determinant of the fate of NPCs in the stressful environment of the developing brain. To more definitely uncouple the mechanism and function of p53 activation in neurogenesis, we sought to use a human based model system that would allow us to determine temporal effects of p53 during neurogenesis and further examine the forms of genomic stress that lead to p53 activation. hiPSC-based neurogenesis models early human cortical development in a consistent manner that mirrors the timeline and significant events observed from human post-mortem tissue and mouse models of cortical development.

Development of Induced Pluripotent Stem Cells

In 1952, it was shown that normal tadpoles could be produced by transplanting nuclei from blastula cells to enucleated eggs of frogs. A few years later, that same research group tried to transplant nuclei from older blastula cells but they were not able to produce normal tadpoles. They concluded that as cells differentiate, their nuclei undergo stable changes that lead to a loss in totipotency. In 1962, John B. Gurdon proved that conclusion was incorrect by demonstrating that nuclei taken from intestinal epithelial cells and transplanted into enucleated eggs can produce normal adult frogs (Gurdon, 1962). This led to the conclusion that differentiated cells do not actually lose the genes required to become any cell type, but it would be almost 50 years before this knowledge would be applied to other model systems and eventually to humans.

After the sperm fertilizes the egg, the morula forms and eventually the blastocyst is created. The blastocyst has an inner cell mass that contains pluripotent embryonic stem cells. In the developing embryo, these cells last for a very short period of time, however in 1998 James Thomson was able to dissociate the inner mass and propagate these cells for the first time (Thomson *et al.*, 1998). These embryonic stem cells had the potential to become any of the three germ layers: endoderm, mesoderm, or ectoderm. This finding was exciting to scientists across many fields because human embryonic stem cells (hESCs) could greatly impact transplant research and regenerative medicine. Unfortunately, the ethical complications of using a human fetus to acquire hESCs have made them a difficult tool for the scientific community to use.

In 2006, Yamanaka discovered that the forced expression of four transcription factors, Oct3/4, Sox2, c-Myc, and Klf4, was sufficient to convert adult mouse fibroblast cells to pluripotent stem cells (Takahashi & Yamanaka, 2006). Only a year later human fibroblasts were reprogrammed (Takahashi *et al.*, 2007). In that same year, Thomson and colleagues demonstrated that cells could be reprogrammed with Lin28 as the fourth factor instead of c-Myc, alleviating concerns that c-Myc, as a mitogen, could increase the risk of cancer in stem cell recipients (J. Yu *et al.*, 2007). Since that time, the reprogramming process has become more efficient and human-induced pluripotent stem cells (hiPSCs) are used to model complex neurological and psychiatric disorders (Ardhanareeswaran, Mariani, Coppola, Abyzov, & Vaccarino, 2017; Brennand *et al.*, 2011).

Modeling Neurodevelopment with induced Pluripotent Stem Cells

As previously discussed, neurodevelopment is an intricate and complicated process that involves determination of polarity, precisely timed cell divisions, cell migration, and eventually cell differentiation (Gotz & Huttner, 2005). Many of the elements of neural development observed in the mammalian cortex are also conserved in iPSC-derived neurogenesis.

During the neural rosette stage of iPSC differentiation, neural rosette cells display features that are consistent with the neuroepithelium *in vivo*. They have apical-basal polarity and express markers such as CD133, aPK, and ASPM on the apical or luminal surface of the rosettes (Y. Shi, Kirwan, & Livesey, 2012; Y. Shi, Kirwan, Smith, Robinson, & Livesey, 2012). Furthermore, in iPSC neurogenesis, interkinetic nuclear migration (IKNM) takes place. IKNM is a unique feature of neuroepithelia in which the nuclei of progenitor cells migrate basally during G1 and return to the apical surface during G2 to undergo mitosis (Farkas & Huttner, 2008). Time lapse imaging of rosettes demonstrate that their nuclei migrate and predominately undergo mitosis at the apical membrane (Y. Shi, Kirwan, Smith, *et al.*, 2012). Additionally, Zo1 and N-cadherin are also expressed on the luminal surface of neural rosettes which is present in the human cortex *in vivo* (Y. Shi, Kirwan, Smith, *et al.*, 2012).

Cortical rosettes also produce RGCs and basal progenitors as seen *in vivo.* Neural rosettes stain positively for a variety of different markers replicating the diversity of progenitor cells in mammalian development. Tbr2+/Pax6- without a basal process are present, which indicate intermediate basal progenitors, and Tbr2-/Pax6+ cells are present which indicate RGCs. iPSC-derived neurogenesis also follows *in vivo* human cortical development temporally. Deep layer neurons are made before outer layer neurons. The Shi group studied the order of neuronal subtypes that appear during the first 70 days in neuron media and they observed that deep, layer 6 neurons (Tbr1+) came first, next were CTIP2-expressing layer 5 and 6 neurons, and then upper layer, Brn2/Cux1 callosal projection (layer 2–4), and finally Satb2 (superficial layer) expression (Y. Shi, Kirwan, Smith, *et al.*, 2012). Glutamatergic

neurons are made before glial cells and exhibit mature physiological properties (Hansen, Rubenstein, & Kriegstein, 2011). Cortical neurogenesis also takes approximately over two months once the neural induction is started, which mirrors the ~100 day period for human neurogenesis (Caviness, Takahashi, & Nowakowski, 1995).

Many groups have studied the validity of iPSCs by transplanting them into mouse cortex or culturing them on mouse slices to see if they migrate to the correct layers. The cortical slice culture assay has been used to demonstrate that iPSC-derived neurons can migrate, terminally differentiate, and orient themselves within the mouse cortex (Polleux & Ghosh, 2002). Several groups have transplanted iPSC derived neurons into the mouse neonatal brain and observed that neurons not only establish axonal projections and dendritic patterns matching the native cortical neurons, but also developed more complex synaptic connections and functional circuitry as the mouse developed (Espuny-Camacho *et al.*, 2013; Qi *et al.*, 2017).

Finally, advances in single-cell sequencing have led to studies examining transcriptomes to determine cell identity and subsequently the heterogeneity within cell populations. Handel et. al conducted a critical study assessing the similarities in transcriptomes of primary tissue and iPSC-derived cortical neurons. They discovered that iPSC-derived neurons had mixed layer identities based on expression of specific upper and deep layer markers (Handel *et al.*, 2016). However, this heterogeneity in cell layer marker expression was also present in primary fetal and post-mortem adult neurons, suggesting that there is neuronal diversity throughout neurogenesis and that iPSC-derived cortical neurons may provide us with an accurate model to examine how that diversity is formed.

hiPSCs Model Neurological and Psychiatric Illness

hiPSCs have been used to model numerous diseases including: Rett Syndrome (Marchetto *et al.*, 2010), Down Syndrome (Mou *et al.*, 2012), Bipolar Disorder (Chen *et al.*, 2014), Autism (Griesi-Oliveira *et al.*, 2015; Marchetto *et al.*, 2017), Schizophrenia (K. Brennand *et al.*, 2015; Brennand *et al.*, 2011), and Parkinson's Disease (Byers, Lee, & Reijo Pera, 2012). Importantly, hiPSC-derived neurons from diseased patients maintain the phenotypes that have been observed in patients and provide the opportunity to understand more about the cellular mechanisms that lead to those phenotypes. Nguyen *et al.* found that hiPSC-derived neurons from patients with a common mutation in Parkinson's Disease had increased expression of oxidative stress genes and α-synuclein protein (Nguyen *et al.*, 2011). hiPSC-derived neurons from patients with Rett Syndrome exhibit smaller cell bodies, fewer synapses, lower spine density, and various electrophysiological defects compared to control cells. These abnormal phenotypes were rescued with drugs that have been effective in mouse models of Rett Syndrome (Marchetto *et al.*, 2010). These two examples illustrate that hiPSC-derived neurons produce phenotypes that are consistent with their respective diseases and offer insight into pathophysiology and potential human treatments.

hiPSCs also provide the opportunity to study more complex diseases that may have a mixture of genetic causes. Schizophrenia, a disorder characterized by perturbed language, thinking, and perception, affects more than 21 million people worldwide (van Os & Kapur, 2009) and affects patients with a wide variety of mutations in numerous genes. Kristen Brennand was one of the first to use hiPSC-derived neurons to model schizophrenia (Brennand *et al.*, 2011). Brennand and colleagues found reduced neural connectivity and altered signaling in the Wnt pathway; they were able to rescue the defects in neural connectivity with Loxapine, a commonly prescribed antipsychotic used to treat the disorder. Additional studies revealed an increase in oxidative stress in the hiPSC-derived NPCs from schizophrenic patients (SZD) as well as abnormal expression of cytoskeletal genes

and aberrant neural migration (K. J. Brennand *et al.*, 2015). Some groups have used hiPSCs to study rare genetic causes for schizophrenia. One study derived hiPSCs from patients with a DISC1 mutation and found increased Wnt signaling and altered expression of neuronal fate markers (Srikanth *et al.*, 2015). Others have discovered that a majority of the mutations in schizophrenia are in neural genes involved in synaptic transmission or development (Soliman, Aboharb, Zeltner, & Studer, 2017).

Many research groups have been combining hiPSC-derived neurons with single cell analysis to further investigate how specific cell types play a role in disease. The Pearse research group sought to understand secretion patterns of amyloid beta (Aβ) and soluble amyloid precursor protein-alpha (sAPPα) from hiPSC-derived neural cells of both control and Alzheimer's Disease (AD) patients on a single-cell level (Liao *et al.*, 2016). Using a novel nanowell antibody capture technique to collect single cell analytes and a nanostring assay to analyze gene expression, they found that several subpopulations of neural cells expressed high levels of Aβ and sAPPα and that expression levels increased during neural differentiation. Previously it was thought that neurons were the main cell type expressing Aβ, but this study yielded the novel finding that astrocytes have the ability to express Aβ as well. Additionally, when they looked into the subneuronal populations they expected to see an enrichment of Aβ secretion from excitatory neurons; instead they discovered a majority of the neurons were GABAergic. This study highlights the depth of information that hiPSC-derived neurons and single cell analysis can contribute to the field.

Single-Cell Approaches to Study a Diverse Brain

Once of the challenges of studying brain development is the immense diversity present in the cortex. NPCs give rise to diverse neuronal and glial progeny during brain development (S. Lodato & Arlotta, 2015; Masland, 2004). While Golgi and Cajal first glimpsed the extraordinary morphological diversity of neurons in the cerebral cortex over a century ago (Cajal, 1890, 1891; Golgi, 1886), careful accounting of neural diversity at the molecular level has become an increasingly

common approach in neurodevelopment research. Tissue-wide measurement of any brain region obscures the underlying molecular diversity so rare cell types go unmeasured and diversity among common cell types becomes population-averaged (Figure 1). Thus, measurement of single cells is essential to define neuronal diversity (Eberwine & Kim, 2015).

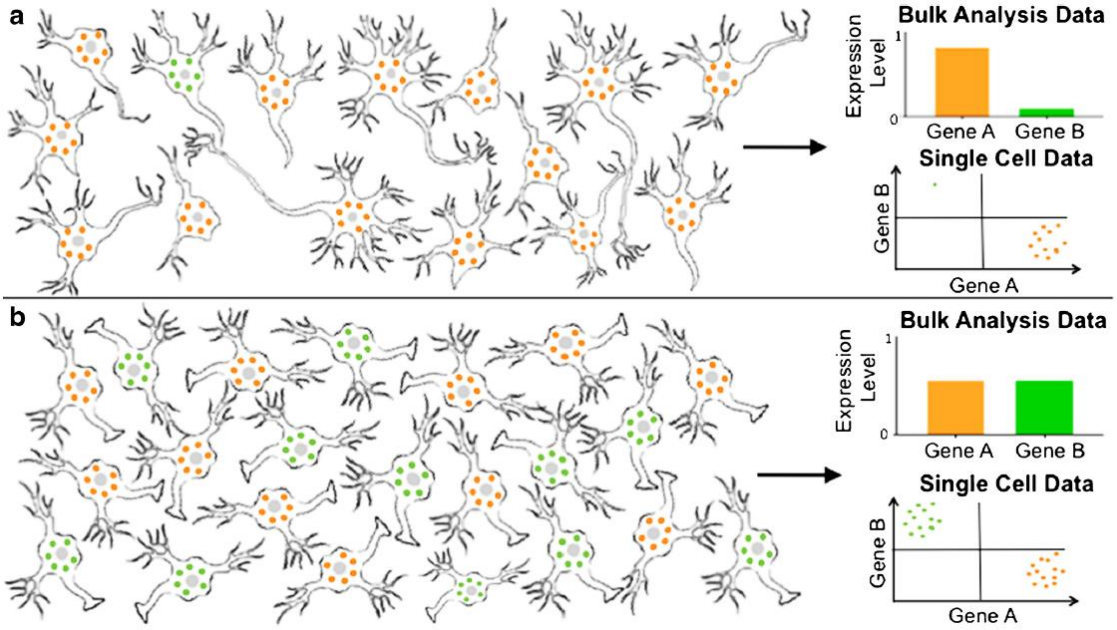

Figure 1. Single cell approaches are essential to measure neuronal diversity. **(A)** In a morphologically diverse population of neurons (left), transcriptomic diversity present only in a rare population of neurons is lost in bulk measurement. Schematized gene expression measurements from bulk tissue and from single cells (right) are used for illustration. Bulk analysis indicates that all neurons express high levels of gene A (orange), and low levels of gene B (green); whereas, single cell measurement identifies neuronal diversity. **(B)** Diversity among morphologically similar neurons (left) is also obscured by bulk measurement. As in (A, right), bulk measurement indicates that all neurons express equal levels of genes A and B; whereas, single cell measurement can reveal distinct subpopulations.

Single Neuron Transcriptome Analysis

Transcriptomic analysis is routinely employed to validate pluripotency and lineage potential in hiPSC lines (Muller *et al.*, 2011; Tsankov *et al.*, 2015). Likewise, transcriptomic analysis has become a central tool for phenotyping patient-derived hiPSC lines. Several groups have taken this approach to study hiPSCs derived from patients with neuropsychiatric disorders such as schizophrenia (K. Brennand *et al.*, 2015; Brennand *et al.*, 2011). Studies looking at the transcriptome of hiPSC-derived neurons are typically performed on large cell populations, which necessarily obscure neuron-to-neuron diversity. With the development of single-cell transcriptomic approaches, fine-grained maps of neuronal diversity are emerging rapidly.

Transcriptome Diversity *In Vivo*

Various single cell approaches have been used to better understand cellular diversity within known subpopulations of primary NPCs and neurons. Specific neural subtypes are purified from bulk tissue using fluorescence activated cell sorting (FACS). Single cell transcriptomes can then be measured on targeted collections of hundreds of specific genes using multiplexed qPCR and microfluidic devices (i.e., Fluidigm Biomark) or comprehensively on RNA libraries by next generation sequencing. Two examples of these approaches are highlighted from human cerebral cortex; however, several similar studies have also examined other populations of NPCs and neurons (Dulken, Leeman, Boutet, Hebestreit, & Brunet, 2017; S. J. Liu *et al.*, 2016; Tasic *et al.*, 2016).

Johnson and colleagues (Johnson *et al.*, 2015) isolated two cortical progenitor cell populations (apical and outer (i.e., non-apical) radial glia from fetal human brain based on expression of known proteins (i.e., GLAST and LexA) and differential abundance of the apical marker prominin. Diversity in these human cortical progenitor cell types is of particular interest because the development of large, complex germinal zones is associated with evolutionary expansion of the human neocortex. Multiplexed qPCR was performed on 546 single progenitor cells to

query the expression levels of dozens of genes. In contrast to previous bulk analysis of micro dissected germinal zones, this single cell study identified new markers of outer radial glia and found diverse transcriptional states involving co-expression of both classic radial glia markers and pro-neural transcription factors in both apical and non-apical cell types.

A second single cell study by the Zhang and Chun labs used NeuN expression to separate neuronal nuclei from non-neuronal nuclei and investigated cortical neuron diversity in 6 discrete regions of the human cerebral cortex (Lake *et al.*, 2016). Notably, they found that sequencing of nuclear RNA (Grindberg *et al.*, 2013; Lacar *et al.*, 2016) was superior to laser microdissection of intact neurons. A total of 3,227 neuronal data sets were classified based on 10-fold differentially expressed genes using an iterative clustering approach, then excitatory and inhibitory populations were identified based on expression of known marker genes. Neuronal diversity was classified into 8 excitatory and 8 inhibitory subtypes with additional diversity associated with regional identities. However, the authors note that even within one region there is still heterogeneity in gene expression among single cells that remains to be explored.

An unbiased alternative to these FACS-based approaches is to perform RNAseq analysis on all single cells in a defined brain region. Zeisel *et al.* (Zeisel *et al.*, 2015) performed RNAseq on 3,005 single cells from mouse somatosensory cortex and hippocampal CA1 region. Cluster-based analysis identified pyramidal neurons and interneurons, as well as 6 non-neuronal subtypes including oligodendrocytes, astrocytes, microglia, vascular endothelial cells, mural cells, and ependymal cells. Distinct subclasses of cells were identified retrospectively based on expression of cell marker genes. Sixteen subclasses of interneurons were discovered and the authors noted that interneurons within the same region had the most similar transcriptomic profiles.

Transcriptome Diversity *In Vitro*

Single cell transcriptome analysis of primary neurons provides an essential benchmark for hiPSC-derived neurons. As mentioned earlier, Handel and colleagues conducted a critical study assessing the similarities in transcriptomes of primary tissue and hiPSC-derived cortical neurons (Handel *et al.*, 2016). The discovery of mixed layer identity neurons in both primary tissue and hiPSC-derived neurons led to two important conclusions. One is that iPSC-derived cortical neurons provide us with a reliable model to examine how neural diversity is formed and the other is that relying on a few markers to distinguish cortical layer identify is an insufficient approach. This makes transcriptomic and other multidimensional forms of single-cell analysis fundamental to understand neuronal diversity.

The direct comparison between *in vivo* and *in vitro* single-cell transcriptomic analysis has been examined in mice as well. Dulken *et al.* specifically looked at transcriptional dynamics in adult neural stem cell lineage through single cell RNA-seq of the adult mouse subventricular zone in transgenic GFAP-GFP mice. They observed four cell populations: astrocytes, quiescent neural stem cells (qNSCs), activated neural stem cells (aNSCs), and NPCs. Through PCA analysis they found a continuum of quiescence, activation, and differentiation in aNSCs. Further investigation of this subpopulation revealed differential gene expression depending on the state of the NSC. Earlier aNSCs expressed cell cycle genes while later aNSCs expressed neuronal genes. When the authors compared the *in vivo* NSCs to *in vitro*, they found a greater enrichment for neuronal genes *in vivo* while the *in vitro* NSCs had enrichment for astrocyte genes (Dulken *et al.*, 2017). This study highlights one of the key issues in the study of *in vitro* neurogenesis: determining real versus artificial heterogeneity. The *in vitro* condition showed more heterogeneity than the *in vivo* condition in that there was a greater spectrum of neural stem cells in various stages of activation. The study did not follow the NSCs far into the differentiation process, however, so it is still unclear if the heterogeneity in the NSCs translated into more diverse iPSC-derived neurons compared to primary tissue.

Single Neuron Genome Analysis

As mentioned previously, single cell analysis has also revealed surprising diversity in neuronal genomes due to brain somatic mosaicism. SNVs (Hazen *et al.*, 2016; M. A. Lodato *et al.*, 2015), CNVs (Cai *et al.*, 2014; Knouse *et al.*, 2016; McConnell *et al.*, 2013), and mobile genetic element insertions (Baillie *et al.*, 2011; Erwin *et al.*, 2016; Evrony *et al.*, 2012; Upton *et al.*, 2015) collectively contribute to genomic diversity.

Cell proliferation during development is a prominent source of somatic mutations. Given about 20 billion neurons in human cortex, and more than 50% cell death during neurodevelopment, cortical NPCs must undergo at least 40 billion cell divisions (Lui, Hansen, & Kriegstein, 2011). Errors in DNA replication and repair are estimated to lead to 1 – 3 mutations per cell division (Lynch, 2010); thus, estimates of greater than 1,000 somatic SNVs per neuronal genome (M. A. Lodato *et al.*, 2015) are quite reasonable. However, it is interesting to consider that the distribution of diverse genomes in the cortex is expected to be orthogonal to the arrangement of diverse cell types.

Clonally-related neurons of different cell types are born through a series of asymmetric cell divisions by an individual NPC (Namba & Huttner, 2017). Surviving progeny then reside in functionally connected radial columns (Y. C. Yu, Bultje, Wang, & Shi, 2009) with early born neurons in deep cortical layers and subsequently born neurons migrating to increasingly superficial layers. Neuronal cell type diversity is often described in the context of layer 6 neurons expressing different genes than layer 5 neurons, and so forth. Likewise, neurons in different cortical layers have different morphological and physiological properties. Somatic mutations in NPCs, as a consequence of iterative cell fate decisions, will be shared among many of that NPCs progeny, while cortical columns that arise from other NPCs could have distinctly different genomes (Figure 2).

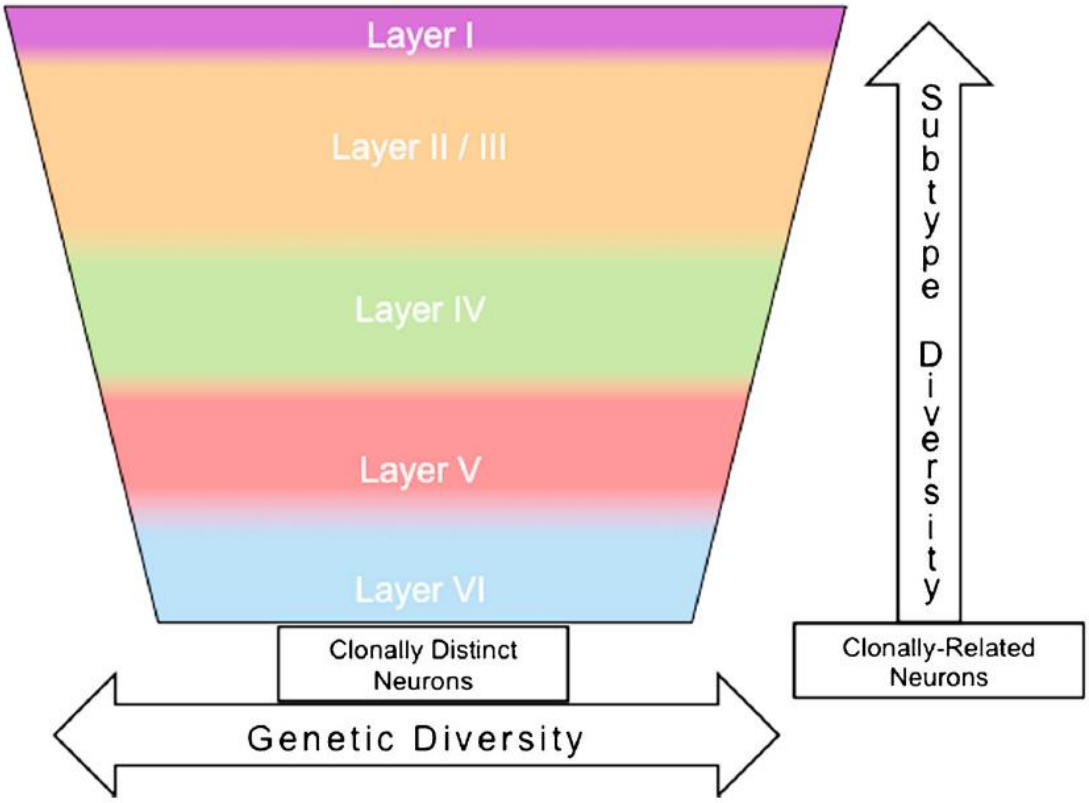

Figure 2. Genomic diversity may be greater within single neuronal subtypes, than among clonally-related neurons. The molecular taxonomy of excitatory cortical neurons is based on laminar residence. Morphological, physiological, and transcriptomic diversity is catalogued by comparing layer VI neurons, to layer V neurons, for example. However, genomic diversity is expected to expand in an orthogonal direction. Radial cortical columns contain neurons of each subtype that were born from the same NPC, these clonally related progeny are expected to share somatic mutations. Tangentially distributed columns, on the other hand, arise from different NPCs and are expected to accumulate distinct mutational profiles from other columns.

A central interest is whether somatic mutations are more prevalent in the brain than in other tissues. Although somatic mosaicism occurs in probably all organs, the long lifespan and direct influence on behavior of neural circuits suggest a direct consequence of somatic mosaicism in both neurotypical and diseased brains. *In vitro* models of human neurogenesis offer some insight into this question.

Single cell genomic analysis showed that NPCs derived from hiPSCs exhibit few CNVs; whereas CNVs are abundant in 8-week differentiated neurons (McConnell *et al.*, 2013). Using an L1 reporter system, L1 retrotransposon activity is likewise absent in hiPSC-derived NPCs, but then observed during the first week of neuronal differentiation (Coufal *et al.*, 2009). Additional study of the L1 promoter shows transcriptional regulation similar to that of the master neuronal transcription factor NeuroD. Hybrid Sox2/TCF-LEF motifs MeCP2-deficient phenotypes (Coufal *et al.*, 2009) support a model wherein Sox2-binding and MeCP2 activity suppress L1 mobility in NPCs, and Sox2 de-repression coupled with Wnt signaling promote L1 transcription during neurogenesis (Kuwabara *et al.*, 2009). If hiPSC-based neurogenesis is faithfully recapitulating the mechanisms that lead to primary brain somatic mosaicism, it will prove to be a valuable model system in defining the intersection between cell type diversity and genomic diversity in human neurons.

Single-Cell Protein Based Approaches

In addition to the single cell approaches highlighted herein, other advances in single cell epigenomic (Farlik *et al.*, 2015; Gravina, Dong, Yu, & Vijg, 2016) and proteomic approaches (Budnik, 2017), as well as multi-omic approaches (Bock, Farlik, & Sheffield, 2016; Macaulay, Ponting, & Voet, 2017), a high-resolution molecular taxonomy of neuronal diversity is taking shape rapidly. Multiplex protein measurement approaches such as flow cytometry provide additional quantification of diverse neural types in specific brain regions. Pruszak et al used FACS to sort heterogeneous hESC derived neural stem cells at various stages of differentiation and showed that specific surface antigens corresponded to the development or maintenance of neural precursor cells or neurons (Pruszak, Sonntag, Aung, Sanchez-Pernaute, & Isacson, 2007). Mass cytometry extends multiplex

capability to at least 50 separate analytes on single cells by conjugating antibodies with heavy metals rather than fluorophores (Bandura *et al.*, 2009; Bendall *et al.*, 2014). Together with novel computational approaches, Zunder et. al used mass cytometry to track the dynamic process of iPSC reprogramming by looking at markers of pluripotency, differentiation, cell cycle status, and cell signaling (Zunder, Lujan, Goltsev, Wernig, & Nolan, 2015).

Development of improved approaches for hiPSC-based neurogenesis is likewise proceeding with great pace. Three-dimensional culture approaches such as cerebral organoid technology (Lancaster *et al.*, 2013) show improved tissue patterning over standard two-dimensional approaches; however, additional advances are required to fully recapitulate neuronal diversity in primary tissue. For example, neural vasculature is known to provide an important NPC niche, yet existing organoids are avascular. Without such a niche, limited diversity is not unexpected.

Concluding Remarks

The role of p53 in human-based cortical development has yet to be examined. In the studies described in this thesis, we investigated the dynamics of DNA DSBs in neural cells at different timepoints of differentiation by using imaging flow cytometry to quantify DNA DSBs in hiPSC-derived NPCs during neurogenesis (Chapter II). We then examined the role of p53 in hiPSC-derived neurogenesis by examining how decreased levels of p53 alters neurogenesis and differentiation, applied genomic stress to NPCs to determine which stressors activate p53, and mapped the location of DNA DSBs arising from transcriptional stress (Chapter III). Finally, we applied single-cell RNA sequencing and high sensitivity cytokine detection to examine whether p53 has a functional role in neuroinflammatory phenotypes (Chapter IV). This work is the first to explore the dynamics of DNA damage, cell death, and neuronal differentiation using hiPSCs at a single-cell level. Specifically, this work investigates what cellular conditions activate p53 during neurodevelopment and provides possible mechanisms for selective p53 activation during replication versus transcriptional stress during development.

Chapter II

Imaging Flow Cytometry Quantifies Neural Genome Dynamics

Abstract

Somatic mosaicism is a common consequence of normal development. DNA repair is simply not perfect, and each cell's genome incurs continuous DNA damage as a consequence of transcription, replication, and other cell biological stressors. Brain somatic mosaicism is particularly noteworthy because the vast majority of an individual's neurons are with that individual for life and neural circuits give rise directly to behavioral phenotypes. Brain somatic mosaicism, now revealed and tractable due to advances in single cell 'omic approaches, has emerged as an intriguing and unexplored aspect of neuronal diversity. Furthermore, the study of DNA damage during early neurodevelopment, when the rate of mutagenesis is high, is the perfect starting point to understand the origins of brain mosaicism.

Flow cytometry is a highly efficient technique to study cell cycle and intracellular proteins of interest; particularly those related to DNA damage, but lacks the high resolution of microscopy to examine the localization of these proteins. In this study we outline a novel single-cell approach to quantify DNA Double-Strand Break (DNA DSB) dynamics during early human neurodevelopment by applying imaging flow cytometry (IFC) to human-induced pluripotent stem cell derived neural progenitor cells (NPCs) undergoing neurogenesis. We establish an increase of DNA DSBs by quantifying γH2AX foci in mildly stressed NPCs using various single-cell approaches in addition to IFC including fluorescent microscopy, conventional flow cytometry, and measuring DNA DSBs with the comet assay. We demonstrate the dose-dependent sensitive detection of γH2AX foci through IFC and reveal the dynamics of DNA DSBs in proliferating and differentiating neural cells in early neurogenesis.

Introduction

Human neuronal genomes exhibit signs of neurodevelopmental genomic stress (McConnell *et al.*, 2017). Hundreds of somatic single nucleotide variants (SNVs) are observed in young human neurons (Abyzov *et al.*, 2017; M. A. Lodato *et al.*, 2018), some of these are clonal indicating that they occurred in a common NPC lineage. More extensive genomic stress in the form of megabase-scale copy number variants (CNVs) are observed in a subset (~30%) of young cortical neurons (Cai *et al.*, 2014; Knouse *et al.*, 2016; McConnell *et al.*, 2013). Recent data from our lab indicate that neurons with large CNVs are selectively vulnerable to aging-related atrophy(W. Chronister *et al.*, 2018); thus, understanding the origin of CNV neurons is important for both development and aging. The abundance of young neurons with complex karyotypes indicates that human neurogenesis tolerates high levels of genomic stress, yet the cellular basis for this tolerance is not known.

Genomic stress, arising from ongoing transcription, replication, and metabolism, contributes to the accumulation of DNA damage during neurodevelopment. The abnormal accumulation of DNA damage in neurons is a shared pathological feature among neurodegenerative diseases (Bushman *et al.*, 2015; Lovell & Markesbery, 2007), and it is also correlated with normal aging (Chow & Herrup, 2015). Transgenic mouse models further demonstrate a specific requirement for DNA repair during neurogenesis (Barnes, Stamp, Rosewell, Denzel, & Lindahl, 1998; Frank *et al.*, 2000; McConnell *et al.*, 2004). Previously, studying neural genomic dynamics during human neurogenesis has been incredibly challenging because post-mortem tissue is difficult to acquire and is not amenable to longitudinal studies. With the development of human-induced pluripotent stem cells (hiPSCs)(K. Brennand *et al.*, 2015; Takahashi *et al.*, 2007), we now have an *in vitro* model of human neurodevelopment that also accurately captures the immense cellular and genetic heterogeneity present in human neurons (Handel *et al.*, 2016).

This heterogeneity requires single-cell approaches that will inform how subpopulations of NPCs and neurons respond to genomic stress acutely and how stress exposure alters developmental trajectories (Harbom, Michel, & McConnell, 2018). H2AX is a histone subunit that is rapidly phosphorylated (γH2AX) when a DNA Double-Strand Break (DNA DSB) occurs making it an optimal marker of DNA damage (Rogakou, Pilch, Orr, Ivanova, & Bonner, 1998). To assess acute stress in neurodevelopment, we quantified DNA DSBs through the detection of γH2AX foci through IFC, an approach that has been used to study human cell lines with defective DNA repair (Bourton *et al.*, 2012). To our knowledge, this is the first application of imaging cytometry to hiPSC-derived neural cells. In addition to describing a novel approach to simultaneously quantify DNA DSBs and other cellular phenotypes, we also employ this assay to gain additional insight into genome dynamics during early hiPSC-based neurogenesis.

Results

DNA-DSB Heterogeneity Revealed by Single-Cell Approaches

In order to evaluate our IFC approach (Figure 1), we employed traditional assays to measure DNA DSBs in hiPSC-derived NPCs. NPCs were exposed to 400nM aphidicolin for 24 hours, a DNA polymerase α inhibitor, to induce mild replicative stress (Figure 2A). Bulk analysis (Western Blot) of NPCs exposed to stress did not show a significant difference in γH2AX protein levels compared to cells treated with DMSO (Figure 2B). To detect DNA DSBs at a single-cell level we employed the comet assay, in which single cells are electrophoresed and the length and intensity of the DNA fragmentation corresponds to the level of DNA DSBs, (i.e. Comet Tail Moment) which is readily measured with imaging software. When similarly treated NPCs were analyzed by comet assay (OpenComet Figure S2), stressed NPCs showed significant heterogeneity with more DNA DSBs in stressed compared to controls (Figure 2C, D). Flow cytometry also confirmed a higher percentage of γH2AX positive cells in stressed versus control NPCs (Figure 2E) (unpaired t-test, $p<.01$). Likewise, immunostaining (Figure 2F) revealed that NPCs

exposed to aphidicolin had significantly more puncta per nucleus compared to DMSO controls (Figure 2G, KS test, p<.01).

Figure 1. Gating Strategy to Detect DNA Double-Strand Breaks in hiPSC-Neural Cells.

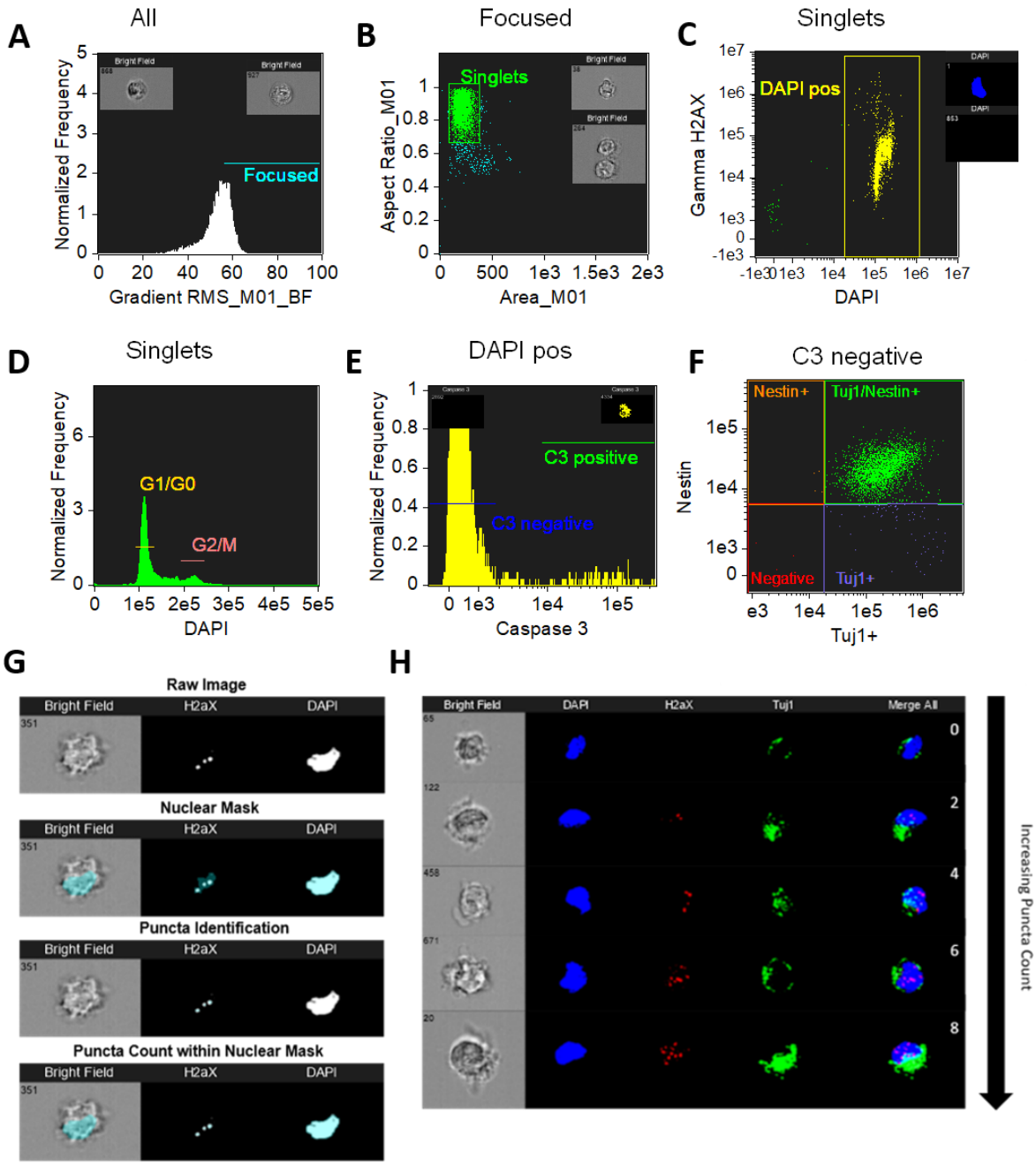

Figure 1. Gating Strategy to Detect DNA Double-Strand Breaks in hiPSC-Neural Cells. (A) Cells in focus were gated using IDEAS® 6.2 software. (B) Singlets were gated out of the focused cell population, examples of singlets within the gate (top small box) are compared to doublets outside of the gate (lower small box). (C) Singlets were separated into DAPI positive and negative populations to continue spot count analysis on DAPI positive cells. (D) A typical representation of singlets plotted on a histogram with DAPI is shown. (E) DAPI positive cells were further categorized into Caspase-3 (C3) negative and positive populations. Only C3 negative DAPI positive cells were used for further spot count analysis. (F) Cells were gated into subpopulations of Nestin, Tuj1 (β-Tubulin III), and Nestin/Tuj1 double positive cells. (G) Components of the Spot Mask include a nuclear mask based on DAPI staining, puncta identification in the channel containing γH2AX, and merging puncta counts within the nuclear mask that are within an optimal intensity. (H) The spot count mask has accurate γH2AX puncta counts and shows increasing puncta counts per nucleus.

Figure 2. Genomic Stress Induces DNA Double-Strand Breaks in hiPSC-neural cells.

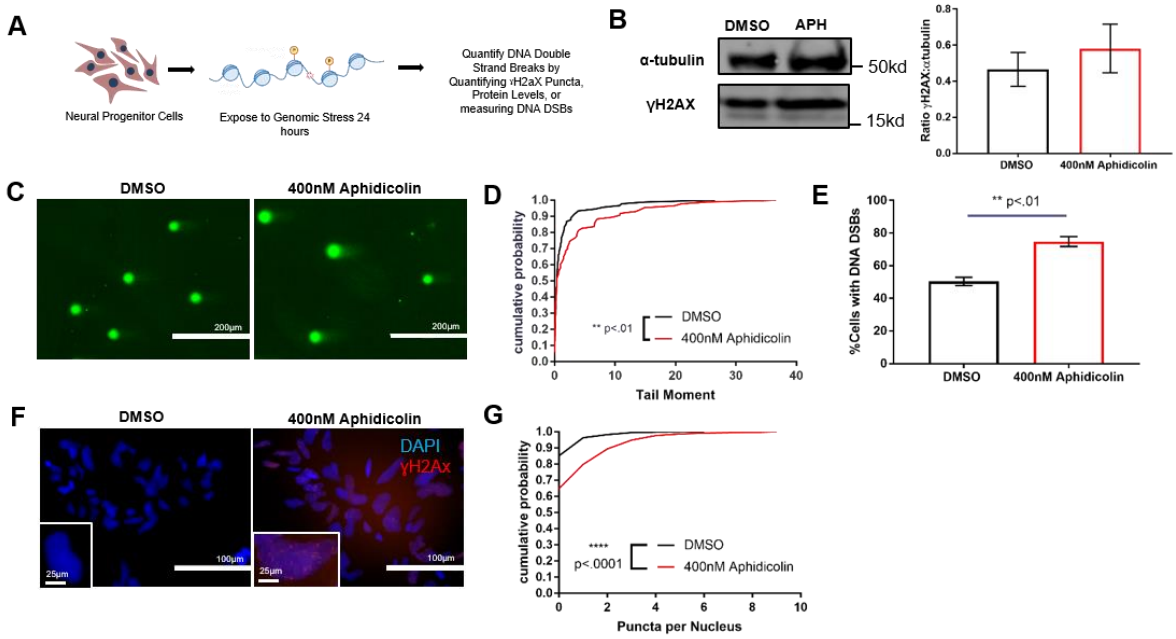

Figure 2. Genomic Stress Induces DNA Double-Strand Breaks in hiPSC-Neural Cells. (A) hiPSC-derived NPCs were treated with Aphidicolin or DMSO vehicle control for 24 hours and harvested for analysis by western blot, flow cytometry, comet assay, or immunocytochemistry. (B) In several independent immunoblotting experiments, NPCs exposed to mild replication stress show no difference in γH2AX protein levels. (C, D) The comet assay was employed to detect levels of DNA breaks and revealed that NPCs exposed to mild replication stress have an increase in the percent of NPCs with tail moments (tail length times %DNA in tail) indicating an increase in NPCs with DNA DSBs (KS test, $p<.01$). (E) Flow Cytometry data also revealed that NPCs exposed to stress for 24 hours have an increased percentage of cells that are positive for γH2AX (unpaired t-test $p<.01$). (F) Images of NPCs after 24-hour stress treatment, (G) a cumulative probability plot showing a significant percentage of NPCs have an increase in DNA DSBs per nucleus (KS test, $p<.001$).

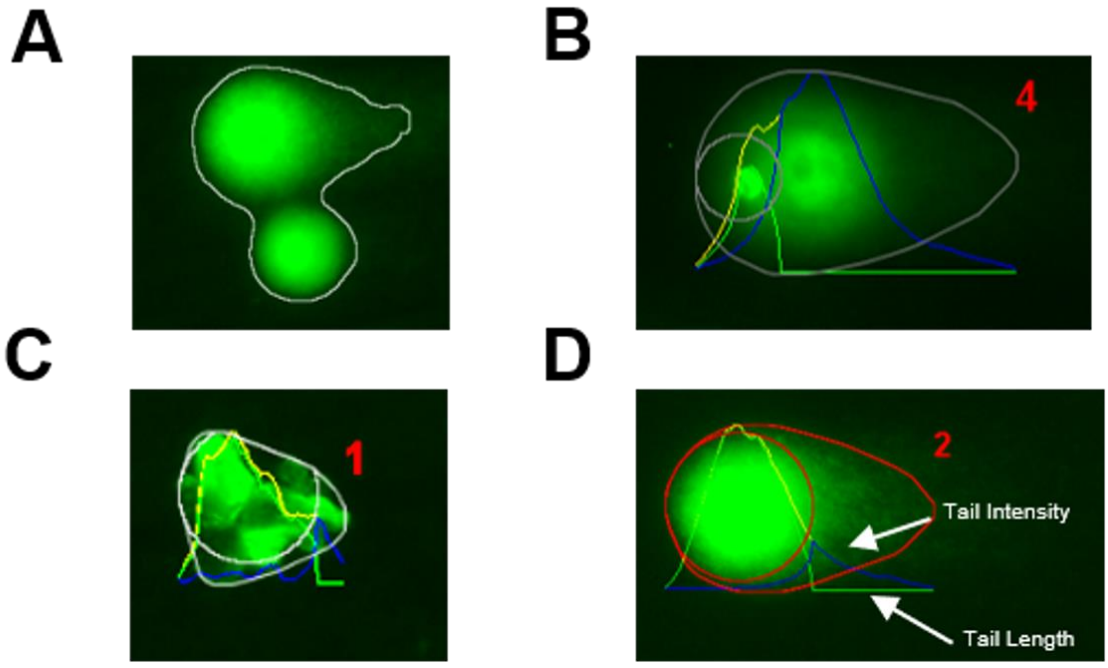

Supplementary Figure 2. Comet Assay Analysis. Representative images of the analysis from the OpenComet software. Gray outlined comets were automatically excluded from analysis because the software could not correctly distinguish cells that are too close in proximity (A). Once the automated software analysis was completed, images were manually reviewed to remove any miscalculated comets due to auto fluorescent particles or doublets (B, C). An accurate comet is shown, the red circle indicates the comet head and the red line outlines the entire comet (D). The blue line shows the intensity of the comet tail and the green line is the length of the tail. Tail moment is the intensity of the tail (which represents the %DNA) multiplied by the length of the tail.

Imaging Flow Cytometry to Quantify DNA DSBs

We sought a higher throughput and less labor-intensive approach to further explore neuronal genome dynamics. IFC permitted the quantification of DSBs along with other antigens and cell cycle measurements in thousands of NPCs and neurons. We found that active caspase-3 positive cells contained high levels of γH2AX staining and unquantifiable foci (Figure S3) and therefore, were excluded from subsequent analysis of non-apoptotic associated DNA DSBs. In the active caspase-3 negative population we observed a corresponding increase in the number of single cells with γH2AX foci and the number of γH2AX foci per nucleus with increasing concentrations of drug. NPCs treated with 40nM Aphidicolin have an average of 2.4 puncta per nucleus, a significant increase over DMSO controls (KS test, p<.0001). Elevated levels of aphidicolin led to a corresponding increase (100nM, 2.8 +/-3.3, KS test p<.05; 400nM, 3.6 +/-3.2, KS test p<.0001) in the number of puncta per cell (Figure S4A). Compared to controls (Figure S4B) NPCs treated with higher doses of aphidicolin demonstrated cell cycle arrest (Figure S4C-E).

S3. Caspase-3 Positive Cells Have Indistinguishable Spots

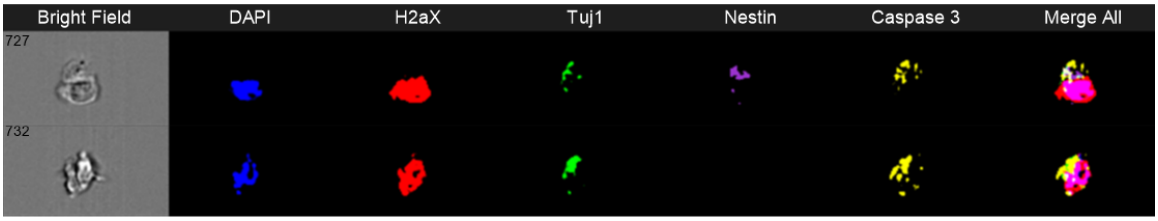

Supplementary Figure 3. Caspase-3 Positive Cells are Refractory to Accurate Puncta Counts. Caspase-3 positive cells have high levels of DNA damage and consequently too many puncta to be quantified accurately by the IDEAS® spot mask. Therefore, Caspase-3 positive cells were excluded from puncta analysis.

S4. Drug Titration of Aphidicolin

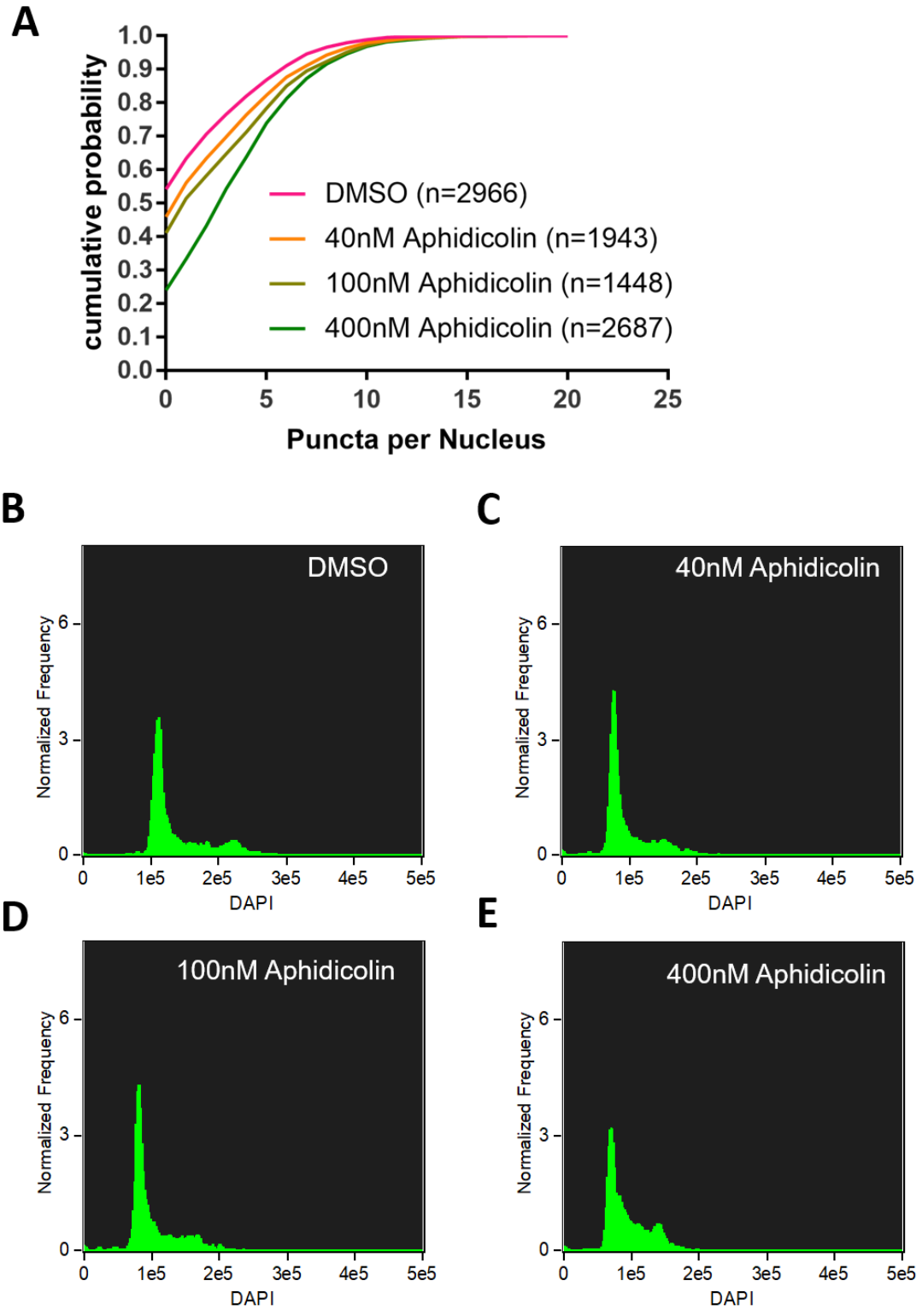

Supplementary Figure 4. Replication Stress Elevates DNA DSB Burden and Leads to Cell Cycle Arrest. (A) NPCs were treated with DMSO, 40nM, 100nM, or 400nM aphidicolin for 24 hours. A cumulative probability plot shows the distribution of single cells with puncta per nucleus. NPCs treated with 40nM aphidicolin have significantly more DNA DSBs than DMSO controls ($p<.0001$, KS test). Elevated levels of aphidicolin also led to a corresponding increase in DNA DSBs at 100nM aphidicolin ($p<.05$) and 400nM aphidicolin ($p<.0001$). (B-E) Cell cycle profile of the NPCs reveal that cells treated with 400nM aphidicolin show cell cycle arrest.

Assessing Population Dynamics with IFC

Proliferative NPCs can be induced to differentiate into neurons by removing mitogens and adding neurogenic factors to the culture media. After several weeks of differentiation this protocol typically results in ~80% β-tubulin III positive cells (Brennand *et al.*, 2011). We sought to employ IFC to evaluate population dynamics during the first two weeks of hiPSC-based neurogenesis using well established markers. Beta-Tubulin III expression is characteristic of post-mitotic neurons while Nestin is expressed by NPCs. Caspase-3 and γH2AX were also used to assess apoptosis and DNA DSBs during neurogenesis.

We analyzed neurogenesis in non-apoptotic cells. Spontaneous neuronal differentiation was observed at low levels (16.1% +/- 0.9) in NPC media. Neurons represented 27.05% +/- 12.05 by four days in neuron media and increased to 51.35% +/- 3.4 on day 7 and to 75.65% +/-3.4 on day 14 in neuron media. We observed a concomitant decrease in NPCs starting at 19.95% +/-0.05 in NPC media to 9.3% +/- 1.7 at four days in neuron media to 2.2% +/- 0.28 by day 7 and to 0.23% +/-.03 by day 14 in neuron media. In addition to Nestin positive and β-tubulin III positive cells, Nestin and β-tubulin III double positive cells as seen by others (Bardy *et al.*, 2016) were also observed at various timepoints. In NPC media there were 41.45% +/-4.85, then 55.1% +/-16 at 4 days in neuron media, then decreased to 33.85% +/-2.3 at 7 days, and down to 17.5% +/-3.3 by day 14.

It is likely that double positive cells represent a transitional population between NPCs and Neurons, as observed by others at a transcriptional level (Hoffman *et al.*, 2017). We evaluated evidence in our data that supported this notion. The double positive population peaked on day 4 and then diminished while the neuronal population expanded over this time (Figure 3A). Likewise, the G1/G0 cell cycle state of the double positive population increased steadily from 77.2% in NPC Media to > 90% after two weeks (Table 2). Furthermore, representative images of each cell type (Figure 3C) show that Nestin/ β-tubulin III double positive cells have lower mean β-tubulin III intensity compared to β-tubulin III positive cells (paired t-test, $p<.01$, Figure S5). In summary, β-tubulin III positive cells emerged (Neurons)

and Nestin (NPCs) and Nestin/ β-tubulin III positive cells diminished (Figure 3A) over time (two-way ANOVA, $p<.001$).

Although caspase-3 positive cells were the minority of cells at most timepoints, the majority of apoptotic cells were β-tubulin III positive (Figure 3B) across all of the timepoints (two-way ANOVA, $p<.0001$). All populations showed similar levels of DNA DSBs in NPC media (Figure 3D). After 4 days in neuronal differentiation media, remaining undifferentiated NPCs (Nestin positive) contained higher levels of DNA DSBs than differentiating neurons (KS test, $p<.0001$). All populations showed equal and very low levels of DNA DSBs after 7 days in neuronal differentiation media, but at 14 days in neuronal differentiation media DNA DSBs were present in a subset of all remaining cell populations (KS test, $p<.0001$, Figure 3D). At day 14, there was also an increase in the number of apoptotic cells (Figure 3B).

Figure 3. Imaging Cytometry Combines Quantifying DNA Double-Strand Breaks with Cell Fate Detection During Neurogenesis

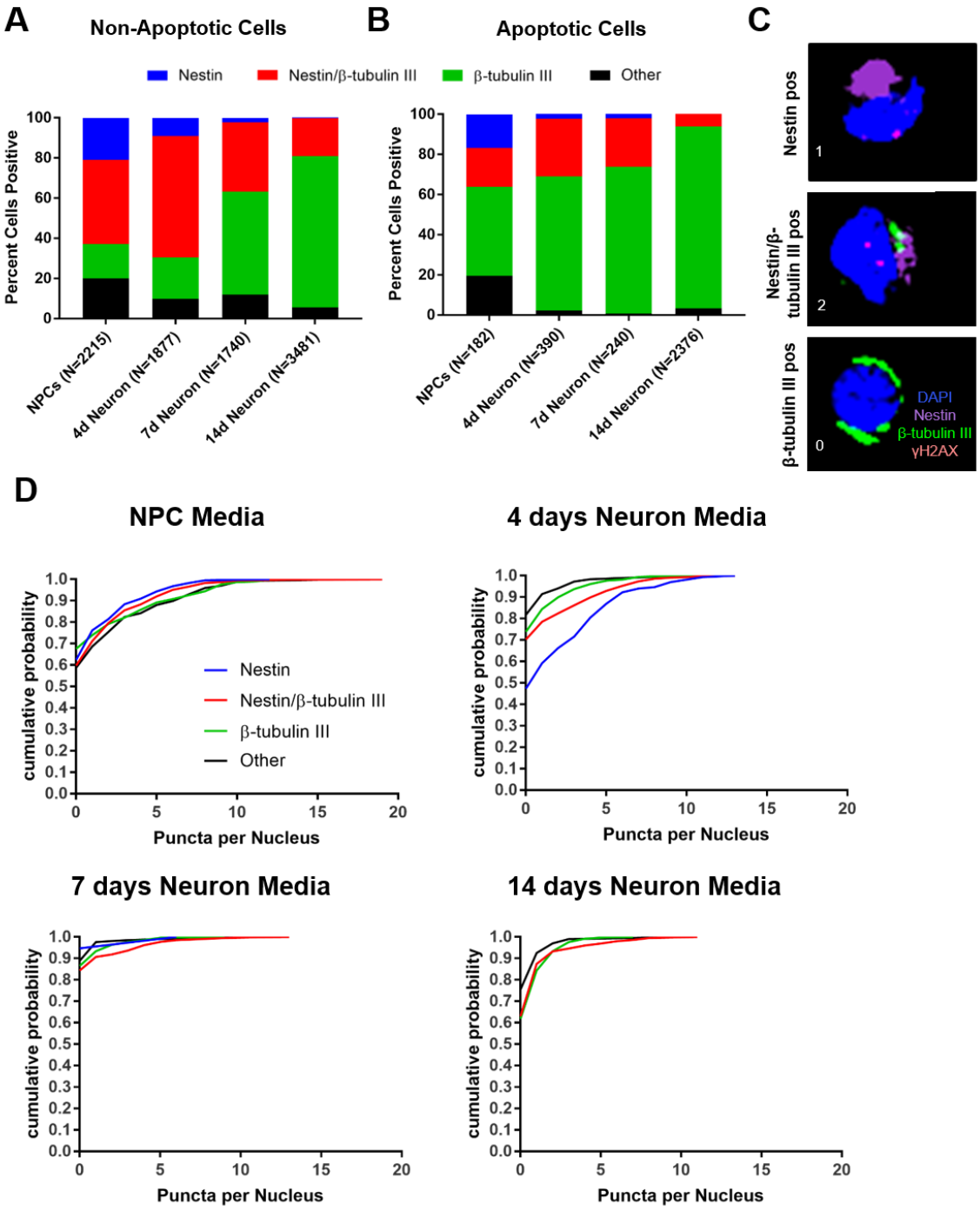

Figure 3. Imaging Cytometry Combines Quantifying DNA Double-Strand Breaks with Cell Fate Detection During Neurogenesis. hiPSC-derived NPCs were either collected in standard culture media and after 4, 7, or 14 days in neuronal differentiation media. (A) As NPCs undergo neuronal differentiation the number of non-apoptotic Nestin and Nestin/ β-Tubulin III positive cells decreased while the number of β-Tubulin III positive cells increased (two-way ANOVA, $p<.001$). (B) β-Tubulin III positive cells were the majority of Caspase-3 positive cells at every timepoint (two-way ANOVA, $p<.0001$). (C) Representative images of Nestin positive, Nestin/ β-Tubulin III positive cells, and β-Tubulin III positive cells with puncta counts are shown. (D) IFC reports heterogenous DNA DSB frequency in different populations of non-apoptotic cells over this two-week period.

Timepoint	% Cells G1/G0	% Cells S or G2/M
NPC Media	77.2	22.8
Day 4 Neuron Media	82.6	17.4
Day 7 Neuron Media	88.3	11.7
Day 14 Neuron Media	90.3	9.7

Table 2. Nestin/β-tubulin III Cell Cycle Dynamics During hiPSC-based Neurogenesis. Double positive cells show an increase in the percentage of cells in G1/G0 and a decrease in the percentage of cells at other stages of the cell cycle.

Actively Replicating NPCs Harbor More DNA DSBs During hiPSC-derived Neurogenesis

Non-apoptotic cells at each timepoint (see Figure 3D) were analyzed for DNA content using DAPI staining with IFC. Gates were created on G1/G0 and G2/M peaks (see Figure 1D) and analyzed as detailed previously (see Figure 1). In NPC media (Figure 4A) and at 4 days in neuron media (Figure 4B) the G2/M population have significantly more cells with breaks (KS test, $p<.0001$). At 7 days neither population has significant breaks (Figure 4C), but at 14 days G2/M cells have more DNA DSBs (KS test, $p<.05$) although they make up a smaller percentage of cells (2.03%) than earlier timepoints (Figure 4D).

Figure 4. Mitotically Active Cells Incur More DNA Double-Strand Breaks During Early Neurogenesis

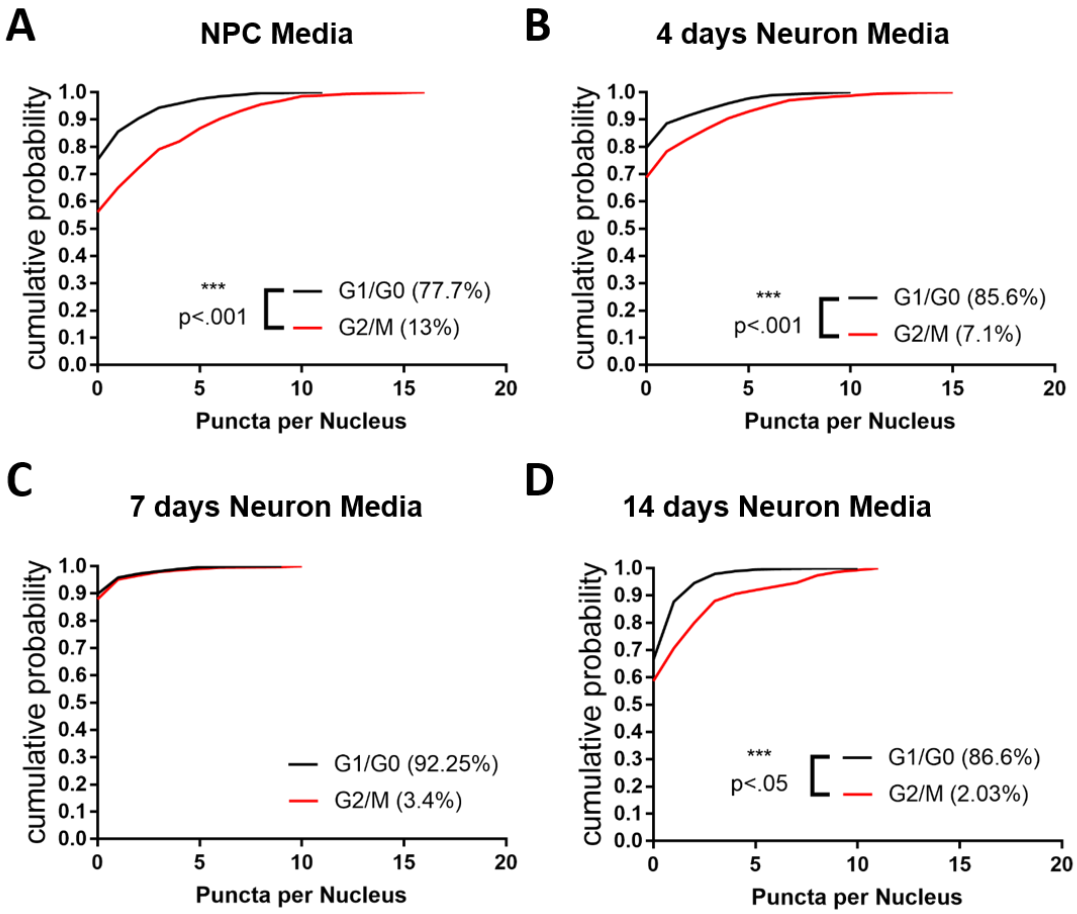

Figure 4. Mitotically Active Cells Incur More DNA DSBs During Early Neurogenesis. (A-D) Cells were collected as in Figure 3. Caspase-3 negative G1/G0 and G2/M populations were determined based on DAPI fluorescence intensity (see Figure 1D). The G2/M population was most abundant under NPC conditions (A). When γH2AX puncta were prevalent in the population (see Figure 3D), these were observed most frequently (KS test p<.001 in NPC Media and 4 days in Neuron Media, p<.05 at 14 days in Neuron Media) in the G2/M population (A, B, D).

Discussion

Neural cells are heterogenous and bulk studies are unable to discern diversity generated during neurogenesis (Harbom *et al.*, 2018). In this study we demonstrate that IFC can measure neural genome dynamics with better resolution and higher throughput than other methods. We showed that replication stress induces DNA DSBs in a subpopulation of hiPSC-derived NPCs, but this difference was not detectable by bulk Western Blot (Figure 2B). Subsequent single cell studies both dependent (Figure 2E, F, G) and independent (Figure 2C, D) of γH2AX show that subpopulations of NPCs respond to mild genomic stress with an increase in DNA DSBs similar to what is observed in mouse neural progenitor cells (Wei *et al.*, 2016). IFC produced the same results in addition to anticipated changes in expression of neuronal and progenitor cell markers during neurogenesis (C. Liu, Zhong, Apostolou, & Fang, 2013; Zhang & Jiao, 2015). The novel component of our approach stems from examining which neural subpopulations and cell cycle phases have the highest DSB burden during neurogenesis. We observed that replicating cells contain more DNA DSBs as NPCs and during the fourth day in neuron media (Figure 4A, B), this suggests that the DSBs are predominately from replicative stress. Interestingly the level of breaks decreases on the seventh day in neuron media and rises again one week later (Figure 4C, D) when the cells are predominately β-tubulin III positive and in G1/G0. DNA DSBs in this cell population could likely arise from transcriptional stress which has been observed to cause DNA DSBs in early neurons (Madabhushi *et al.*, 2015). Although the percentage of cells with DNA DSBs is higher in proliferating cells (Figure 3, 4), the majority of apoptotic cells were Neurons (β-tubulin III positive) (Figure 3B). In addition, the number of Caspase-3 positive cells were highest at two weeks of differentiation when the cells are predominately neurons and only 2% of the cells are mitotically active (Figure 4D). These results indicate that the source of DNA DSBs may be different in neural sub-populations; this finding requires further future study.

While we cannot track the fate of any single cell our study also revealed Nestin and β-tubulin III double positive cells, which have been seen in other single cell studies (Bardy *et al.*, 2016; K. Brennand *et al.*, 2015). Multiparameter snapshots of population dynamics changing over time can be used to infer molecular changes in this process as demonstrated in mass cytometry (Zunder *et al.*, 2015). Here we show that IFC can produce multiparametric data on a scale and through-put that is comparable to mass cytometry, albeit with fewer antigens. Despite this limitation, IFC provides additional information such as subcellular localization, quantification of puncta, and DNA content-based cell cycle profiling. We employed these tools to support the idea that β-tubulin III/Nestin positive cells are a transitional cell population during hiPSC-based neurogenesis (Figure S5, Table 2).

IFC provides high-throughput and high-resolution single-cell information efficiently (Table 3). In this study we simultaneously acquired data for four antigens (Nestin, β-tubulin III, Caspase-3, and γH2AX) and cell cycle data (DAPI). While flow cytometry could provide some of these measurements, it would not be able to quantify γH2AX foci. Puncta counting is also possible with immunocytochemistry (Figure S6); however, it would require additional markers and assay design (BrdU incorporation) to reveal cell cycle. With respect to time, IFC yields more cells in a shorter time frame compared to conventional microscopy; and consequently, more samples can be analyzed (Table 3).

In this study EDF was used during the acquisition of cells with IFC. Since EDF collapses the image over a wide focal range within the cell (16μm), any spot or point within the same Z position will overlap during image processing of the focal length into a single plane of focus (Ortyn *et al.*, 2007). Samples with more puncta likely have several stacked foci which are consolidated to one plane with EDF. Therefore, it is likely that the differences in populations with high number of puncta are underestimated. In the case of looking at DNA DSBs in non-apoptotic cells, where the number of puncta is expected to be lower, the use of EDF ensured that when there were low number of puncta the spot would not be missed due to being out of the plane of focus.

We have demonstrated how IFC can reveal multiparametric information about cell state and fate during hiPSC-based neurogenesis. This technique could be readily applied to hiPSC-derived patient cell lines, such as cell cycle re-entry phenotypes in Alzheimer's diseases (Seward *et al.*, 2013). γH2AX is a common marker for cell toxicity assays (Geric, Gajski, & Garaj-Vrhovac, 2014), thus our IFC approach could easily be used to test the genotoxicity of various environmental mutagens. Similarly, the measurements we are obtaining can be used to better understand the cause and consequence of somatic mutations that occur during human neurogenesis (McConnell *et al.*, 2017). IFC is a high-throughput method that allows the simultaneous study of cell morphology, cell cycle, and protein quantification and localization. Combined with hiPSC technology, IFC provides a novel tool to research human brain development, aging, and DNA damage dynamics in the study of neuropsychiatric and neurodegenerative disease during human neurogenesis.

S5. β-tubulin III Fluorescence Intensity is Lower in Double Positive Cells

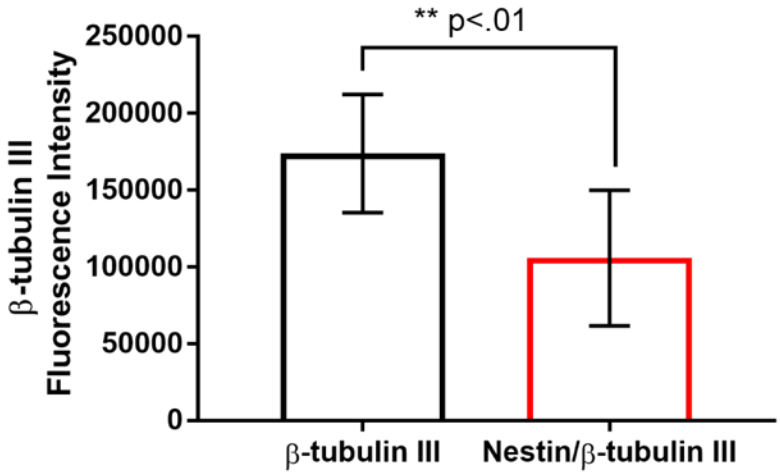

Supplementary Figure 5. Nestin/β-tubulin III Positive Cells Have Lower Fluorescence Intensity than β-tubulin III Positive Cells. The mean fluorescence intensity was measured using the intensity feature in IDEAS® 6.2 to quantify intensity values for single-cells gated as β-tubulin III or Nestin/β-tubulin III positive. β-tubulin III positive cells had significantly higher fluorescence intensity than Nestin/β-tubulin III positive cells (paired t-test, p<.01).

S6. Immunocytochemistry of DNA DSBs During Neurogenesis

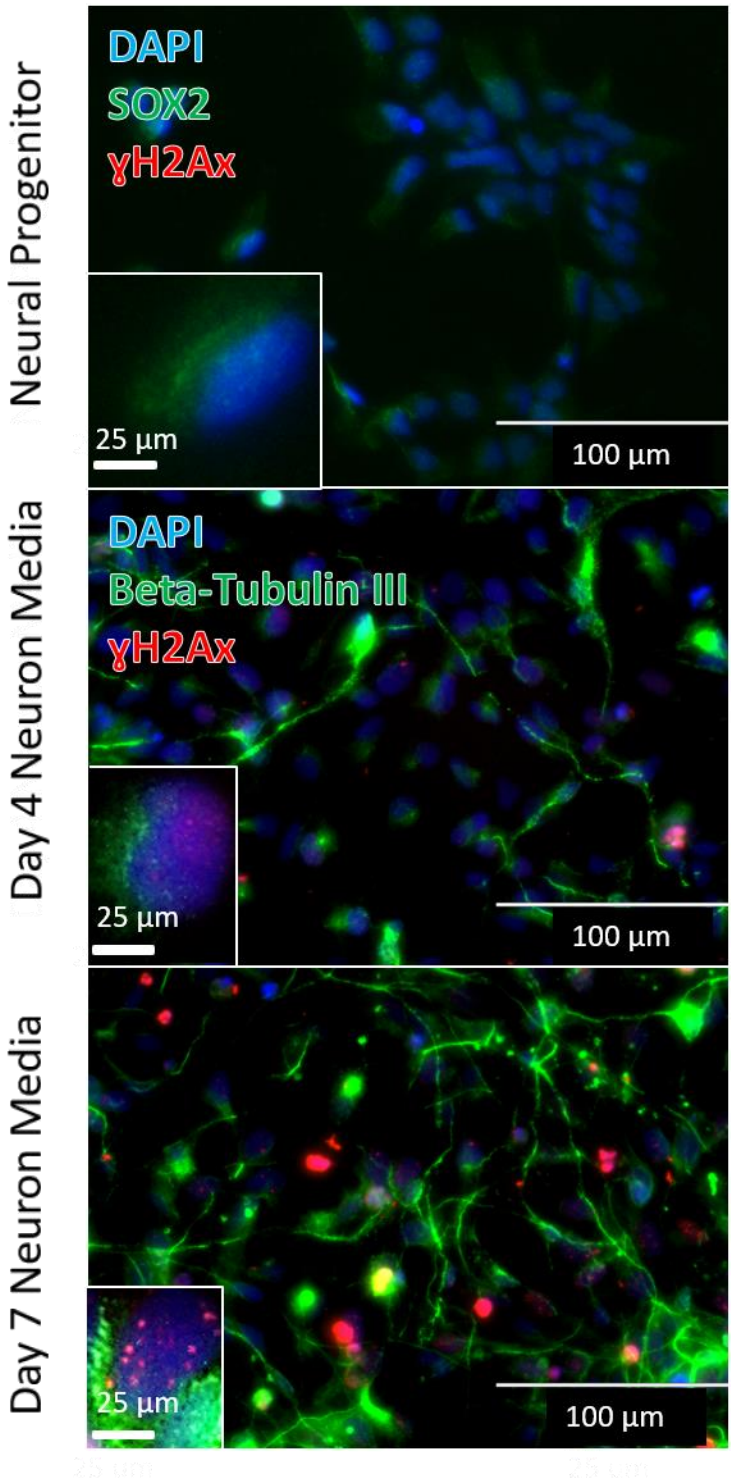

Supplementary Figure 6. Immunocytochemistry of DNA DSBs During Neurogenesis. NPCs were fixed after several days in NPC Media, four days in Neuron Media, and seven days in Neuron Media. Neural cells were stained for DAPI, SOX2 (NPC), β-Tubulin III (Neuron), and γH2AX. Scale bars are 25 microns.

Technique	Number of Markers	Number of Samples Acquired per Hour	Resolution		Fluorescence Localization	Cell Cycle
			Biological	Imaging		
Flow Cytometry	>15	18	Single-cell	n/a	No	Yes
Fluorescence Microscopy	4	4	Single-cell	10x*	Yes	Yes**
Western Blot	1	1	Bulk	n/a	No	No
Imaging Flow Cytometry	10	8	Single-cell	60x	Yes	Yes

Table 3. Throughput and Resolution of Approaches. IFC provides sub-cellular resolution similar to fluorescence microscopy but with the high throughput of flow cytometry. Representative comparisons of time, specificity, resolution, and multiparameter capabilities are shown. *A 10x field of view is required to reasonably obtain sufficient N. **An additional marker, such as BrdU is required for this analysis.

Material and Methods

Cell Culture

9429 Human Fibroblasts (Coriel Cell Repository) were reprogrammed to induced pluripotent stem cells and induced to neural progenitor cells in house according to the methods outlined by Brennand and colleagues (Brennand *et al.*, 2011). 5535 NPCs were obtained from the Brennand laboratory (Flaherty *et al.*, 2017). hiPSC-derived NPCs were plated on Matrigel (Fisher) or Poly-Ornithine (Sigma)/ Laminin (Invitrogen) and passaged 1:6 every four days. NPCs were cultured in NPC medium (DMEM/F12 +Glutamax (Invitrogen), 1x N2 (Invitrogen), 1X B27-Vitamin A (Invitrogen), 1ug/ml Laminin (Invitrogen), 20ng/ml FGF-2 (Peprotech) and dissociated in Accutase (Fisher) for 5 min at 37°C. hiPSC-derived neurons were cultured on Matrigel in Neuron Medium (DMEM/F12 +Glutamax, 1x N2, 1X B27 with Vitamin A (Invitrogen), 20ng/ml BDNF (Shenandoah Biotechnology), 20ng/ml GDNF (Shenandoah Biotechnology), 1mM dibutryl-cyclic AMP (Sigma), and 200nM ascorbic acid (Stem Cell Technologies) for all experiments.

Aphidicolin Treatment

9429 NPCs were exposed to 40nM, 100nM, or 400nM Aphidicolin (Sigma) for 24 hours. DMSO was used as a vehicle control. After drug treatment the cells were collected for lysis for immunoblotting, fixation for immunocytochemistry, or fixation for flow cytometry and Image Stream analysis.

Immunocytochemistry

5535 NPCs were cultured for 24 hours with Aphidicolin or DMSO vehicle control and rinsed with PBS. NPCs at ~80% confluency were fixed on 18mm glass coverslips with 4% PFA for 15 minutes at room temperature and rinsed (3 times for 5-minute washes) in PBS. Cells were permeabilized with .5% Triton-X 100 for 20 minutes and incubated in blocking buffer (3% BSA in PBS-T (.1% Triton-X 100)) for one hour at room temperature. The cells were probed overnight with anti-phosphorylated H2AX, DAPI, Nestin, and Cleaved Caspase-3 followed by labeling

with secondary staining and incubated for one hour at room temperature (see Table 1 for reagents).

Detection of H2AX Foci

NPCs were imaged on a fluorescent EVOS Microscope at 10x magnification. RGB images were analyzed through a Cell Profiler (Broad Institute) pipeline that takes the original RGB image, isolates the channels, identifies the nuclei, enhances the foci, identifies the foci, and counts the number of foci per nucleus (Figure S1). The generated counts per nucleus were compared to counts made by blinded technicians and each step of the pipeline was optimized.

Reagent	Clone	Catalogue	Fluorophore	Vendor	Target	Application
Rabbit Anti-Active Caspase-3	C92-605	550821	PE	BD Pharmingen	Cleaved Caspase-3	Flow
Mouse Anti-Beta Tubulin, Class III	Tuj1	560338	Alexa Fluor 488	BD Pharmingen	Neuron specific tubulin	Flow
Mouse anti-Nestin	25/Nestin	561231	PerCP-Cy 5.5	BD Pharmingen	NPC specific neurofilaments	Flow
Mouse anti-H2AX(pS139)	N1-431	560447	Alexa Fluor 647	BD Pharmingen	Phosphorylated Histone H2AX	Flow
DAPI		62248	DAPI	Thermo Fisher Scientific	A-T regions in DNA	Flow, Immunostaining
Rabbit Anti-Nestin	Polyclonal	ab92391		Abcam	NPC specific neurofilaments	Immunostaining
Mouse Anti-H2AX (pS139)	JBW301	05-636		Millipore Sigma	Phosphorylated Histone H2AX	Immunostaining, Western Blot
Goat anti-Mouse IgG (H+L)		A-21424	Alexa Fluor 555	Thermo Fisher Scientific		Immunostaining
Donkey anti-Mouse IgG (H+L)		P/N 925-68072	IRDye®680RD	Li-Cor		Western Blot
Donkey anti-Rabbit IgG (H+L)		A-21206	Alexa Fluor 488	Thermo Fisher Scientific		Immunostaining
Mouse Anti-SOX 2	9-9-3	ab79351		Abcam	SOX2, neural stem cell factor	Immunostaining
Rabbit Anti-Beta III Tubulin	Polyclonal	ab18207		Abcam	Neuron specific tubulin	Immunostaining
Mouse Anti-Tubulin alpha Ab-2	DM1A	MS581PABX		Thermo Scientific	Microtubules	Western Blot

Table 1. Table of Reagents used for Flow Cytometry, Imaging Flow Cytometry, and Western Blot.

S1. Cell Profiler Workflow

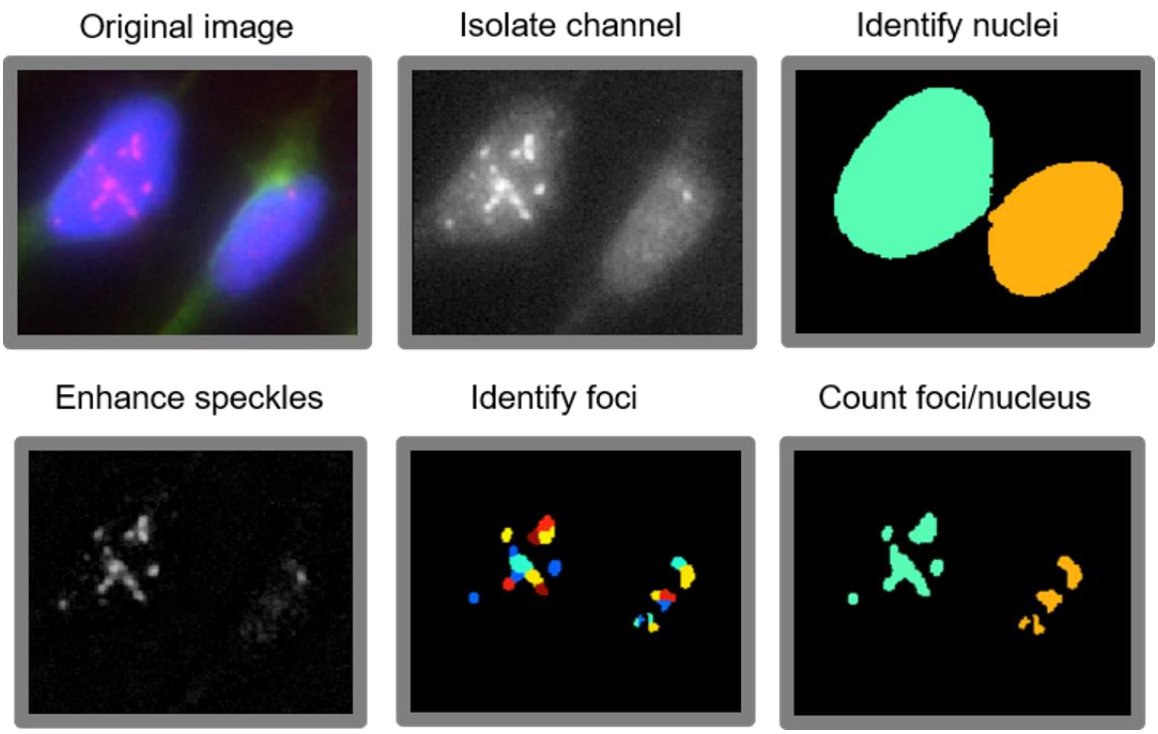

Supplementary Figure 1. Cell Profiler Workflow. Original RGB images of treated and control NPCs were taken and analyzed using the pipeline above. RGB images were isolated into red, green, and blue channels. The blue channel was used to identify nuclei (DAPI) and the red channel was used to identify and enhance foci. A nuclear mask was added to the pipeline analysis so that only foci within the nucleus were counted and the number of foci per nucleus could be generated.

Cumulative Probability Plots

Cumulative probability plots were generated by exporting single cell counts of γH2AX from Cell Profiler (for immunocytochemistry) and IDEAS® 6.2 (for IFC) to PRISM Graphpad Software. The cells were ranked based on the total number of γH2AX puncta and plotted as a function of the frequency of the population of cells with a given number of foci. To determine statistical significance the Kolmogorov-Smirnov test was used.

Bar Graphs

Stacked bar graphs were created by adding the total number of each cell type at each timepoint over several IFC experiments. The percentages were obtained by dividing the total number of cells positive for each sub type by the total number of cells at the corresponding timepoint obtained using IDEAS® 6.2. All bar graphs were generated using PRISM Graphpad software.

Comet Assay

The Comet Assay was performed using the protocol outlined from the Neutral Comet Assay Reagent Kit (Trevigen). NPCs were harvested after 24-hour exposure to Aphidicolin, combined with molten LMAgarose at a ratio of 1:10 (v/v), and added to CometSlides™. The slides were immersed in Lysis Solution (Trevigen) overnight and transferred to Neutral Electrophoresis Buffer for 30 minutes. Slides were then placed in an electrophoresis chamber at 21 volts for 45 minutes at 4°C and then submerged into DNA Precipitate Solution for 30 minutes at room temperature. After being immersed in 70% ethanol for 30 minutes at room temperature, the samples were dried at 37°C, and SYBR Green (Life Technologies) was added to the slides before they were dried and imaged on an EVOS Microscope (Thermo Fisher). All buffers and solutions for the Comet Assay were made according to protocols outlined in the Comet Assay Kit (Trevigen). Images were taken at 20x and analyzed using OpenComet software (Figure S2). OpenComet software generates measurements and images that can be reviewed; allowing for the removal of miscalculated comets. Examples of excluded comets

(Figure S2A-C) and good comets (Figure S2D) are included in supplementary figures. The red circle indicates the comet head and the red line outlines the entire comet (Figure S2D). The blue line shows the intensity of the comet tail and the green line is the length of the tail. Tail moment (tail length times %DNA in tail) was used to detect levels of DNA DSBs.

Western Blots

NPCs were cultured for 24 hours with Aphidicolin or DMSO vehicle control before being lysed with 2x Laemmli buffer (4% SDS, 10% 2-mercaptoethanol, 20% glycerol, .004% bromophenol blue, 0.125M Tris HCl, pH 6.8) and boiled for 10 minutes at 95°C. For immunoblotting, total cell lysate was resolved by 4-15% Mini-PROTEAN precast gradient gel (Biorad). Proteins were transferred to a PVDF membrane for 90 minutes at 100V and incubated at room temperature for 1 hour in blocking buffer (3% Bovine Serum Albumin (Thermo Fisher) in TBS-T (Tris-buffered Saline .1% Tween-20)). The blots were incubated at 4°C overnight in blocking buffer with anti-phosphorylated H2AX and anti-alpha tubulin. Alexa Fluor 800 (mouse) Secondary antibodies were used and the blots were visualized on a Licor Odyssey Imaging System. (see Table 1 for reagents)

Cell Fixation and Antibody Staining for Cytometry

Neural cells were exposed to various doses of Aphidicolin or DMSO for 24 hours depending on the specific experiment. For all cells the following protocol was used to prepare cells for imaging flow cytometry: Cell culture media was removed from the cells and 1 mL of Accutase was added per well of 6 well plate. The cells were incubated at 37°C for 5 minutes and collected for centrifugation after 2mL of basal media (DMEM/F12 +Glutamax) was added to each well. The cells were spun down at 300xg for 5 minutes and all of the media was removed from the cells. 500µL of 2% PFA in PBS was added to the cells and they were resuspended and filtered through a 40µM strainer into an eppendorf tube containing 500 µL of 2% PFA in PBS. The cells incubated at room temperature for 15 minutes. Cells were then spun down at 600xg for 5 minutes and the PFA was removed from the cells.

1 mL of 1%BSA/PBS-Triton 100 (.1%) was added to each tube and the cells were resuspended and counted using a countess slide (Thermo Fisher). Each sample was aliquoted into samples containing $1x10^6$ cells, spun down at 600xg for 5 minutes and resuspended in 100µL of 1%BSA/PBS-T containing the following directly conjugated antibodies: 5µL of Nestin and Tuj1, 10µL Active Caspase-3, 1.75µL of Gamma H2AX (see Table 1 for reagents). Single stain controls were also added to cells and incubated at room temperature for 30 minutes in the dark. Samples and controls were centrifuged at 600xg for 5 minutes and reconstituted in 35µL of DAPI staining solution (1%BSA PBS-T with DAPI 1µg/mL) was added to each sample and to the DAPI single stain control. Samples were stored at 4°C in the dark until they were run through the imaging flow cytometer or a Cytek modified FACSCalibur™ cytometer. Samples used for flow cytometry had 500uL of DAPI staining solution.

Flow Cytometry

Flow cytometry was conducted on a Cytek modified FACSCalibur™ using the 488 Blue, 637 Red, and 407 Violet lasers to excite Active Caspase-3 (PE), emission collected with a 580/20 filter, γH2AX (AlexaFluor 647) with a 661/16 filter, and DAPI with a 450/50 filter respectively. 10,000 cells were collected per sample at low pressure. Single stain controls were used for compensation and gating was determined through unstained and Fluorescence Minus One controls (FMOs)(Roederer, 2002), which are experimental cells stained with all the fluorophores minus the one fluorophore for which positive and negative cutoffs are determined. Gating and analysis were performed using FCS Express 6 (DeNovo Software).

Imaging Flow Cytometry

Imaging flow cytometry (IFC) was performed using the Imagestream Mark II System (Amnis Inc/Luminex Corp.). This technology allows the image capture of cells going through the cytometer using six optical channels per camera. Using INSPIRE® software, cells were collected for 10 minutes or until 10,000 cells were

acquired. Following excitation with the 405nM laser at a power of 50mW, the 488nM laser at a power of 200mW, the 561nM laser at a power of 100mW, and the 642nM laser at a power of 150mW, all cells were captured with 60x magnification (Numerical Aperture 0.9) using the enhanced depth field optic (EDF) at low speed (60mm per second) with an average rate of ~10 cell images per second. EDF keeps the entire cell in focus across 16 µm (instead of a single plane)(Ortyn *et al.*, 2007) and through IDEAS® software deconvolution produces an image similar to a collapsed confocal image stack.

Emitted light was collected using the following filters: Channel 1 (Camera 1 420-480nm) and 9 (Camera 2 570-595nm) for brightfield (BF), channel 2 (Camera 1 480-560nm) for Alexa Fluor 488, channel 3 (Camera 1 560-595nm) for phycoerythrin (PE), channel 5 (Camera 1 660-740nm) for PerCP Cy5.5, channel 7 (Camera 2 420-505nm) for DAPI, and channel 11 (Camera 2 660-740nm) for AlexaFluor 647. All data were analyzed using IDEAS® software (version 6.2) and FCSExpress Plus 6.0.

Image Compensation

Image compensation was conducted on samples that were exposed to aphidicolin for at least 24 hours prior to being stained because they had the brightest γH2aX foci. Cells stained with only DAPI, Tuj1-Alexa Fluor 488, H2AX-Alexa Fluor 647, Nestin-PerCP Cy5.5, and Active Caspase 3-PE were collected without BF illumination or Scatter and IDEAS® 6.2 was used to generate the compensation matrix. The compensation wizard detects light from each cell image and places it into the appropriate channel. IDEAS® generates a table of coefficients with normalized values from 0 to 1 which represent the spectral overlap of fluorochromes into juxtaposed channels. New calculated compensation matrices from temporally matched single stain controls were applied to the images from all data sets to generate compensated image (.cif) files for subsequent analysis.

Analysis of Cell Images and Calculation of Foci Number

Cells treated with aphidicolin (400nM for 24 hours) were analyzed first to determine a masking strategy and calculate foci number since they had the brightest and highest number of foci. The optimal fluorescence display for fluorescence imagery was determined by adjusting the image gallery properties in a linear fashion and applied to all images. To analyze the cells several steps and gating strategies were employed based on IDEAS® 6.2 software and incorporated wizards. The first step identified cells that are in focus using a histogram of the Gradient RMS of CH01 Bright Field. Using select bins within the histogram an image gallery displays the cells within the selected bin. Gating was determined based on finding a bin where most cells are in focus (Figure 1A). The focused cells were then gated using a plot of Area (BF1) vs. Aspect Ratio (BF1) to determine singlets (low area and high aspect ratio). An accurate gating of singlets was confirmed by selecting various data points within the gate and validating that they are indeed single cells (Figure 1B). Single cells were used to gate for DAPI positive staining (Figure 1C). Only DAPI positive cells were of interest because γH2AX should only be present in the nucleus. A histogram of DAPI intensity was also used for cell cycle information for each cell sample (Figure 1D). DAPI positive cells were separated into Caspase-3 negative and Caspase-3 positive subpopulations. Caspase-3 positive cells, likely to be apoptotic cells, tend to have very high number of foci (Figure S3) which make them difficult to quantify and distinguish; frequently leading to inaccurate spot counts. Furthermore, DNA DSBs in non-apoptotic cells were of interest for this study, therefore caspase-3 positive cells were excluded from further analysis (Figure 1E). Finally, the caspase-3 negative cells were separated into four subpopulations, Nestin positive, β-tubulin III positive, Nestin/ β-tubulin III double positives, and other (negative). Nestin is a neurofilament present in neural progenitor cells and indicates that an NPC is proliferative and has not exited the cell cycle to begin neuronal differentiation (Park *et al.*, 2010) . β-tubulin III is a microtubule predominately found in mature neurons (Caccamo *et al.*, 1989). The cells in the negative quadrant were categorized as “Other” because they are DAPI positive cells that were negative for the markers used in this particular study. The

gates were created using the polygon gating tool and determined based on FMOs (Figure 1F).

Masking Strategy

To determine the number of γH2AX foci within the nucleus several sequential masks were created using the masking tools in IDEAS® 6.2 software (Figure 1G). A nuclear morphology mask based on the DAPI Channel was used to identify the nucleus of the cell. An additional step including dilation of the DAPI mask was added to optimize the accuracy of the morphology mask. After the morphology mask was established, a spot mask was created from the γH2AX foci using Ch11 (Alexa Fluor 647). An optimal spot-to-background ratio was established with the addition of an intensity mask to remove background fluorescence. The final spot mask provided optimal quantification of γH2AX foci: Intensity (Spot (Dilate (Morphology (M07, DAPI),1), H2AX, Bright, 6, 3, 0), H2AX, 258-4095) and show appropriate counts with increasing foci (Figure 1H). Using export features, the foci count for different cell populations were exported to PRISM software where they could be plotted into various graphs and analyzed statistically. Once all of these parameters were optimized a template file was created and saved and the rest of the samples run on the same day were analyzed through batch analysis using the same analysis template.

Quality Control Testing

The ASSIST calibration and testing software was run daily before each acquisition run. Daily QC for the FACSCalibur™ included the running of calibration standards to assess instrument sensitivity, linearity, and alignment.

Chapter III

p53 Mediates Transcription Associated DNA DSBs During hiPSC-based Neurogenesis

Abstract

Neurons are overproduced during cerebral cortical development. Neural progenitor cells (NPCs) divide rapidly and incur frequent DNA double-strand breaks (DNA DSBs) during neurogenesis. Although half of the neurons born during neurodevelopment die, many neurons with inaccurate DNA repair survive leading to brain somatic mosaicism. Currently it is unknown how these neurons escape DNA damage response-mediated cell death during neurodevelopment. In this study we examine the role of p53 in DNA DSB-induced NPC death during human induced pluripotent stem cell-based neurogenesis. We observe that p53 knockdown ($p53^{KD}$) leads to a 3-fold increase in neuronal survival after 6 weeks of differentiation due to continued proliferation in the absence of p53 during the first week of differentiation. Furthermore, DNA DSBs incurred from transcriptional stress lead to p53 activation and consequent cell death in NPCs. In $p53^{KD}$ NPCs, DNA DSBs accumulate in highly transcribed genes that are associated with neurological disorders.

Introduction

Evolution has devoted significant cellular resources to genome maintenance and the prevention of somatic mutations. Numerous DNA repair pathways employ distinct biochemical means to counteract a myriad of DNA lesions brought about by ongoing replication, transcription, and metabolism (Shrivastav, De Haro, & Nickoloff, 2008). DNA damage signaling pathways promote DNA repair by engaging cell cycle checkpoints that stall cell cycle progression until repair is complete (Dasika *et al.*, 1999). When DNA repair fails, persistent DNA damage signaling initiates cell death (Roos & Kaina, 2006). Following from this basic mechanistic model, DNA repair mechanisms have been thought of as cellular caretakers. DNA damage signaling mechanisms, in turn, play the role of cellular gatekeepers protecting an individual from potentially tumorigenic somatic mutations. The tumor suppressor protein p53 is a prototypical gatekeeper, sometimes referred to as “the guardian of the genome” (Levine, 1997; Levine & Oren, 2009).

Human development requires hundreds of billions of cell divisions to reach and maintain a steady-state level of ~10^{15} cells in an adult. Human brain development is additionally constrained by limited regeneration (Bhardwaj *et al.*, 2006; Rakic, 2006).The human cerebral cortex is comprised of 15 - 20 billion neurons that are among the longest-lived and most diverse mammalian cells. These arise from a discrete neural progenitor cell (NPC) pool in the ventricular zone of the developing cerebral cortex (Lui *et al.*, 2011). NPCs overproduce neurons by ~2-fold, thus requiring at least 40 billion NPC divisions during a few months of development (Blaschke *et al.*, 1996; Thomaidou, Mione, Cavanagh, & Parnavelas, 1997; F. K. Wong & Marin, 2019). This presents an enormous burden for genome maintenance, notably in the NPC response to DNA double strand breaks (DNA DSBs) (Abyzov *et al.*, 2017). The abundance of somatic mutations (D'Gama & Walsh, 2018; M. A. Lodato *et al.*, 2018; McConnell *et al.*, 2017; Paquola, Erwin, & Gage, 2017) in human brains prompts the question, why doesn’t p53 delete mutant neurons?

DNA DSBs are potent somatic mutagens. Mouse mutants that lack nonhomologous end-joining (NHEJ) DNA DSB repair proteins exhibit extensive NPC death that precludes neurodevelopment and perinatal survival (Chun & Schatz, 1999; Ferguson, Sekiguchi, Chang, *et al.*, 2000; Ferguson, Sekiguchi, Frank, *et al.*, 2000; Gu *et al.*, 2000). However, NHEJ-deficient mice survive in a p53-deficient background, albeit with an increased occurrence of medulloblastoma (Yan *et al.*, 2006). Together with previous work, neurodevelopmental DNA DSBs in NHEJ / p53 deficient mice implicate genomic stress at long, neuron-expressed genes in autism and schizophrenia (King *et al.*, 2013; Schwer *et al.*, 2016; Wei *et al.*, 2016). Neurodevelopmental origins for schizophrenia and autism are supported by several lines of evidence (K. Brennand *et al.*, 2015; Brennand *et al.*, 2011; Marchetto *et al.*, 2017). In addition to increased NPC proliferation, p53 has been identified as a risk allele for schizophrenia (Ni *et al.*, 2005).

We sought to investigate the relationship between DNA DSB prevalence and p53 activity in human brain development using induced pluripotent stem cell (hiPSC)-based neurogenesis. NPC lines that expressed an shRNA targeting *p53* ($p53^{KD}$) produced 3-fold more neurons after 6 weeks of differentiation. Treatment with the indirect p53 agonist Nutlin (Arva *et al.*, 2008; Shangary & Wang, 2009; Vassilev *et al.*, 2004) was lethal to control NPCs, but restored $p53^{KD}$ NPCs to control levels in multiple assays. Further investigation with single cell imaging flow cytometry (IFC)(Michel, Majumdar, Lannigan, & McConnell, 2019a) and genome-wide DNA DSB capture (Lensing *et al.*, 2016) approaches find that $p53^{KD}$ leads to an elevated but not lethal DNA DSB burden. Despite some level of additional proliferation in $p53^{KD}$ neurogenesis, additional DNA DSBs in $p53^{KD}$ NPCs are associated with transcriptional rather than replicative stressors. Toward better understanding of human neuronal genome dynamics, our data show that proposed mechanisms of brain somatic mosaicism (i.e., polymerase collisions) are unlikely to directly engage p53-dependent mechanisms (Weissman & Gage, 2016).

Results

Reduced p53 activation promotes neurogenesis

To examine the role of p53 in early neuronal differentiation, NPCs from two neurotypic hiPSC lines (Figure S1A-E) were transduced to express a short hairpin RNA (shRNA) targeting p53 transcripts (Figure 1A), these showed markedly diminished p53 protein relative to shRNA control (Figure 1B, C). We grew NPCs to equivalent densities and switched to neuron media to induce neurogenesis in paired cultures. After six weeks of differentiation, the $p53^{KD}$ NPCs produced almost 3 times more cells than control cultures (Figure 1D, E, G, S1F). A slight increase in the percentage of neurons (Tuj1+) was observed in $p53^{KD}$ cultures relative to controls (data not shown). To assess whether genome maintenance was compromised in $p53^{KD}$ neurons DNA DSBs were measured by examining fluorescence of a phosphorylated histone epitope (γH2AX) that marks DNA DSBs (Figure 1F). We quantified γH2AX foci through imaging flow cytometry (IFC) (Bourton *et al.*, 2012; Geric *et al.*, 2014; Michel, Majumdar, Lannigan, & McConnell, 2019b) and observed both increased numbers of neurons containing DNA DSBs and increased γH2AX foci per neuron in cultures differentiated from $p53^{KD}$ NPCs (Figure 1F, H). Taken together, these data indicate that $p53^{KD}$ increased neurogenesis and elevated the number of differentiated neurons with unrepaired DNA DSBs.

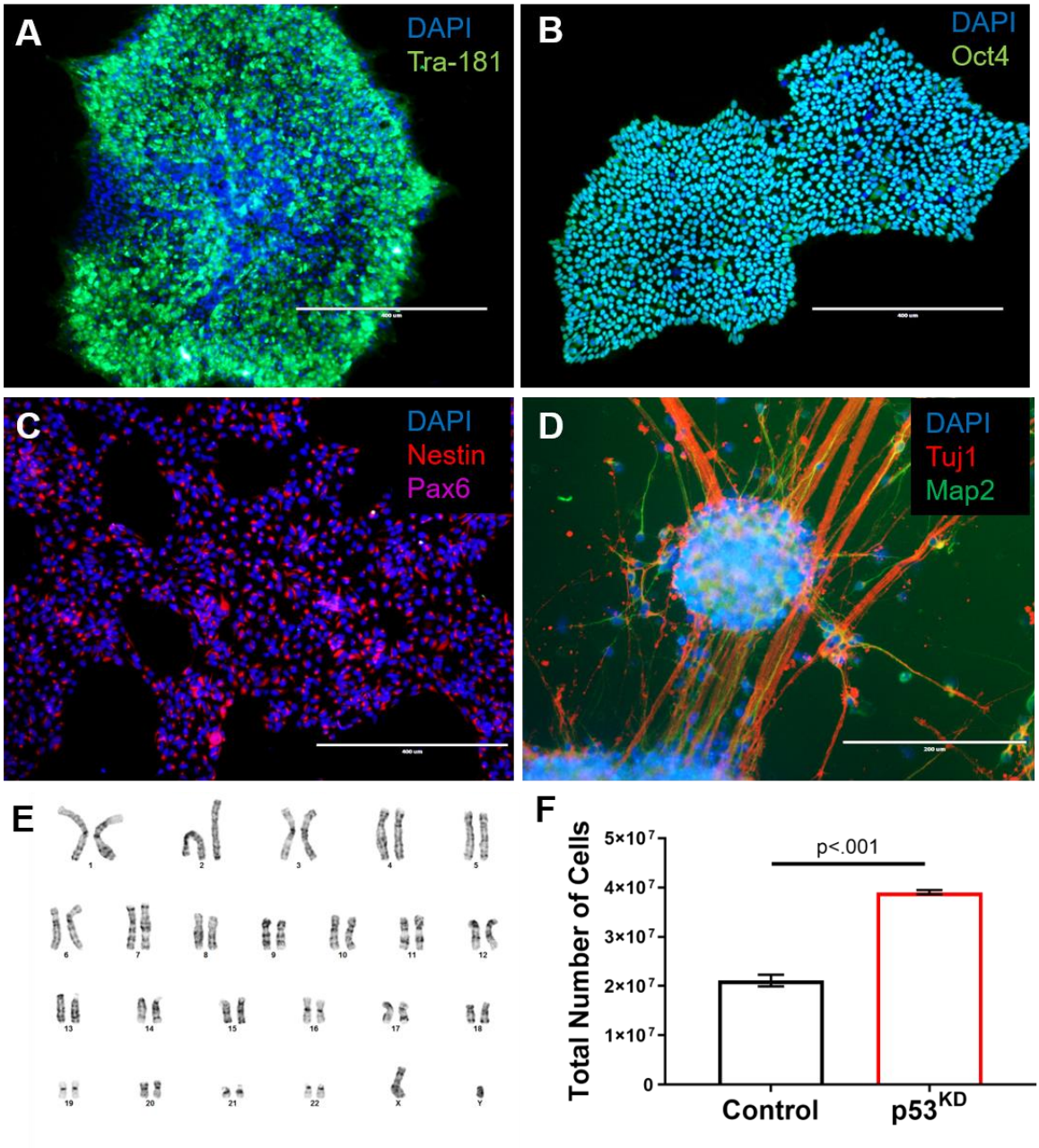

Figure S1. Related to Figure 1 | hiPSC validation and Cell Count in p53^{KD} Neurons.

Figure S1. Related to Figure 1 | hiPSC validation and data. (A and B) Representative images of neurotypic lines reprogrammed from human fibroblasts to hiPSC (human-induced pluripotent stem cells) are positive for pluripotency markers Tra-181 and Oct 4. (C) Neural progenitor cells derived from hiPSCs show expression of NPC markers Nestin and Pax6. (D) Six-week neurons differentiated from NPCs are positive for neuronal markers Tuj1 and Map2. (E) All neurotypic cell lines used in this study had normal karyotypes. (F) $p53^{KD}$ neuronal cultures have fewer cells at 6 weeks in 9429 hiPSC-derived neurons ($p<.001$, unpaired t-test, N=3 biological replicates).

Figure 1. Reduced p53 activation promotes neurogenesis

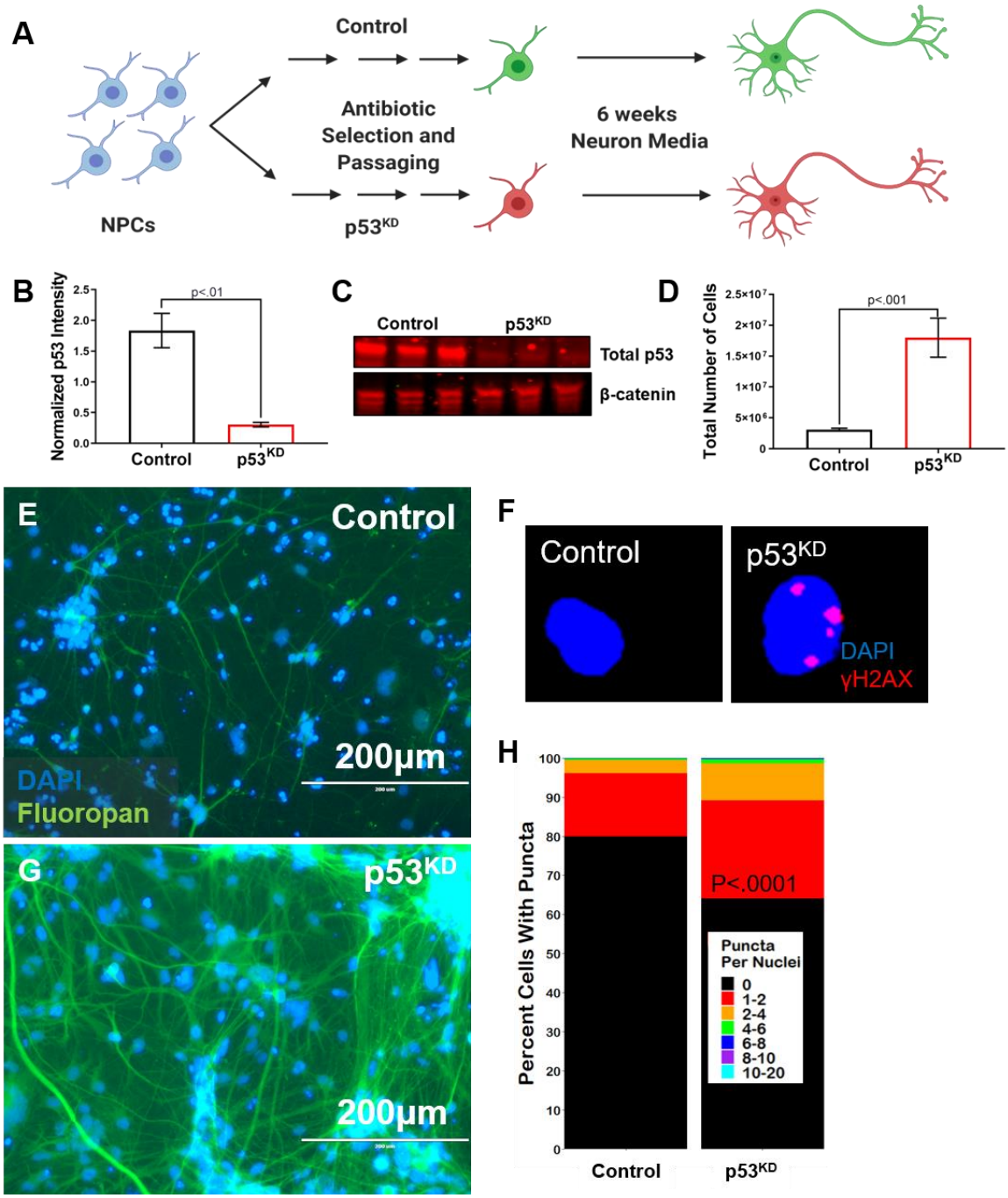

Figure 1. p53 shRNA NPCs generate more neurons with DNA DSBs at 6 weeks. (A) $p53^{KD}$ neurons were generated by transducing NPCs with a lentivirus containing a shRNA scramble or p53 shRNA plasmid. After antibiotic selection the NPCs were differentiated into neurons for six weeks. (B, C) The knockdown was validated in NPCs during the first week in neuron media through Western Blot Analysis (Unpaired t-test, $p<.01$). (D) $p53^{KD}$ neurons have more total cells when collected at 6 weeks (Error Bars= Mean +/- SEM, unpaired t-test, $p<.001$). (E, G) Representative images of Control and $p53^{KD}$ neuronal cultures stained with DAPI and Fluoropan (Neuron Specific Cocktail antibody). (F) Representative IFC images of neurons with γH2AX foci. (H) Pooled stacked histogram of γH2AX puncta per nucleus from two neurotypic cell lines. $p53^{KD}$ neurons (Tuj1+) have significantly more DNA DSBs (N= 47,406 cells from 3-6 biological replicates per cell line, Chi-squared test, $p<.0001$).

p53 deficiency promotes NPC expansion during early neurogenesis

We reasoned that an abundance of neurons in 6-week-old $p53^{KD}$ neuronal cultures may reflect diminished cell death or increased proliferation during early neurogenesis (Figure 2A). To examine this, control and $p53^{KD}$ NPC cultures were initiated at equivalent densities and cell number was determined after one week in neuron media. After one week of differentiation $p53^{KD}$ cultures had three-fold more cells than controls (Figure 2B, S2A). A role for p53-dependent early neurogenic death was further investigated using the small molecule Nutlin-3 which promotes p53 activation by inhibiting MDM2 (Arva *et al.*, 2008). Unsurprisingly, Nutlin treatment led to extensive cell death in control cultures, but it also returned $p53^{KD}$ cultures to control levels of neurogenesis (Figure 2B). While we observed a 50% decrease in caspase-3 positive cells in $p53^{KD}$ neurogenesis, cell death alone did not seem sufficient to account for the 3-fold increase in cell number (Figure S2B).

An alternative means to account for increased neuron number is continued proliferation of $p53^{KD}$ NPCs. IFC was used to quantify Tuj1-positive and Nestin-positive cells in caspase-3 negative populations. The Tuj1 antibody is immunoreactive for β-III tubulin, a marker of mature neurons (Caccamo *et al.*, 1989). Nestin is neurofilament specific to NPCs (Park *et al.*, 2010). As expected, few Nestin-positive cells and an abundance of Tuj1-positive cells were observed in control cultures (Figure 2C, E). However, $p53^{KD}$ cultures showed an abundance of Nestin/Tuj1 double positive cells, many of which showed G2 DNA content suggesting continued proliferation (Figure 2C, E). Nutlin treatment again returned $p53^{KD}$ cells to control levels of Tuj1 positive neurons (Figure 2D). To determine whether there were more proliferating cells in $p53^{KD}$ cultures, we quantified Ki67 immunostaining, a graded (i.e., not binary) marker of cell proliferation (Gerdes *et al.*, 1984; I. Miller *et al.*, 2018). We examined the median fluorescent intensity of Ki67 levels, and observed higher Ki67 levels in $p53^{KD}$ compared to controls (Figure 2F, H, S2C, S2D) and Nutlin-treated $p53^{KD}$ cells (Figure 2F, H). To further examine whether $p53^{KD}$ cells had more cells in non-G1 phases of the cell cycle, cell cycle statistics were acquired based on DNA content (Figure 2G). $p53^{KD}$ cells had fewer

cells in G1 compared to controls (Figure 2G, I, S2E, S2F), and $p53^{KD}$ cells treated with Nutlin had no differences in G1 compared to controls (Figure 2I). Taken together, these findings suggest that $p53^{KD}$ NPCs exhibit (1) less cell death; thereby increasing the number of progenitors that can become neurons and (2) increased proliferation in neuronal media; leading to an increase in the progenitor pool.

Figure 2. p53 deficiency promotes NPC expansion in early neurogenesis

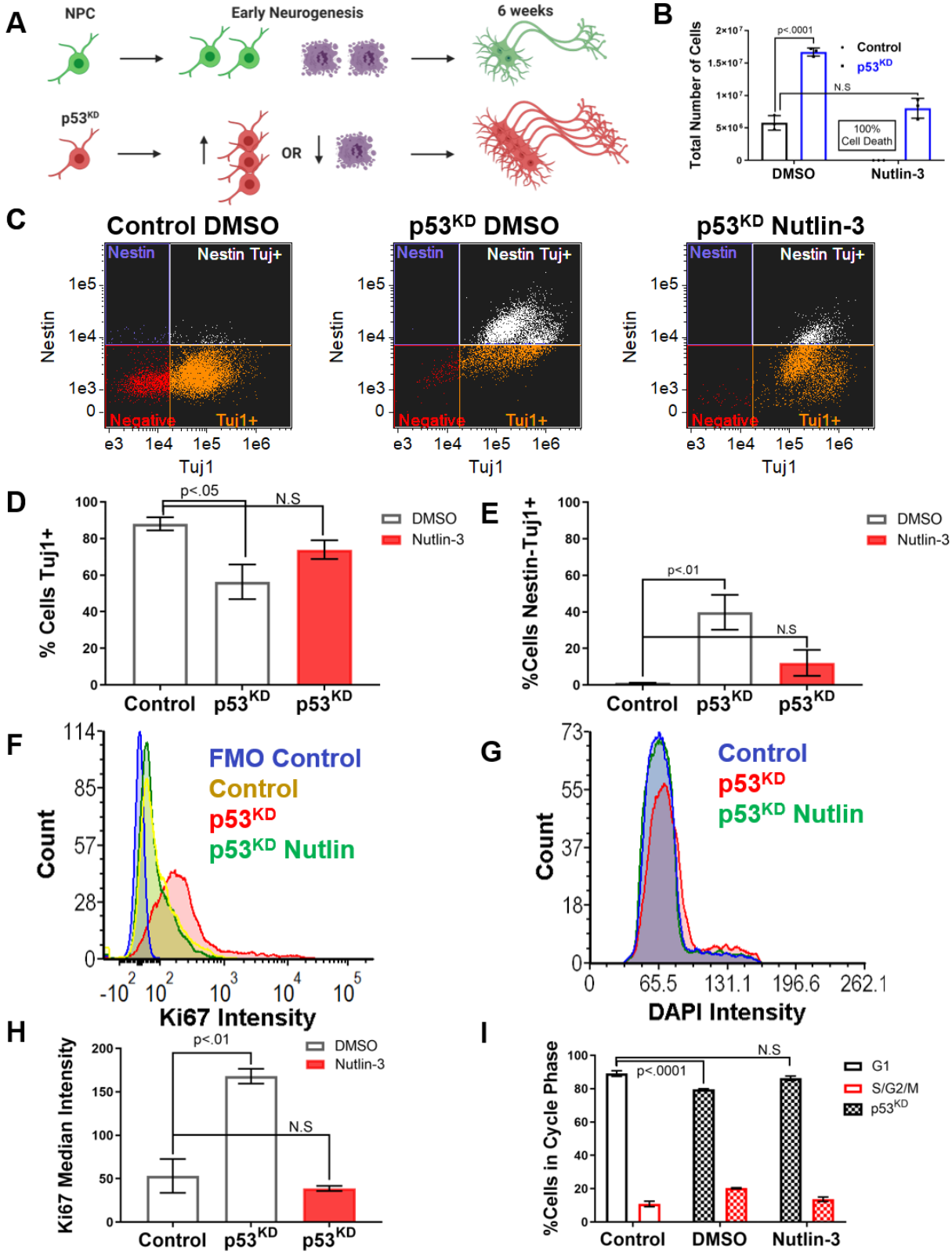

Figure 2. p53 deficiency promotes NPC expansion in early neurogenesis. (A) Model of hypothesis that more $p53^{KD}$ neurons are generated at 6 weeks due to fewer neurons dying during early neurogenesis or because more progenitor cells are still dividing in neuron media. Control and $p53^{KD}$ NPCs were either treated with15μM Nutlin-3 or DMSO control and cultured in neuron media for one week. (B) $p53^{KD}$ NPCs treated with DMSO had significantly more cells than control NPCs treated with DMSO (2-way ANOVA, Dunnett's Test $p<.0001$, N=3 biological replicates), the $p53^{KD}$ NPCs treated with Nutlin-3 had comparable cell numbers as the control NPCs (2-way ANOVA, Dunnett's Test $p=.059$). (C) The remaining three samples were processed and analyzed through imaging flow cytometry and stained with Nestin and Tuj1. (D) The percentage of Tuj1 only positive cells was quantified to determine the number of mature neurons in the population at one week in neuron media from two neurotypic lines. Control cells treated with DMSO had the highest percentage of neurons compared to $p53^{KD}$ cells treated with DMSO (One-way ANOVA, Dunnett's test, $p<.05$, pooled data from 2 neurotypic lines). There was no significant difference between controls and $p53^{KD}$ treated with Nutlin (One-way ANOVA, Dunnett's Test $p=.10$). (E) Nestin-Tuj1 double positive cells were assessed to investigate transitioning cells that were not post mitotic neurons. $p53^{KD}$ cells treated with DMSO had significantly more double positive cells (One-way ANOVA, Dunnett's Test $p<.01$, pooled data from two neurotypic cell lines). The quantity of double positive cells was not significantly different between Control NPCs treated with DMSO and p53 deficient NPCs treated with Nutlin (One-way ANOVA, Dunnett's Test, $p=.51$). (F, H) Flow cytometry histograms show more mitotically active cells (Ki67 positive) in p53 shRNA neuronal cultures at one week than control or Nutlin treated p53 shRNA neurons as quantified by Ki67 median fluorescent intensity (One-way ANOVA, Dunnett's Test $p<.01$). (G, I) Fewer p53 KD cells in G1/G0 phase of the cell cycle compared to controls (One-way ANOVA, Dunnett's Test $p<.0001$, p53 KD Nutlin treated cells had similar percentages of cells in G1/G0 as controls (One-way ANOVA, Dunnett's Test $p=.41$). Patterns inside the bar graphs are p53 KD cells.

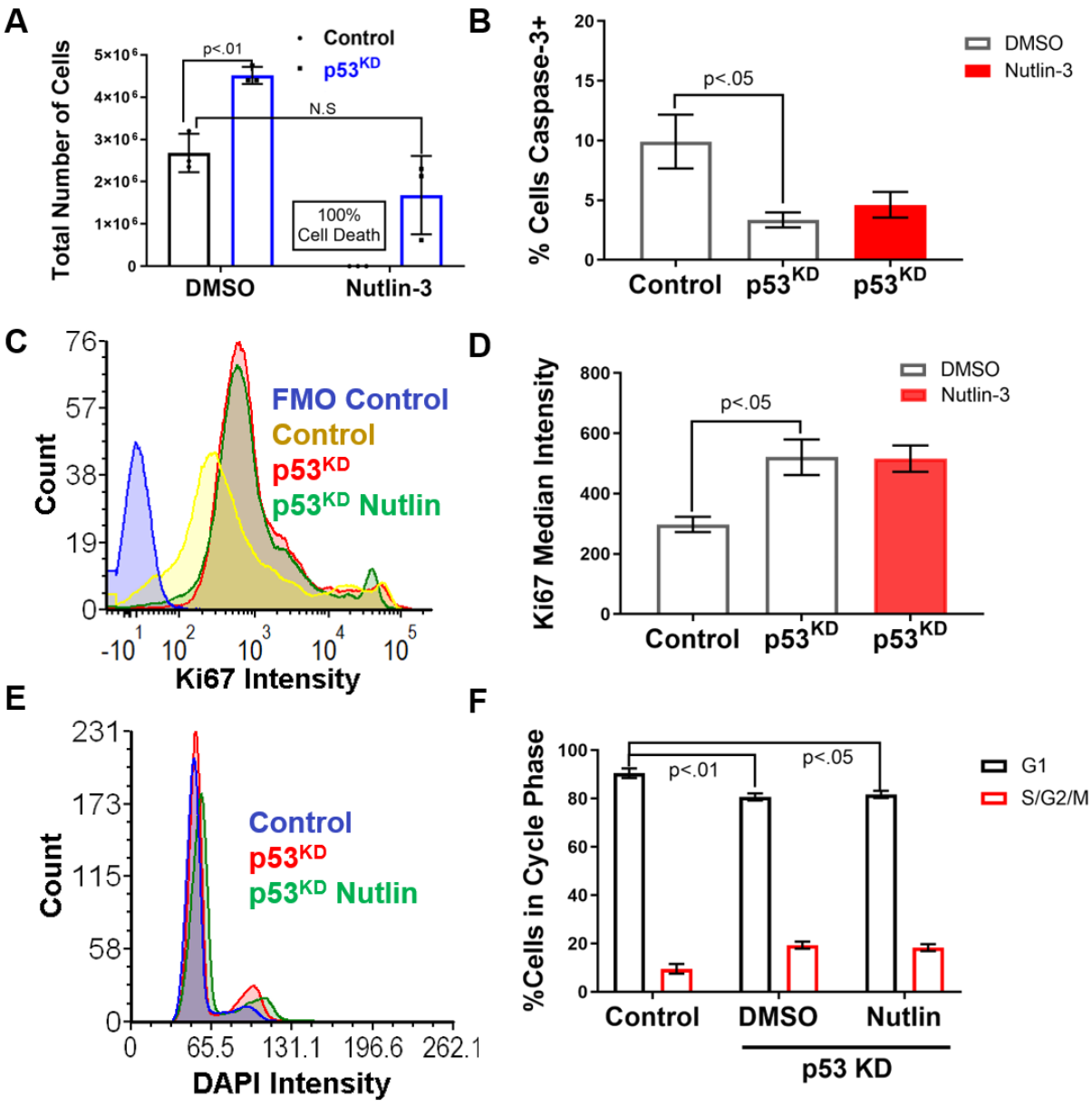

Figure S2. Related to Figure 2 | Cell death and p53^{KD} in a different neurotypic cell line.

Figure S2. Related to Figure 2 | Cell death and p53 KD in a different neurotypic cell line. (A) $p53^{KD}$ NPCs treated with DMSO had significantly more cells than control NPCs treated with DMSO after one week in neuron media (2-way ANOVA, Sidak's Test $p<.01$, N=3 biological replicates, Error Bars=SEM), the p53 knockdown NPCs treated with Nutlin-3 had comparable cell numbers as the control NPCs (2-way ANOVA, Dunnett's Test $p=.13$, N=3 biological replicates, Error bars=SEM). (B) $p53^{KD}$ have less cell death than controls at one week in neuron media (One-way ANOVA, Dunnett's Test, $p<.05$, pooled data from 2 cell lines, n=3 biological replicates per cell line). (C, D) Flow cytometry histograms show more mitotically active cells (Ki67 positive) in p53 KD neuronal cultures at one week than controls (One-way ANOVA, Dunnett's Test $p<.05$) in a different neurotypic cell line. (E, F) Fewer p53 KD cells in G1/G0 phase of the cell cycle compared to controls (One-way ANOVA, Dunnett's Test $p<.01$), Nutlin partially rescued the percentage of cells in G1/G0 (One-way ANOVA, Dunnett's Test $p<.05$).

p53 is activated during transcriptional stress in human NPCs

The rapid proliferation of NPCs during expansion and changes in gene expression during neurogenesis are known sources of genomic stress that activate various stress response signaling pathways (McKinnon, 2017), but the connection between p53 activation and genomic stress in human neurons is not known. We sought to determine whether replication or transcriptional stress more strongly activated p53 in NPCs by exposing cells to small-molecules that inhibited events associated with either DNA replication or mRNA transcription. We treated control NPCs with an inhibitor of DNA polymerase α known as aphidicolin (APH) (Rodriguez-Acebes, Mouron, & Mendez, 2018), or a topoisomerase I inhibitor known as camptothecin (CPT) (Capranico *et al.*, 2007) to create replication (APH) or transcriptional (CPT) stress. We used traditional cytometry to count the total percentage of cells containing DNA DSBs in treated cultures. From these data we identified concentrations of APH and CPT that increased the percentage of γH2AX positive NPCs (Figure S3A). Imaging flow cytometry permits single cell quantification of genomic stress by counting γH2aX puncta in single NPCs. We used this approach to quantify DNA DSBs per nucleus to assess whether NPCs were more sensitive to replication or transcriptional stress, and to what degree effect these stressors had on the numbers of DNA DSBs per cell. Among APH and CPT treated NPCs, those exposed to CPT had significantly more DNA DSBs per cell (Figure 3A, S3B).

To examine which DNA damage response proteins were activated by DNA DSBs resulting from transcriptional stress we assayed levels of pATM, pChk2, and phosphorylated p53 because these proteins are part of a canonical DNA DSB response pathway (Marechal & Zou, 2013; Matsuoka *et al.*, 2007; Sancar, Lindsey-Boltz, Unsal-Kacmaz, & Linn, 2004). Transcriptionally stressed NPCs had higher levels of phosphorylated p53, pChk2, and γH2AX compared to controls and replication stressed NPCs (Figure 3B, S3D). In addition, transcriptionally-stressed NPCs also had higher levels of pATM activation compared to controls and APH-treated NPCs (Figure 3C, D). To determine whether the increase in DNA DSBs

leads to cell cycle arrest, we collected cells after drug treatment and measured DNA content by flow cytometry. APH and CPT treated cells were predominantly arrested in S-phase compared to DMSO controls (Figure 3E, 3F, S3C).

NPCs exposed to replication stress had similar levels of cell death (i.e., Caspase 3 positive cells) relative to controls but this population was more prevalent in transcriptionally stressed cells (Figure 3G). Notably, even in an individual neurotypic cell line that responded to CPT and APH with similar distributions of puncta per nucleus, more cells died from transcriptional stress than replication stress (Figure S3B, 9429).

To further characterize the NPC response to transcriptional versus replicative stress we stressed NPCs for 24 hours and collected them for single-cell RNA sequencing (scRNA-seq). We observed three distinct transcriptional groups present in all conditions (Figure 3H, S3E). Actively proliferating NPCs were abundant in the two controls (Not Treated, DMSO) and APH treated cells (blue cluster), but minimally present in the CPT treated cells (Figure 3H, J, S3E). CPT treated cells had a significant emergence of cells upregulating genes involved in the DNA damage checkpoint, p53 mediators, and cell death (Figure 3I). These data confirm transcriptional, not replicative, genomic stress leads to p53 activation.

Figure 3. DSB mediated activation of p53 in NPCS undergoing transcriptional stress

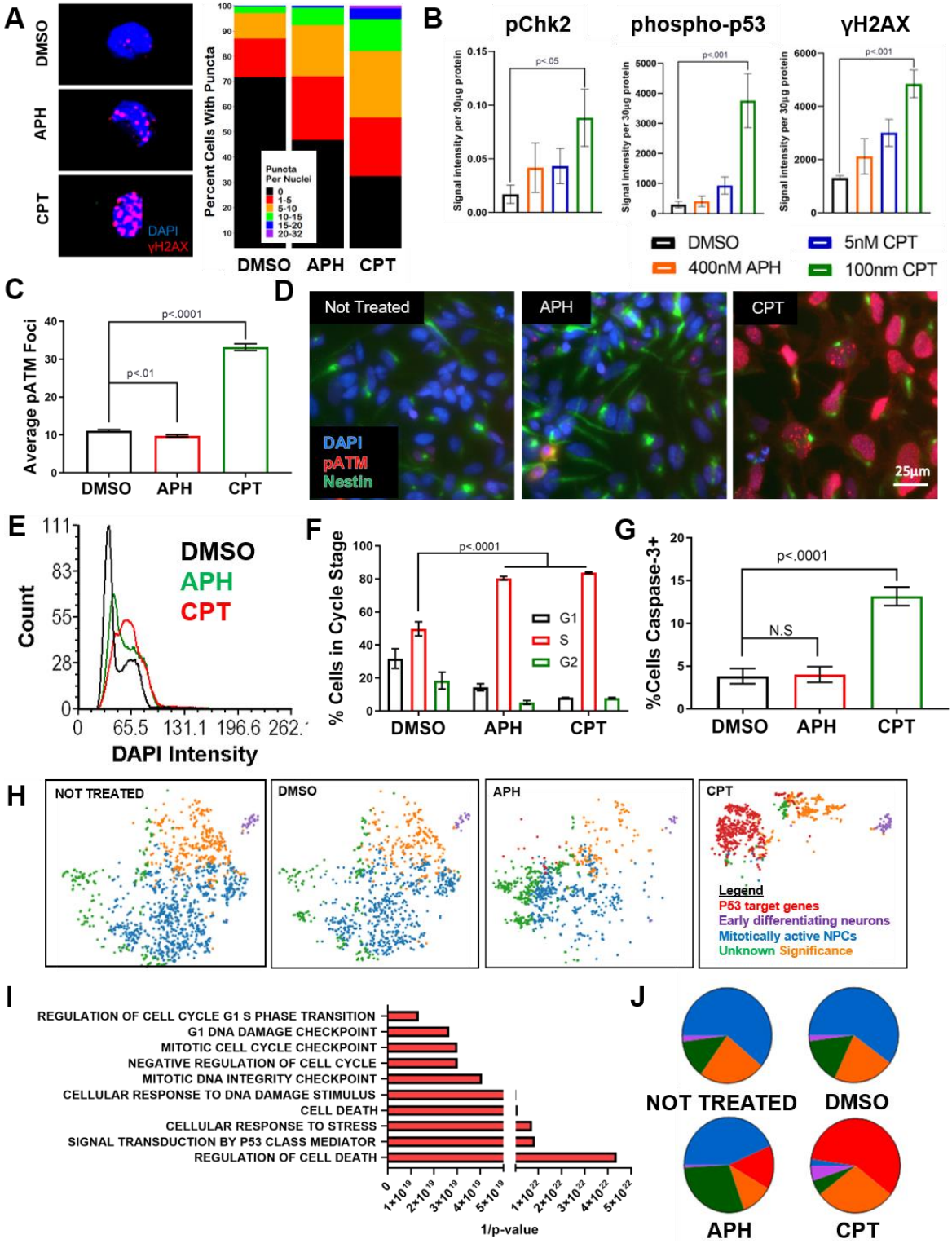

Figure 3. DNA DSB mediated activation of p53 in NPCs undergoing transcriptional stress. (A) NPCs were exposed to vehicle control (DMSO), 400nM of Aphidicolin (APH), or 100nM Camptothecin (CPT) for 24 hours and processed for imaging flow cytometry. Stressed NPCs had significantly more DNA DSBs per nucleus (Chi-squared, p<.0001, N= 63436 cells from two neurotypic lines, 3 biological replicates each) but the distribution of cells with more puncta per nucleus was higher in CPT treated cells (KS test, p<.0001, N= 63436 cells from two neurotypic lines, 3 biological replicates each). (B) Transcriptional stress (100nM CPT) increases phosphorylated p53 (unpaired t-test, p<.001), γH2AX (unpaired t-test, p<.001), and pChk2 (unpaired t-test, p<.05) protein levels as measured through Western Blot Analysis (N=3 biological replicates per cell line (2 lines)). (C, D) NPCs have more pATM foci per nucleus in transcriptional stress (CPT) (One-way ANOVA, Dunnett's Test, p<.0001, N=3 biological replicates per cell line (2 lines)) and less pATM foci per nucleus in replication stress (APH) (One-way ANOVA, Dunnett's Test, p<.01, N=3 biological replicates per cell line (2 lines)). (E, F) NPCs exposed to replication (APH) and transcriptional stress (CPT) are significantly more arrested in S-phase compared to controls (Two-way ANOVA, Dunnett's Test p<.0001). (G) CPT treated cells had more caspase-3 positive than controls (One-way ANOVA, Dunnett's Test p<.0001) while APH treated cells did not (One-way ANOVA, Dunnett's Test, p=.98, N=3 biological replicates per cell line (2 lines)). (H) Single-cell RNA seq revealed that transcriptionally stressed NPCs have differential expression of p53 target genes involved in DNA damage response, cell cycle arrest, and cell death (N=4598, n is number of cells). (I) Functional pathway analysis of the top 100 highest variant genes from the 592 cells in the red cluster (enriched in CPT treatment) are involved cellular processes related to DNA damage checkpoint (p<1.37E-22), cell death (p<1.16E-22), and p53 mediators (p<1.16E-22). (J) The percentage of cells in each cluster per condition is shown in a pie chart.

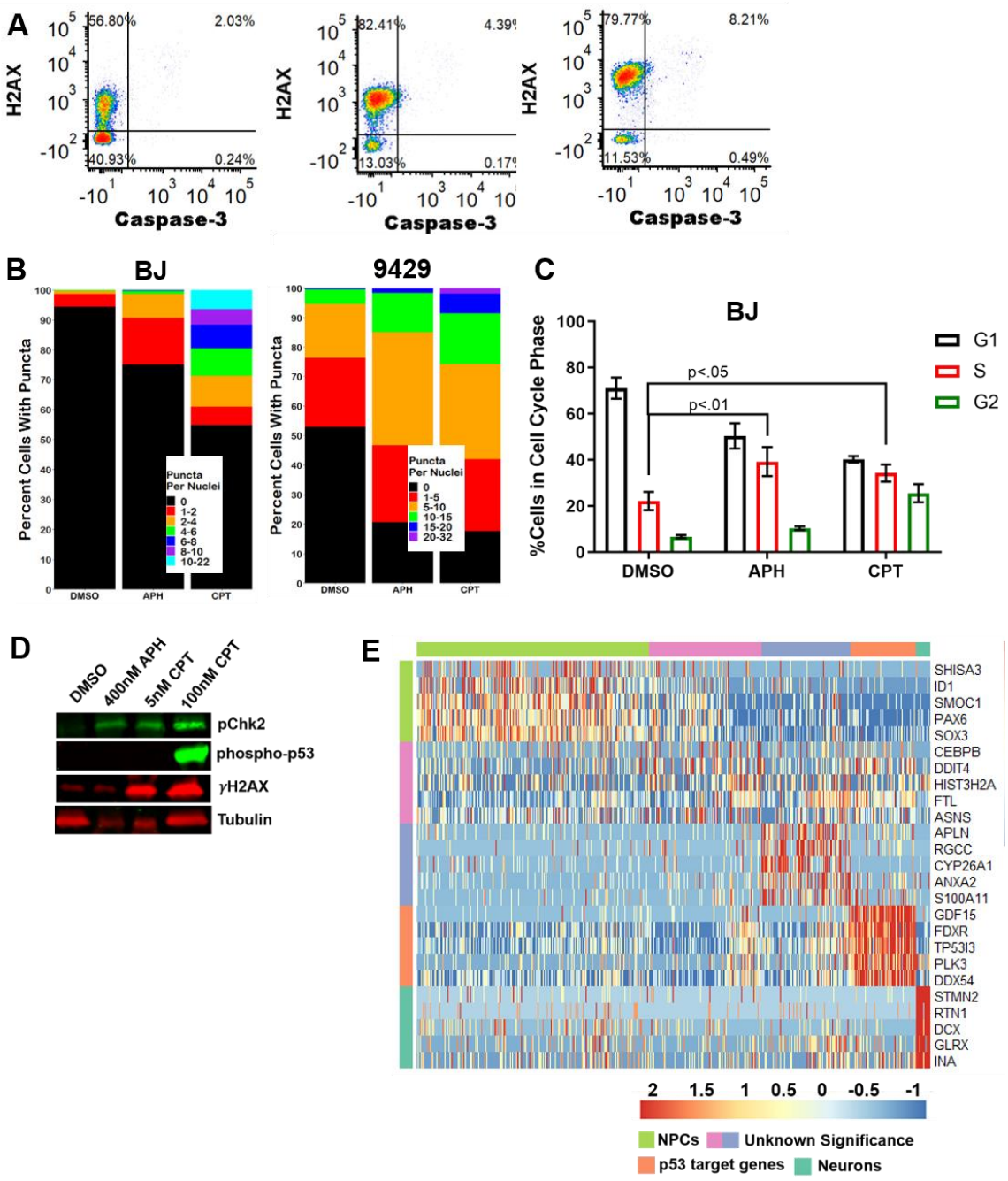

Figure S3. Related to Figure 3 | p53 activation from transcriptional stress in individual neurotypic cell lines.

Figure S3. Related to Figure 3 | p53 activation from transcriptional stress in individual neurotypic cell lines. (A) NPCs were exposed to vehicle control (DMSO), 400nM of Aphidicolin (APH), or 100nM Camptothecin (CPT) for 24 hours and processed for flow cytometry. NPCs exposed to genomic stress (APH or CPT) had significantly more NPCs with DNA DSBs than controls (One-way ANOVA, Dunnett's Test $p<.0001$). (B) DNA DSB plots of NPCs (9429 and BJ) that were exposed to 24 hours of replication stress (APH), transcriptional stress (CPT), or vehicle control (DMSO). Both cell lines have an increase in DNA DSB in response to stress but vary in the extent of DNA DSBs in each cell line (Chi-squared $p<.001$). (C) NPCs exposed to genomic stress are significantly more arrested in S-phase compared to controls (APH, Two-way ANOVA, Dunnett's Test $p<.01$, CPT, Two-way ANOVA, Dunnett's Test $p<.05$). (D) Representative western blot of pooled data from two neurotypic NPC lines exposed to stress for 24 hours. (E) Differential expression heatmap of the top five genes in each transcriptional cluster from scRNA-seq of NPCs stressed for 24 hours.

Unrepaired DNA DSBs in p53KD NPCs are in highly transcribed genes associated with neurological disorders

Many neuronally-expressed genes are among the longest genes in the human genome (King *et al.*, 2013; Zylka, Simon, & Philpot, 2015). Long genomic loci are transcribed into S-phase leading to potential collisions between RNA and DNA polymerases and ensuing DNA DSBs (Wilson *et al.*, 2015). In addition to gene length, rapid transcription of immediate early genes is enabled by DNA DSBs (Madabhushi *et al.*, 2015). Our biochemical and pharmacological data suggest that $p53^{KD}$ leads to an elevated DNA DSB burden due to transcriptional, not replicative stressors. We further tested this hypothesis by mapping DNA DSB location in control and $p53^{KD}$ NPCs.

Unrepaired DNA DSBs were captured using a genome wide DNA Break Mapping/Sequencing approach and mapped with single nucleotide-level resolution (Lensing *et al.*, 2016). Two biological replicates of 9429 NPCs (control and $p53^{KD}$) showed strong concordance and were pooled for subsequent analysis (Table S1, S4A). Consistent with elevated DNA DSB burden in $p53^{KD}$ NPCs observed in other assays, we detected more DNA DSBs in $p53^{KD}$ NPCs compared to control (Figure 4B). Moreover, DNA DSB location was associated with gene length in all NPCs (Figures S4B). We examined transcriptional stress as the origin of additional DNA DSBs in $p53^{KD}$ NPCs by assessing DNA DSB location in the most (top 10%) and least (bottom 10%) expressed genes based on scRNA seq data (Figure 3H-J). Extant DNA DSBs in $p53^{KD}$ NPCs occurred more frequently in the most highly expressed genes (Figure 4A).

Table S1. Sequencing and alignment statistics for paired-end Illumina sequencing libraries prepared from NPC9429.

Samples	Biological duplicates	# Sequenced read pairs[a]	Alignment rate	% Duplication[b]	# Proper read pairs[c]	# Mapped DNA DSBs[d]	% Mapped DNA DSBs[e]
CONTROL	N1	20,182,000	96.26	15.73	18,613,470	14,127,449	70.00
	N2	15,662,240	93.67	30.55	13,635,779	8,490,542	54.21
p53KD	N1	20,695,451	96.26	11.50	19,011,211	15,256,854	73.27
	N2	18,175,752	92.63	19.42	15,883,396	11,684,734	64.29

[a] Number of raw paired read1-read2s following Illumina paired-end sequencing and quality filtering

[b] PCR duplicates are marked and removed meaningfully using read1 and read2 alignment, and "% Duplication" is based on original "# Sequenced read pairs".

[c] Following the quality control removal of all unmapped, non-primary, supplementary and low-quality reads, the remaining number of paired read1-read2s are indicated.

[d] For each proper read pair, only read1 is kept, and the 5' most nucleotide of read1 defines the DNA break position.

[e] "% Mapped DNA DSBs" was calculated by dividing "# Mapped DNA DSBs" by "# Sequenced read pairs".

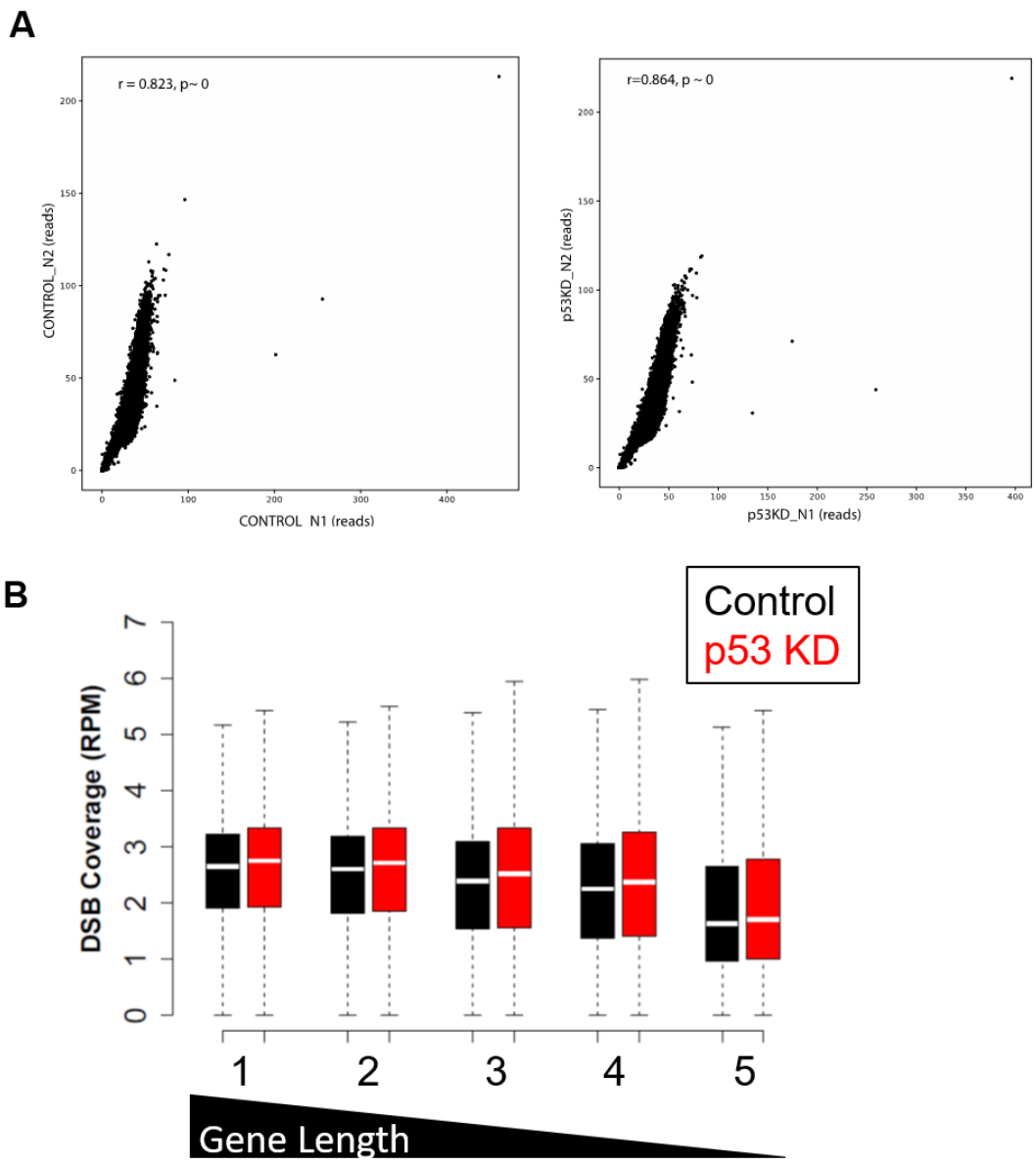

Figure S4. Related to Figure 4 | p53 DNA DSBs in long genes and reproducibility of genome-wide DSB mapping/sequencing in 9429 NPCs.

Figure S4. Related to Figure 4 | p53 DNA DSBs in long genes and reproducibility of genome-wide DNA DSB mapping/sequencing in 9429 NPCs (A) Scatter plots of genome-wide DNA DSB mapping/sequencing reads from two biological duplicates (N1 and N2) of the control (left panel) and the $p53^{KD}$ (right panel) samples show strong correlations (Pearson's correlation r = 0.82 and 0.86, respectively, p ~ 0). Read-normalized DNA DSB coverage for each preparation was calculated for 100 kb genome-wide, non-overlapping windows (n=30,895 bins), and Pearson's correlation was calculated. (B) DNA DSB read coverage is plotted against gene length in 5 bins based on all genes spanning the TSS +/- 2kb (n=2536 genes). $p53^{KD}$ has significantly more DNA DSBs than Controls at all gene lengths (Wilcoxon signed-rank test, two-sided, paired test, p<.00001).

Figure 4. Absence of p53 leads to more DNA DSBs in highly transcribed genes associated with neurodevelopment and neurodegeneration

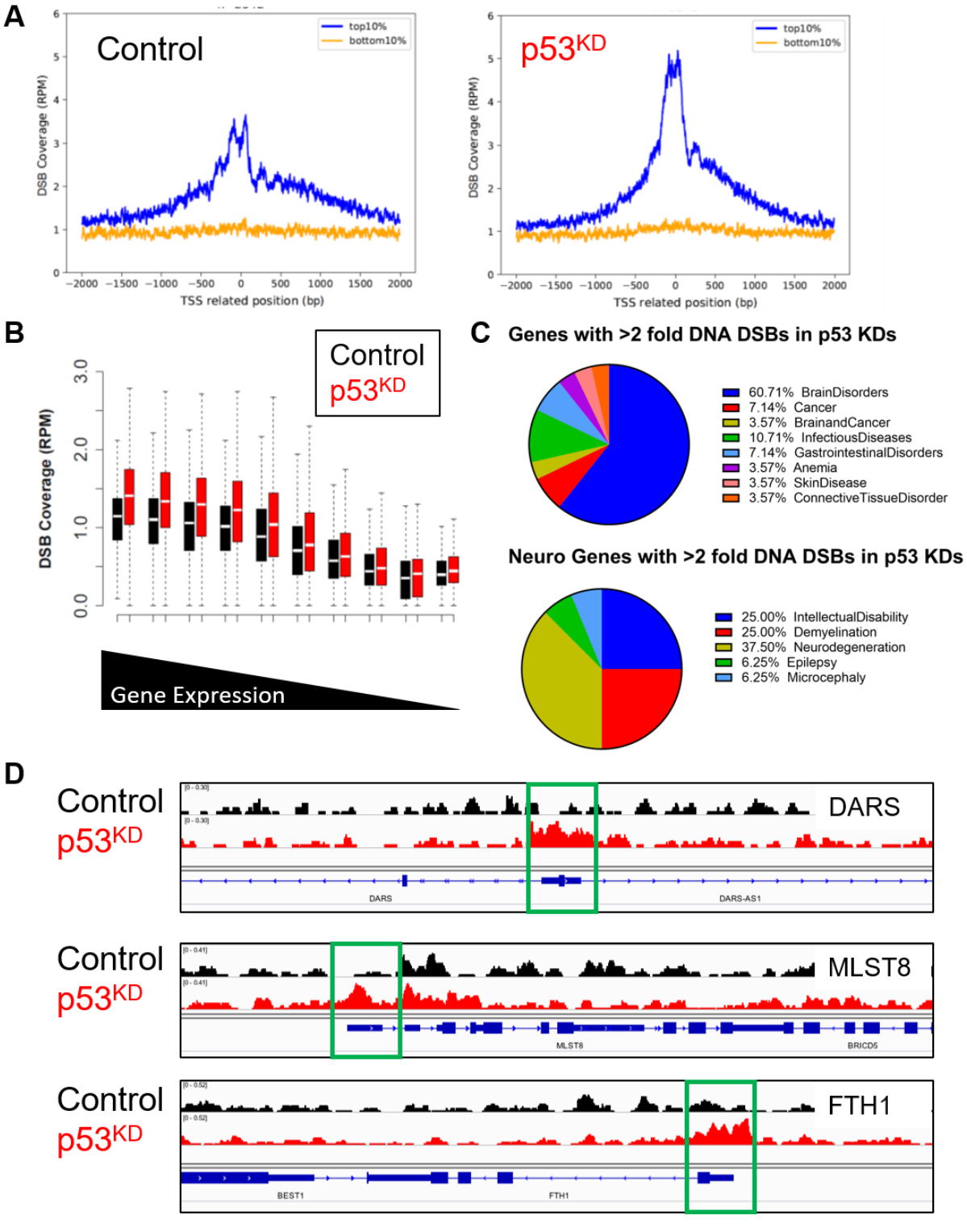

Figure 4. Absence of p53 leads to more DNA DSBs in highly transcribed genes associated with neurodevelopment and neurodegeneration. (A) DNA DSB coverage in the top 10% highly expressed (n=2542 genes) and low expressed genes (n=2542) TSS regions in (A, left) Control cells and (A, right) $p53^{KD}$ NPCs show that the breaks are enriched in the regions with high expression. (B) Boxplot of DNA DSB coverage (TSS+/-500 bp) in 10 equal bins based on the gene expression. $p53^{KD}$ NPCs have more DNA DSB in highly transcribed genes compared to control cells at every bin (Wilcoxon signed-rank test, two-sided, paired test, $p<.00001$). The box plot shows the 25th and 75th percentile; the middle line is the median. Outliers are not shown. (C) The top 50 genes with greater than 2 DNA DSBs in $p53^{KD}$ NPCs were analyzed for known associations with disease. Over 60% of the genes related to clinical diseases and disorders were specific to brain disease. Of those brain specific genes over ~37% were involved in processes related to neurodegenerative disorders. (D) An IGV plot of three genes associated with brain disorders showing an increase in DNA DSBs in p53 KD NPCs compared to Control NPCs are shown (from top to bottom: DARS, MLST8, FTH1). Green boxes highlight the TSS where the differences in DNA DSBs were quantified.

We sought to examine whether $p53^{KD}$ increased the prevalence of DNA DSBs in genes with neuronal function or causal links to brain disease. We performed gene ontology (GO) analysis of expressed genes that had >2-fold enrichment per transcription start site (TSS) in p53KD NPCs. Of the top 50 genes, half were associated with known human diseases, and out of that group 60% were associated with brain disorders (Figure 4C, top). We analyzed the brain disorder genes further and observed that 25% were involved in demyelinating disorders, 25% in intellectual disabilities, and more than 37% in neurodegenerative disease (Figure 4C, bottom). Specifically, some of the genes bearing additional DNA DSB burden in p53KD NPCs include DARS (Hypomyelination with Brainstem and Spinal Cord), MLST8 (Childhood Absence Epilepsy), and FTH1 (Superficial Siderosis of the CNS) (Figure 4D, Table 1). Together these data show that a lack of p53 is associated with more DNA DSBs in highly transcribed genes involved in brain disease.

Table 1. Top 10 Genes with >2-fold DNA DSB enrichment in p53 KD.

Rank	Gene Name	DNA DSB Fold Change	Function	Disease Association	Overlapping Gene(s)
1	**DARS**	3.7	Mediates the attachment of amino acids to their cognate tRNAs	Hypomyelination with Brainstem and Spinal Cord Involvement and Leg Spasticity	
2	**FTH1**	3.0	Encodes the heavy subunit of ferritin, the major intracellular iron storage protein in prokaryotes and eukaryotes	Superficial Siderosis of the Central Nervous System	
3	**CRIPT**	2.8	Encodes a protein that binds to the PDZ3 peptide recognition domain	Microcephaly	
4	**PPP2R1A**	2.8	Encodes a constant regulatory subunit of protein phosphatase 2	Mental Retardation	MIR6801
5	**RPL7A**	2.8	Encodes a ribosomal protein that is a component of the 60S subunit of cytoplasmic ribosomes (the large subunit)	Leigh Syndrome: severe neurological disorder with progressive mental movement abilities	SNORD24; SNORD36A; SNORD36B; SNORD36C
7	**TOMM20**	2.7	Central component of the receptor complex responsible for the recognition and translocation of cytosolically synthesized mitochondrial preproteins.	Perry Syndrome: characterized by parkinsonism and psychiatric changes	SNORA14B
11	**NDUFB10**	2.6	Encodes an accessory subunit of Complex I, which functions in the transfer of electrons from NADH to the respiratory chain	Mitochondrial Complex I Deficiency: abnormal brain function, epilepsy, intellectual disability, ataxia, dystonia	
14	**COX6B1**	2.6	Encodes the terminal enzyme of the mitochondrial respiratory chain, catalyzes the electron transfer from reduced cytochrome c to oxygen.	Mitochondrial Complex IV: muscle weakness, intellectual disability, ataxia, seizures	
15	**MLST8**	2.4	Subunit of both mTORC1 and mTORC2, which regulates cell growth and survival in response to nutrient and hormonal signals	Childhood Absence Epilepsy	
16	**CTNNB1**	2.4	The protein encoded by this gene is part of a complex of proteins that constitute adherens junctions	Severe Intellectual Disability and Spastic Diplegia	

Table 1. Top 10 Genes with >2-fold DNA DSB enrichment in p53 KD. The top 10 genes with >2-fold DNA DSB enrichment related to brain disorders are listed from highest to lowest DNA DSB fold change. Genes with unknown clinical significance were excluded.

Discussion

A deeper understanding of human neuronal genome dynamics is motivated by increasing recognition that both neurodevelopmental and neurodegenerative human diseases are linked to genome maintenance. Brain somatic mutations altering mTOR-signaling lead to hemispheric overgrowth in hemimegalencephaly (Kurek *et al.*, 2012; Lee *et al.*, 2012) and focal dysplasia in epilepsy (Baulac *et al.*, 2015), and somatic GNAQ mutations contribute to developmental delay and seizures in Sturge-Weber syndrome (Shirley *et al.*, 2013). The abnormal accumulation of DNA damage is a common pathological feature among neurodegenerative diseases including Alzheimer's disease (Coppede & Migliore, 2009; Lovell & Markesbery, 2007), Parkinson's disease (Ogino *et al.*, 2016; Sepe *et al.*, 2016), and Amyotrophic lateral sclerosis (ALS) (Coppede, 2011; Martin, 2008) and is correlated with normal aging (Chow & Herrup, 2015; D. Liu & Xu, 2011). DNA repair is not perfect and somatic mutations accumulate in neurotypical human neurons (Alsina & Silver, 2019), higher frequencies of somatic mutations are observed in neurodegenerative disorders (M. A. Lodato *et al.*, 2018; McConnell *et al.*, 2017). Indeed, genome maintenance is critical in neurons and enhanced DNA repair is a pharmacological target to ameliorate cognitive decline (Chow & Herrup, 2015; McKinnon, 2017). Moreover, mutations affecting DNA repair and damage signaling (e.g., Atm) lead to childhood onset neurodegenerative disease (e.g., ataxia-telangiectasia)(Rothblum-Oviatt *et al.*, 2016) and have emerged as critical mediators of Huntington's Disease onset (Genetic Modifiers of Huntington's Disease Consortium. Electronic address & Genetic Modifiers of Huntington's Disease, 2019).

We show that the cellular gatekeeper p53 monitors transcriptional, not replicative, DNA DSBs (Figure 5). Through an hiPSC-based model system we altered p53 levels in NPCs and measured effects on the abundance of DNA DSBs, neural cell numbers, and neural cell types. Our data show 1) that $p53^{KD}$ NPCs show increased neurogenesis, 2) that increased neurogenesis is the result of both ongoing proliferation and diminished cell death, 3) that p53 is activated by transcriptional,

not replicative, genomic stress, and 4) that persistent DNA DSBs in p53^{KD} NPCs occur in highly transcribed genes linked to human neurological disease. Collectively, these data exclude a predominant role for p53 in mitigating some forms of brain somatic mosaicism.

Figure 5. A model of p53 activation in NPCs undergoing transcriptional stress during neuronal differentiation.

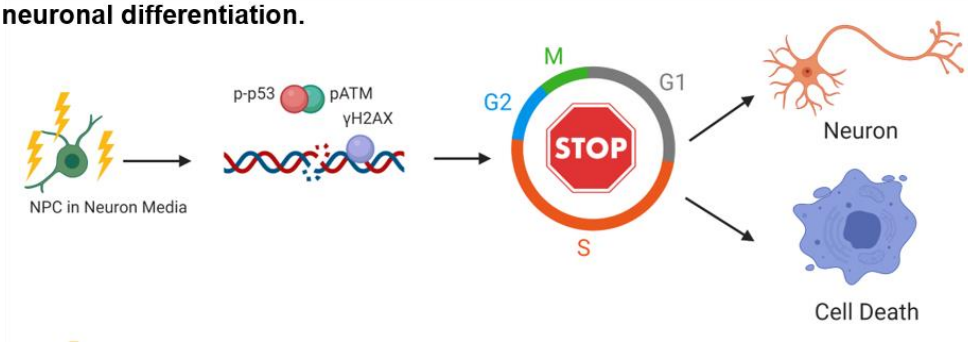

Figure 5. A model of p53 activation in NPCs undergoing transcriptional stress during neuronal differentiation. NPCs undergo various stress during neurogenesis that lead to DNA DSBs. Upon the formation of DNA DSBs from transcriptional stress, H2AX is phosphorylated and ATM is phosphorylated, leading to the phosphorylation of p53. p53 activation leads to cell cycle arrest and cell death in progenitors with significant DNA damage in genes related to neurodegenerative and neurodevelopmental disorders.

Our data indicate a distinct neurodevelopmental role for p53 in the response to transcription-associated DNA DSBs. It has been proposed, based on several lines of evidence, that collisions between DNA and RNA polymerases lead to DNA DSBs and subsequent somatic mosaicism at a subset of neuronal genes that are long and are also risk alleles for psychiatric disease (Wei *et al.*, 2016; Weissman & Gage, 2016; Wilson *et al.*, 2015). Consistent with this mechanism, we find an association between gene length and DNA DSB prevalence in all NPCs. However, it is only when considered with regard to gene expression level that we observe a differential incidence of DNA DSBs in p53^{KD} NPCs.

Longitudinal molecular genetics and biochemical studies of human neurodevelopment have largely been intractable due to practical logistics and ethical considerations. Cross-sectional familial and population-based genetic studies have solidified the notion that most human neurological disease is

polygenic and challenging to interpret. Studies of mouse mutants together with studies of post-mortem human brains have yielded many insights; yet the translation of mouse data to human disease has been imperfect. This barrier to progress is brought about both by species-specific brain differences and by the end-stage nature of most human post-mortem tissue. The study of human neurodevelopment in-a-dish is enabled by hiPSC-based neurogenesis. In addition to providing mechanistic insight and drug development platforms for human neurological disease (Ardhanareeswaran *et al.*, 2017; Brennand *et al.*, 2011; Choi *et al.*, 2014; Flaherty *et al.*, 2017; Y. Liu *et al.*, 2013; Marchetto *et al.*, 2017) hiPSC-based models offer insights into neurotypical neurodevelopment that are uniquely human. Given dramatically different neuronal production requirements and human-specific brain phenotypes, it is not surprising that brain somatic mosaicism is more abundant in human brains (W. D. Chronister *et al.*, 2019; McConnell *et al.*, 2013), relative to mouse brains (Hazen *et al.*, 2016; Rohrback, April, *et al.*, 2018). A human-specific understanding of the interplay between endogenous genomic stress and genome maintenance responses portends new drug targets for neuropsychiatric and neurodegenerative disease.

Materials and Methods

Cell Culture

Fibroblasts from neurotypical individuals (Coriel Cell Repository) were reprogrammed to induced pluripotent stem cells using lentiviral (9319, 9429) or non-integrating Sendai (Invitrogen) vectors (BJ, 7545). NPCs and neurons were generated following methods outlined by Brennand and Livesey (Brennand *et al.*, 2011; Y. Shi, Kirwan, & Livesey, 2012). Briefly, hiPSC-derived NPCs were plated on Matrigel (Fisher) or Poly-Ornithine (Sigma)/ Laminin (Invitrogen) and passaged 1:6 every four days. NPCs (<passage 14) were cultured in NPC medium (DMEM/F12 +Glutamax (Invitrogen), 1x N2 (Invitrogen), 1X B27-Vitamin A (Invitrogen), 1ug/ml Laminin (Invitrogen), 20ng/ml FGF-2 (Peprotech) and dissociated in Accutase (Fisher) for 5 min at 37°C. hiPSC-derived neurons were cultured on Matrigel in Neuron Medium (DMEM/F12 +Glutamax, 1x N2, 1X B27 with Vitamin A (Invitrogen), 20ng/ml BDNF (Shenandoah Biotechnology), 20ng/ml GDNF (Shenandoah Biotechnology), 1mM dibutryl-cyclic AMP (Sigma), and 200nM ascorbic acid (Stem Cell Technologies).

Drug Treatment

NPCs were exposed to various doses of Aphidicolin (Sigma), Camptothecin (Sigma), and Nutlin-3 (Sigma). DMSO was used to solubilize all drugs and was used as a vehicle control. All treatments were added directly to the appropriate cell media. All drugs used in this study were stored appropriately at -20°C and aliquoted.

Immunocytochemistry

NPCs were cultured for 24 hours with various drugs and rinsed with PBS. NPCs at ~80% confluency were fixed on 18mm glass coverslips with 4% PFA for 15 minutes at room temperature and rinsed (3 times for 5-minute washes) in PBS. Cells were permeabilized with .5% Triton-X 100 for 10 minutes and incubated in blocking buffer (2% BSA in PBS-T (.1% Triton-X 100)) for one hour at room

temperature. The cells were probed overnight at 4°C with anti-phosphorylated pATM, DAPI, and Nestin followed by labeling with secondary staining and incubated for one hour at room temperature. pATM foci were quantified as described in our previous studies (Michel *et al.*, 2019a). In short, NPCs were imaged on a fluorescent EVOS Microscope and analyzed through a Cell Profiler (Broad Institute) pipeline that (1) isolates channels from an RGB image, (2) identifies the nuclei, (3) identifies foci within the nucleus, and (4) quantifies the number of foci per nucleus

Western Blots

NPCs were dissociated with Accutase, pelleted, flash frozen with liquid nitrogen, and stored at -80°C. Cells were lysed with 2x Laemmli buffer (4% SDS, 10% 2-mercaptoethanol, 20% glycerol, .004% bromophenol blue, 0.125M Tris HCl, pH 6.8) and boiled for 10 minutes at 95°C. For immunoblotting, total cell lysate was resolved by 4-15% Mini-PROTEAN precast gradient gel (Biorad). Proteins were transferred to a .2μm nitrocellulose membrane for 90 minutes at 100V and incubated at room temperature for 1 hour in blocking buffer (1% Fish Gelatin (Sigma) in TBS-T (Tris-buffered Saline .1% Tween-20)). The blots were incubated at 4°C overnight in blocking buffer in primary antibody and incubated for 45 minutes at room temperature in secondary antibody. Blots were visualized on a Licor Odyssey Imaging System. All gels were run with a positive control (High dose CPT treated HEK 293T cells). Differences in abundance of protein in loading controls (αtubulin, actin, β-catenin) between samples exposed to genomic stress were observed; therefore, samples were normalized by loading equivalent protein (30μg) in each lane (as determined through BCA assay).

Single-cell RNA sequencing

NPCs were exposed to either 400nM APH, 300nM CPT, DMSO (control), or no treatment for 24 hours. High viability cell samples collected for scRNA-seq using the 10x Genomics V2 Kit for reverse transcription and library preparation. Sequencing was performed on the Next-seq 500 and FASTQ files were run

through the cellranger pipeline and further analyzed through loupe browser software and software packages in R program. Gene ontology analysis was performed using Panther. scRNA-seq data can be accessed at the NCBI Sequence Read Archive (SRA), accession number: PRJNA591220.

p53 Knockdown Neurons

hiPSC-derived NPCs were transfected with a lentivirus containing a puromycin resistant plasmid containing a vector backbone control (pLKO.1) or p53 shRNA containing plasmid (AddGene). After 24 hours of exposure to the lentivirus, NPCs were changed to normal NPC media for 24 hours and puromycin selection for 4 days at 0.4µg/mL. Knockdown efficiency was confirmed with Western Blot.

Cell Counts

Cell counts were performed for every sample to quantify the number of cells remaining in culture and accurately add the appropriate dilution of antibody for flow cytometry experiments. NPCs and Neurons were dissociated with accutase, spun down, and filtered through a 40µm strainer into fixative solution (2% PFA in PBS) to obtain single cell suspensions. Cells were then counted using an automated Cell Countess system (Thermo Scientific).

Flow Cytometry and Imaging Flow Cytometry

NPCs and Neurons were collected, fixed, and stained for flow and imaging cytometry as outlined in detail in our previous study (Michel *et al.*, 2019a). Samples were stored at 4°C in the dark until they were run through the Imagestream Mark II System (Amnis Inc/Luminex Corp.) or a Cytek modified FACSCalibur™ cytometer. Single stain controls were used for compensation and gating was determined through fluorescence minus one (FMOs) controls and isotype controls. For flow cytometry experiments gating and analysis were performed using FCS Express 6 (DeNovo Software). Imaging flow cytometry data were analyzed using IDEAS® software (version 6.2). γH2AX foci were quantified using an efficient foci pipeline and masking strategy (Bourton *et al.*, 2012; Michel *et al.*, 2019a). Cell

cycle statistics were acquired using *Modfit* software. See supplemental information for more details on cytometry methods.

Genome-wide break mapping and sequencing

Detection of DNA breaks (DSBCapture) was performed as previously described (Lensing *et al.*, 2016). Briefly, fixed nuclei of the $p53^{KD}$ and the control samples of NPC 9429 were subjected to blunting/A-tailing reactions, and Illumina P5 adaptor ligation to capture broken DNA ends. Genomic DNA was then purified and fragmented by sonication, and subsequently ligated to Illumina P7 adaptor, and the libraries were PCR-amplified for 15 cycles. Prepared libraries were then subjected to whole-genome, 75-bp and 150-bp paired-end sequencing with the Illumina NextSeq 500 and the HiSeq X Ten platforms, respectively. Two biological duplicates were performed for each samples (TableS1).

DNA DSB read processing

Sequencing reads were aligned to the human genome (GRCh38/hg38) with bowtie2 (Langmead & Salzberg, 2012)(v.2.3.4.1) aligner running in high sensitivity mode. Restriction on the fragment length from 100 nt to 2000 nt (-X 2000 -I 100 options) was imposed. Unmapped, non-primary, supplementary and low-quality reads were filtered out with SAMtools (Li *et al.*, 2009)(v. 1.7) (-F 2820). Further, PCR duplicates were marked with picard-tools (v. 1.95) MarkDuplicates, and finally, the first mate of non-duplicated pairs (-f 67 -F 1024) were filtered with SAMtools for continued analysis. For each detected break, the most 5' nucleotide of the first mate defined the DNA break position. Downstream data analysis following DNA DSB read processing has been performed with BEDtools (Quinlan & Hall, 2010)(v. 2.27.1) and standard Linux commands to compute coverages. Results were visualized in Python3 (v. 3.6.5) with matplotlib (v. 2.2.2), numpy (van der Walt, Colbert, & Varoquaux, 2011) (v. 1.15.0), pandas (Hunter, 2007)(v. 0.23.3), and R statistical software (v.3.4.4). DNA DSB mapping data can be accessed at the NCBI Sequence Read Archive (SRA), accession number: PRJNA591220.

DNA DSB Gene Analysis

2500 genes had >2-fold enrichment per transcription start site (TSS) in p53KD NPCs. To examine genes with the highest levels of DNA DSB the top 50 genes were examined using Panther for gene function and GeneCard for clinical risk/association. The genes were further categorized based on clinical risk and disease type.

Statistical Analyses

For all experiments, data are shown as mean +/- standard error of the mean of three to six biological replicates per cell line. Statistical significance was determined by using an unpaired t-test, one-way ANOVA and Dunnett post hoc test for differences, or two-way ANOVA when applicable with a Sidak Multiple Comparison Test. DNA DSBs were plotted as stacked histograms and analyzed using a contingency table and the Chi-squared test.

Supplemental Experimental Procedures

Flow Cytometry

Flow cytometry was conducted on a Cytek modified FACSCalibur™ using the 488 Blue, 637 Red, and 407 Violet lasers to excite Ki-67 (PE), emission collected with a 580/20 filter, γH2AX (AlexaFluor 647) with a 661/16 filter, and DAPI with a 450/50 filter respectively. 15,000 cells were collected per sample at low pressure. Single stain controls were used for compensation and gating was determined through fluorescence minus one (FMOs) controls, isotype controls, and unstained controls. FCS Express 6 (DeNovo Software) was used to perform gating and analysis. Cell cycle was analyzed using statistical modelling from the program *Modfit*.

Imaging Flow Cytometry

Imaging flow cytometry (IFC) was performed using the Imagestream Mark II System (Amnis Inc/Luminex Corp.). Cells were collected, using INSPIRE® software, for 10 minutes or until 10,000 cells were acquired. Following excitation with the 405nM laser at a power of 50mW, the 488nM laser at a power of 200mW, the 561nM laser at a power of 100mW, and the 642nM laser at a power of 150mW, all cells were captured with 60x magnification (Numerical Aperture 0.9) using the enhanced depth field optic (EDF) at low speed (60mm per second) with an average rate of ~10 cell images per second. Emitted light was collected using the following filters: Channel 1 (Camera 1 420-480nm) and 9 (Camera 2 570-595nm) for brightfield (BF), channel 2 (Camera 1 480-560nm) for Alexa Fluor 488, channel 3 (Camera 1 560-595nm) for phycoerythrin (PE), channel 5 (Camera 1 660-740nm) for PerCP Cy5.5, channel 7 (Camera 2 420-505nm) for DAPI, and channel 11 (Camera 2 660-740nm) for AlexaFluor 647. All data were analyzed using IDEAS® software (version 6.2).

Image Compensation

Image compensation was conducted on samples that were exposed to CPT prior to being stained because they had the brightest H2aX foci. Cells stained with only DAPI, Tuj1-Alexa Fluor 488, H2AX-Alexa Fluor 647, Nestin-PerCP Cy5.5, and Active Caspase 3-PE were collected without BF illumination or Scatter and IDEAS® 6.2 was used to generate the compensation matrix.

Analysis of Cell Images and Calculation of Foci Number

Cells treated with CPT were analyzed first to determine a masking strategy and calculate foci number since they had the brightest and highest number of foci. The optimal fluorescence display for fluorescence imagery was determined by adjusting the image gallery properties in a linear fashion and applied to all images. To analyze the cells several steps and gating strategies were employed based on IDEAS® 6.2 software and incorporated wizards. The gates were created using the polygon gating tool and determined based on FMOs. The number of γH2AX foci were quantified using a series of masks and quantification tools that were first tested on cells with brightest foci to ensure accurate foci counts and then applied in to all samples and respective raw data files in batch processing.

Chapter IV

p53 and the Neuroinflammatory Response to Genomic Stress

Abstract

The origins of sporadic neurodegenerative disease are incompletely understood. Rare familial early-onset cases implicate specific genes in Alzheimer's (AD), Parkinson's (PD), and other neurodegenerative diseases. However, several lines of recent evidence indicate that the accumulation of somatic mutations during development and through adulthood can compromise subpopulations of neurons to initiate neurodegeneration. First, rapid proliferation of progenitor cells during development, a high transcriptional burden throughout life, imperfect DNA repair, and a long neuronal lifespan predispose the brain to somatic mutations (McConnell *et al.*, 2017). Second, somatic single nucleotide variants (SNVs) accumulate in neurons (M. A. Lodato *et al.*, 2018). Hundreds are observed in young neurons, but thousands are observed in aged neurons (M. A. Lodato *et al.*, 2018). Third, somatic pseudogene-like accumulation of APP transcript-derived genomic retro insertions are observed more frequently in AD patient neurons than in disease-free individuals (Bushman *et al.*, 2015). Fourth, our laboratory has recently found that neurons harboring megabase copy number variants are selectively vulnerable to aging-related depletion (W. D. Chronister *et al.*, 2019). These lines of evidence motivate our central question. Does genomic stress during brain development and maturation promote somatic mutations in subsets of mature neurons and, in turn, neurodegenerative phenotypes in the aging brain? p53, the guardian of the genome, is an ideal protein to study in the context of neurodevelopmental stress and neuroinflammation as it is known to eliminate NPCs harboring DNA DSBs. Our current studies suggest that p53 may play a unique role in the cytokine response to genomic stress through the increased secretion of Fractalkine and other chemokines. Our single-cell RNA sequencing of aged neurons reveals that approaches for collecting older hiPSC-derived neurons require further optimization.

Introduction

Excessive accumulation of DNA damage is a common pathological feature among neurodegenerative diseases including Alzheimer's disease (Coppede & Migliore, 2009; Lovell & Markesbery, 2007), Parkinson's disease (Ogino *et al.*, 2016; Sepe *et al.*, 2016), and Amyotrophic lateral sclerosis (ALS)(Coppede, 2011; Martin, 2008). It is also known that genomic stress, which often leads to oxidative damage, plays a role in aging and neurodegeneration because it contributes to the accumulation of DNA damage (McKinnon, 2017). Previously, studying aging in the human brain has been incredibly challenging; post-mortem tissue is difficult to acquire and is not amenable to longitudinal studies. Additionally, studies of aging have typically looked at model organisms later in life, meaning that few have assessed how stress exposure impacts the development of the brain and how that ultimately could impact the aging process and predisposition to neurodegeneration.

With the development of human-induced pluripotent stem cells (hiPSCs)(Takahashi *et al.*, 2007), we now have an *in vitro* model of human neurodevelopment that provides a tool to study models of normal and pathological neurodevelopment. hiPSCs provide a unique, longitudinal, human platform to determine if neurodevelopmental events can set the stage for neurodegeneration in later life. Familial AD and PD mutations lead to relevant neurodegenerative phenotypes in hiPSC-derived neurons. The accumulation of DNA damage from ongoing genomic stress is both a major somatic mutagen and a shared pathological feature among neurodegenerative diseases (Alzheimer's disease(Bushman *et al.*, 2015; Lovell & Markesbery, 2007), Parkinson's disease(Ogino *et al.*, 2016; Sepe *et al.*, 2016)) and normal aging (Chow & Herrup, 2015). Notably, hiPSC models of AD and PD exhibit neuroinflammatory phenotypes like those seen in patients (Kim *et al.*, 2015; Sommer *et al.*, 2018).

p53, traditionally studied in cancer biology, has been observed to play a role in mediating pathways underlying neurodegenerative disease. p53 activity can lead to a pro-inflammatory phenotype (Jayadev *et al.*, 2011) and neurodegeneration (Davenport, Sevastou, Hooper, & Pocock, 2010). p53 activation is a precursor of

the synaptic degeneration observed in the early stages of neurodegenerative disease (Conforti, Adalbert, & Coleman, 2007). A study examining rat microglial found that increased p53 activity in microglia led to a significant reduction of synaptic markers and an increase of microglial secretion of inflammatory cytokines (Jebelli, Hooper, & Pocock, 2014).

In the following studies we sought to determine how downregulation of p53 altered cytokine secretion in neurons and astrocytes exposed to genomic stress. Furthermore, we aimed to assess which neuronal cell types were secreting inflammatory cytokines through single-cell RNA sequencing. Our goal was to identify whether genomic stress or p53 altered the inflammatory phenotypes and diversity of neurons, predisposing neurons for degeneration. Our results indicate that regardless of genomic stress exposure, p53 has an effect on cytokine secretion but ongoing work is needed to optimally decipher cell types in older hiPSC-derived neurons.

Results

$p53^{KD}$ Neurons Have Unique Cytokine Secretion

To determine whether lower levels of p53 led to an alteration in the patterns of cytokine and chemokine secretion in cortical neurons, hiPSC-derived neurons were cultured for 8 weeks. Media was collected from these samples and cytokine secretion was quantified using the Human Luminex Assay. 38 cytokines and chemokines were tested but only four factors had significantly more secretion in $p53^{KD}$ neurons: interferon alpha 2 (IFNα2), human growth regulated oncogene (GRO), vascular endothelial growth factor (VEGF), and fractalkine (Figure 1A-D).

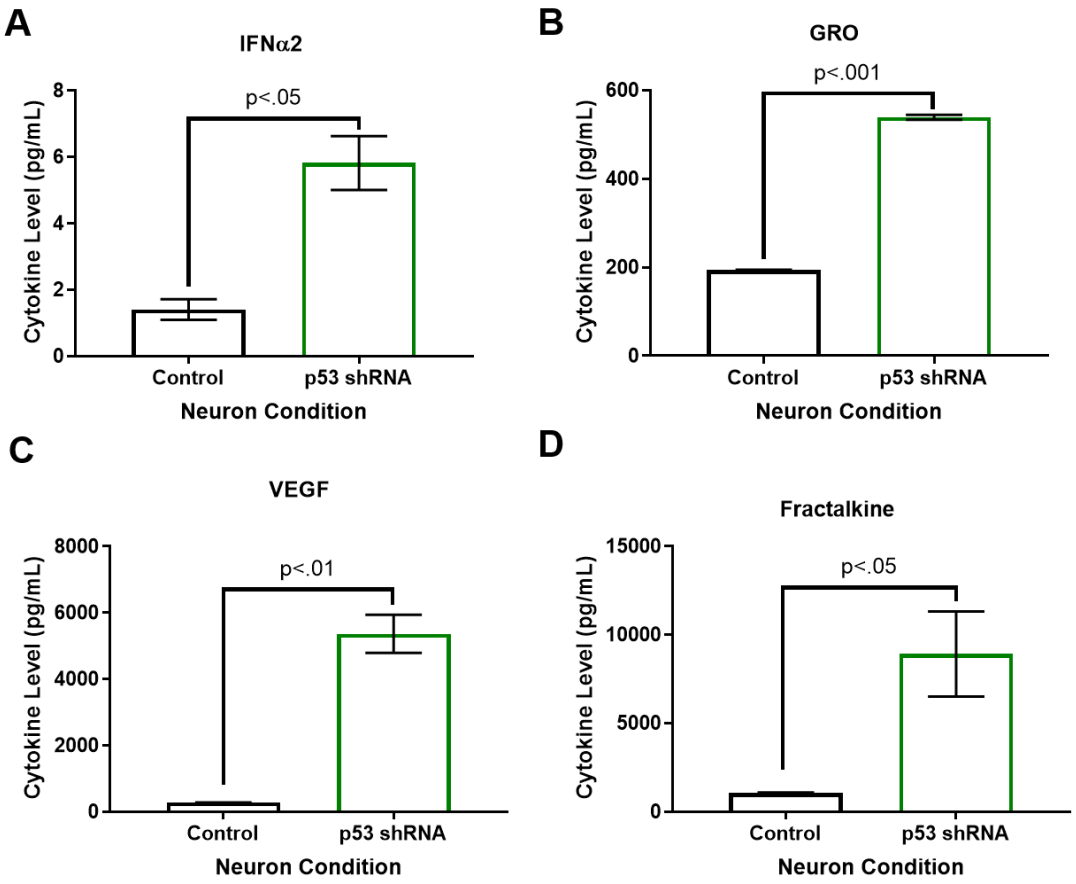

Figure 1. Chemokine Secretion in p53^{KD} hiPSC Neurons. (A) Media collected from 8-week cultures of hiPSC-derived neurons reveal increased IFNα2 secretion in p53^{KD} neurons compared to controls (unpaired t-test, p<.05). (B) p53^{KD} neurons also had increased secretion of GRO (unpaired t-test, p<.001), (C) VEGF (unpaired t-test, p<.01), and (D) Fractalkine (unpaired t-test, p<.01).

Fractalkine Levels Increased in Stressed NPCs

We found the increased level of Fractalkine (FKN) secretion particularly interesting in $p53^{KD}$ neurons because p53 binds directly to fractalkine as a transcription factor and p53 has been proposed to act through immunosurveillance to prevent cells from transforming into malignant cells (Shiraishi *et al.*, 2000). With the knowledge from our previous studies that genomic stress, particularly transcriptional stress from CPT activates p53, we wanted to determine if changes in FKN levels could be observed in NPCs. NPCs were exposed to 24 hours of genomic stress through treatment with DMSO control, Aphidicolin (APH), or Camptothecin (CPT). Stressed NPCs showed a trend of increased FKN (CX3CL1) (Figure 2A-D), however due to low cells numbers from immunostaining and manual counts, the increase was not significant. To address this issue, we turned to a more robust technique, flow cytometry. Genomic stress was validated through flow cytometry which showed increased levels of DNA DSBs in stressed NPCs (Figure 2E). Furthermore, the NPCs were arrested in S-phase due to DNA DSBs (Figure 2F), and stressed cells had greater levels of cell death (Figure 2G). From our previous experiment using immunocytochemistry, we were cognizant that the anti-CX3CL1 antibody had significant background. Consequently, we measured the level of FKN by quantifying the mean fluorescent intensity, a more sensitive metric to detect a shift in levels of FKN. We observed an increase in FKN in both stress conditions (Figure 2H).

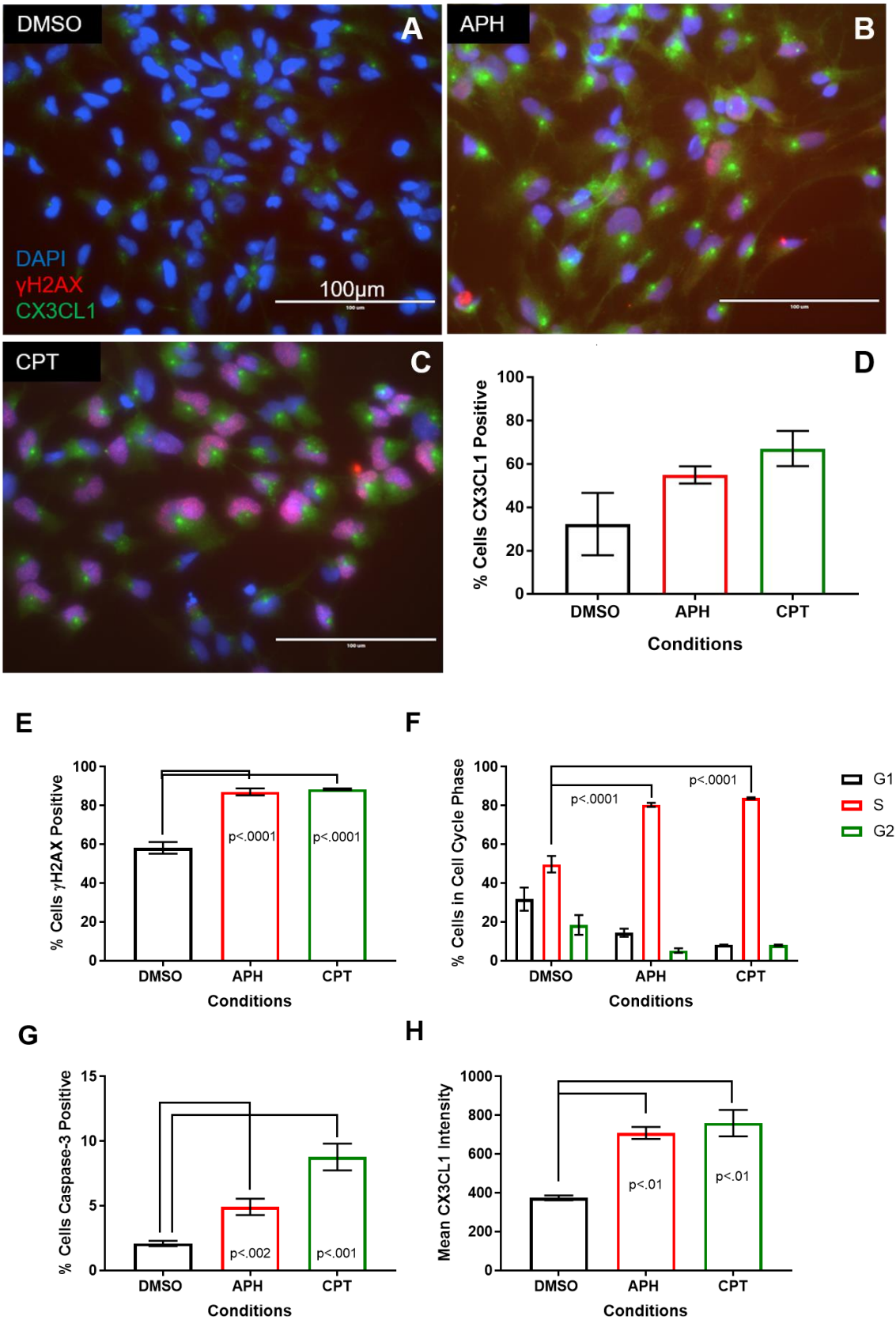
DMSO
A
DAPI
γH2AX
CX3CL1
100μm
APH
B
CPT
C
D
% Cells CX3CL1 Positive
100
80
60
40
20
0
DMSO
APH
CPT
Conditions
E
% Cells γH2AX Positive
p<.0001
p<.0001
F
% Cells in Cell Cycle Phase
p<.0001
p<.0001
G1
S
G2
G
% Cells Caspase-3 Positive
15
10
5
p<.002
p<.001
H
Mean CX3CL1 Intensity
1000
800
600
400
200
p<.01
p<.01

Figure 2. Fractalkine Levels Increase in Stressed NPCs. NPCs were treated with chemicals to induce genomic stress for 24 hours. (A) Cells were either exposed to a vehicle control (DMSO), (B) replication stress (APH), (C) or transcriptional stress (CPT). (D) NPCs exposed to stress trended toward an increase in FKN (One-way ANOVA, Tukey's Test, not significant, $p>.07$). NPCs were treated as previously described and collected for flow cytometry. (E) Stressed cells had more DNA DSBs (Two-way ANOVA, Tukey's Test, $p<.0001$), (F) more cell cycle arrest in S-phase (Two-way ANOVA, Tukey's Test, $p<.0001$), (G) increased caspase-3 positive cells (Two-way ANOVA, Tukey's Test, APH $p<.002$, CPT $p<.001$), and (H) increased levels of FKN compared to control NPCs (Two-way ANOVA, Tukey's Test, $p<.01$).

Genomic Stress Does Not Alter Cytokine Secretion But p53 Does

Since one of the four cytokines with greater secretion (Figure 1) showed an increase with genomic stress, we wanted to determine whether we could detect an increase in several other cytokines in neurons that were stressed as progenitor cells. Essentially, we sought to examine whether exposure to stress as a progenitor predisposed NPCs to inflammatory phenotypes. We exposed two neurotypic cell lines to genomic stress and collected media after 4-8 weeks in culture. While both cell lines had an increase in VEGF secretion in $p53^{KD}$ neurons, only one cell line maintained the increase in FKN observed earlier (Figure 3A), and the other had an additional increase in IL-8 and GRO (Figure 3B). Both cell lines lacked a consistent effect of genomic stress on cytokine secretion, with the exception of VEGF in CPT treated $p53^{KD}$ neurons (Figure 3B).

Different Cytokines and Chemokines Secreted from hiPSC-derived Neurons and Astrocytes

Typically, neurons are not the primary cells secreting cytokines in the brain. Microglia and astrocytes interact more with immune cells and thus are the primary secretors. To examine if genomic stress potentially altered astrocytes we derived astrocytes from the same NPCs used to make neurons (Figure 3B), and collected them after 4 weeks in culture. Although there was no effect of genomic stress on the secretion pattern of astrocytes, we observed distinct secretory phenotypes in neurons compared to astrocytes. Specifically, high secretion of GRO and IL-8 which was lower in neurons, and increased FKN and VEGF in neurons which was lower in astrocytes (Figure 3C).

A

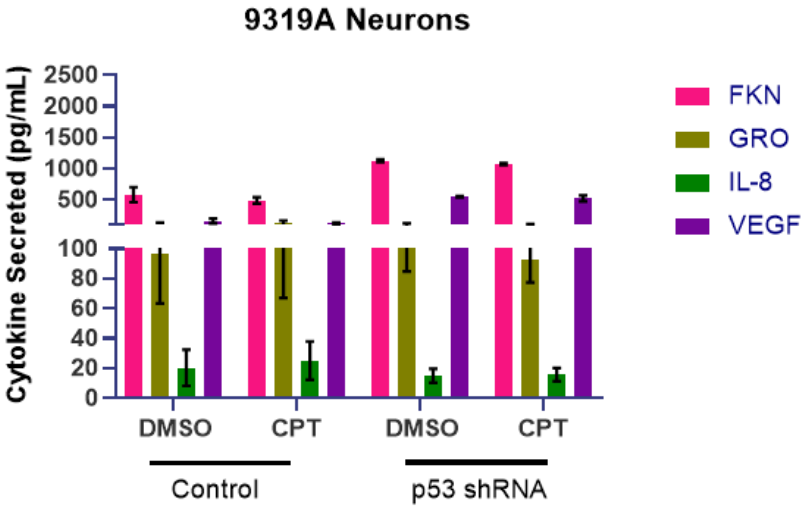
9319A Neurons
Cytokine Secreted (pg/mL)
2500
2000
1500
1000
500
100
80
60
40
20
0
DMSO
CPT
DMSO
CPT
Control
p53 shRNA
FKN
GRO
IL-8
VEGF

B

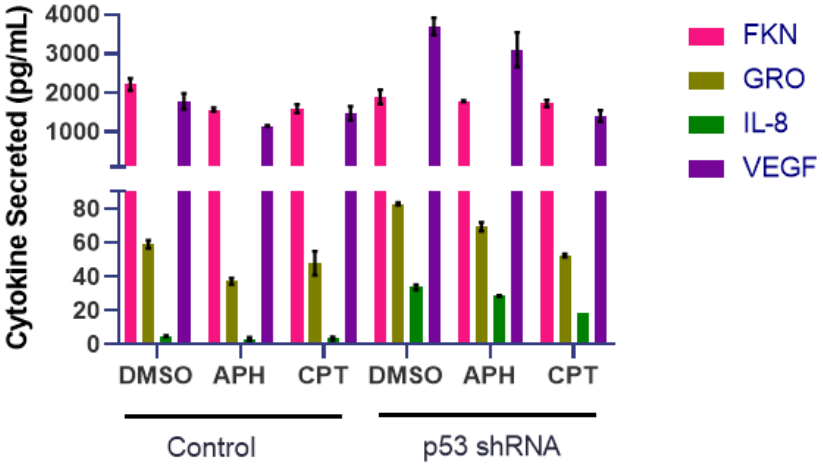
9429 Neurons
Cytokine Secreted (pg/mL)
4000
3000
2000
1000
80
60
40
20
0
DMSO
APH
CPT
DMSO
APH
CPT
Control
p53 shRNA
FKN
GRO
IL-8
VEGF

C

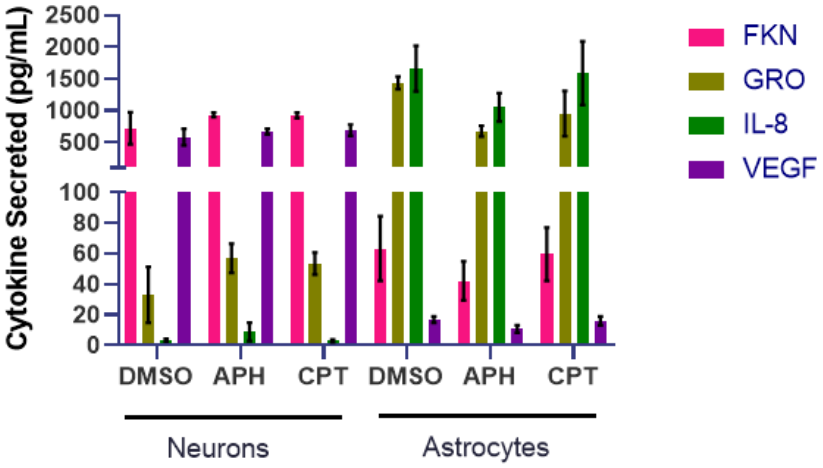
9429 Neurons and Astrocytes
Cytokine Secreted (pg/mL)
2500
2000
1500
1000
500
100
80
60
40
20
0
DMSO
APH
CPT
DMSO
APH
CPT
Neurons
Astrocytes
FKN
GRO
IL-8
VEGF

Figure 3. Cytokine Secretion in Stressed Neurons and Astrocytes. Neurons and astrocytes were cultured for 4-8 weeks and collected media was analyzed for cytokine and chemokine secretion using the Human Luminex Assay. Error bars are standard error of the mean from two biological replicates. (A) $p53^{KD}$ 9319A Neurons had greater FKN secretion (Two-way ANOVA, Tukey's Test, $p<.0001$) and VEGF secretion (Two-way ANOVA, Tukey's Test, $p<.001$). Stress (CPT) had no effect on cytokine secretion within control or $p53^{KD}$ neurons. (B) $p53^{KD}$ 9429A Neurons had greater VEGF secretion (Two-way ANOVA, Tukey's Test, $p<.0001$) and a slight decrease in FKN secretion in control stressed neurons (Two-way ANOVA, Tukey's Test, $p<.05$). (C) 9429A Neurons had greater FKN secretion than 9429A Astrocytes (Two-way ANOVA, Tukey's Test, $p<.05$). 9429A Neurons had less GRO secretion than 9429A Astrocytes (Two-way ANOVA, Tukey's Test, $p<.01$). 9429A Neurons had less IL-8 secretion than 9429A Astrocytes (Two-way ANOVA, Tukey's Test, $p<.01$). 9429A Neurons had greater VEGF secretion than 9429A Astrocytes (Two-way ANOVA, Row Effect, $p<.01$). Stress (CPT or APH) had no effect on cytokine secretion within astrocytes or neurons.

Single-cell RNA Sequencing of hiPSC-derived Neurons

6-Week and 12-week neurons were collected for ssRNA-seq using the 10x genomics platform. Initially the neurons showed a standard number of genes being expressed (Figure 4A), however upon further transcriptional QC validation, the neurons had a significant percent of mitochondrial genes being expressed (Figure 4B). On average the majority of cells had ~30% mitochondrial RNA expression (Figure 4C). Further data analysis was conducted to examine whether genomic stress of p53 altered cell type diversity in neurons. The only distinguishable difference in cell type was a decrease of AQP4, an astrocytic marker, in $p53^{KD}$ neurons compared to controls (Figure 5A, 5B). To examine whether genomic stress or p53 altered cytokine and chemokine expression levels, the expression of several factors that were observed in the human luminex assay (Figure 3) were further assessed. No observable changes were present in GRO, IL8, and IL15 but VEGF was present in 6-week neurons and in 12-week neurons, $p53^{KD}$ neurons had a higher percent of cell expression of FKN than controls.

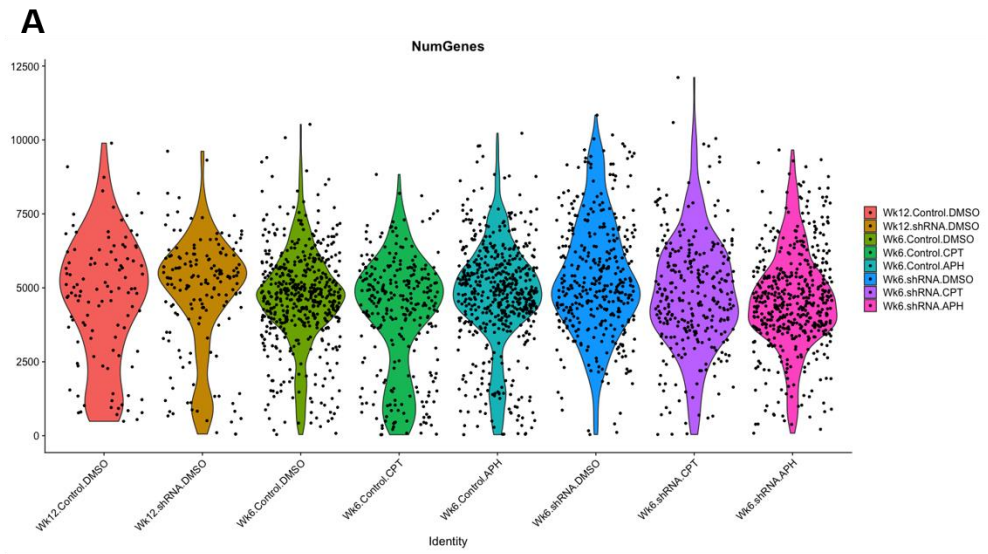
A
NumGenes
12500
10000
7500
5000
2500
0
Wk12.Control.DMSO
Wk12.shRNA.DMSO
Wk6.Control.DMSO
Wk6.Control.CPT
Wk6.Control.APH
Wk6.shRNA.DMSO
Wk6.shRNA.CPT
Wk6.shRNA.APH
Identity

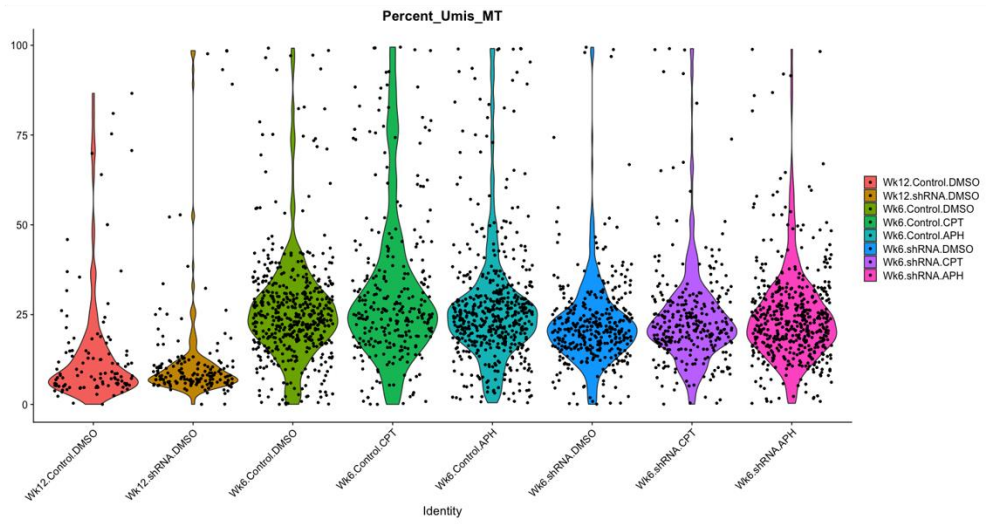
B
Percent_Umis_MT
100
75
50
25
0
Wk12.Control.DMSO
Wk12.shRNA.DMSO
Wk6.Control.DMSO
Wk6.Control.CPT
Wk6.Control.APH
Wk6.shRNA.DMSO
Wk6.shRNA.CPT
Wk6.shRNA.APH
Identity

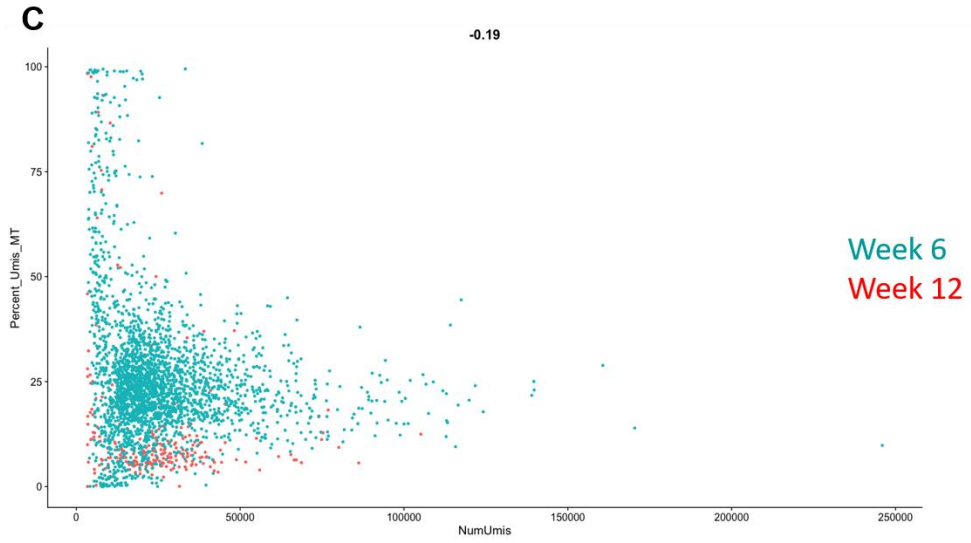
C
-0.19
Percent_Umis_MT
100
75
50
25
0
0
50000
100000
150000
200000
250000
NumUmis
Week 6
Week 12

Figure 4. ssRNA-seq Neurons Express Mitochondrial Genes. To determine whether cells remained viable during ssRNA-seq the percentage of mitochondria genes expressed were calculated. (A) A violin-plot shows the total number of genes expressed per cell. Cell counts are as follows: Wk12.Control. DMSO = 109, Wk12.shRNA. DMSO = 165, Wk6.Control. DMSO = 517, Wk6.Control.CPT = 285, Wk6.Control.APH = 544, Wk6.shRNA. DMSO = 371, Wk6.shRNA.CPT = 295, Wk6.shRNA.APH = 486. (B) A violin-plot of the percent of mRNA transcripts that were mitochondrial. (C) A scatter plot of percent mitochondrial transcripts versus number of total number of transcripts, most cells demonstrate ~25% mRNA transcripts.

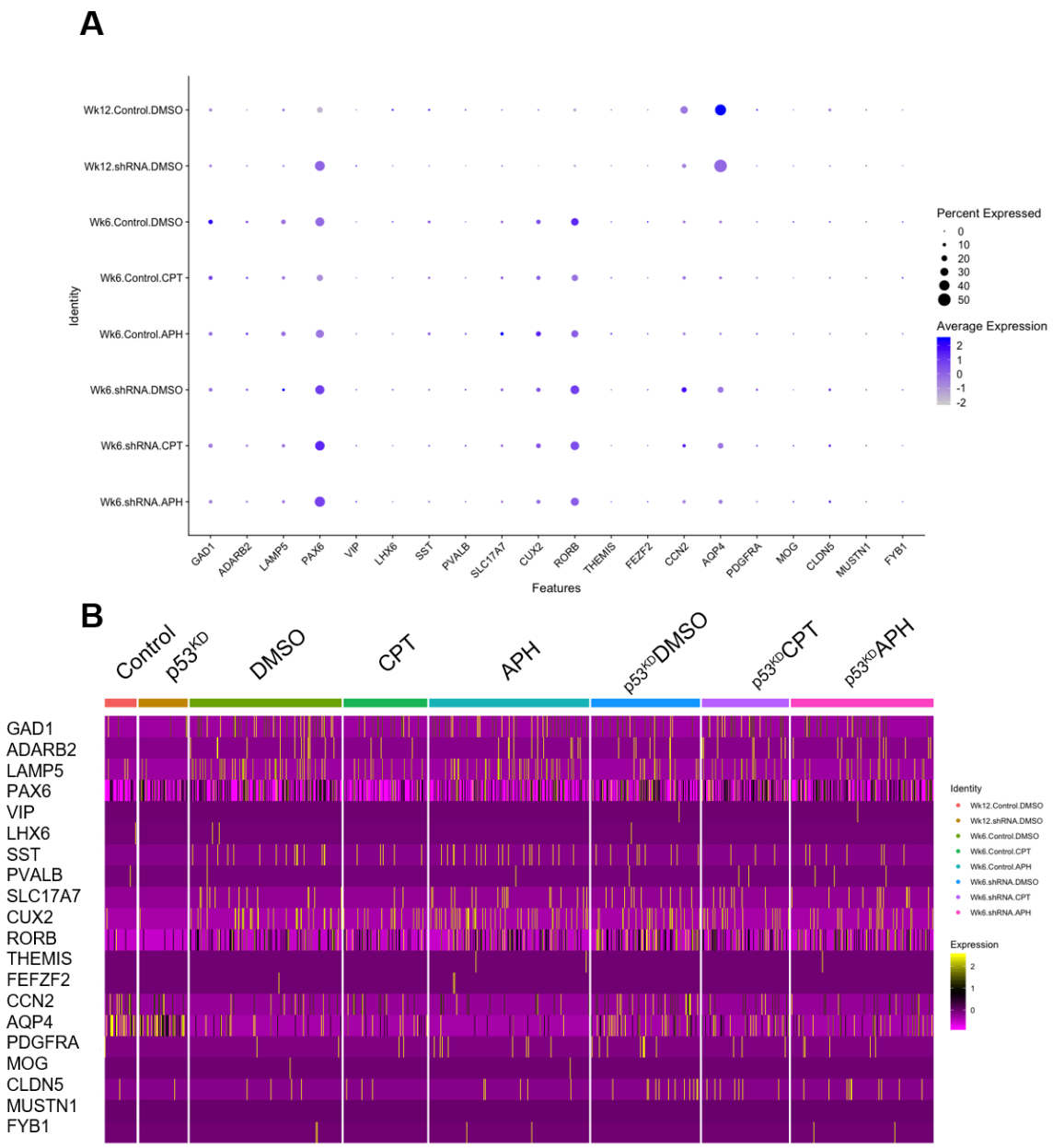

Figure 5. Increased Astrocyte Expression in p53^{KD} Neuronal Cultures.

Figure 5. Increased Astrocyte Expression in p53^{KD} Neuronal Cultures. Transcriptomic data from 6-week and 12-week control and p53^{KD} neurons. Genes listed are different cortical identity markers and neuronal cell types markers. (A) Dot plot of hiPSC-derived neurons. Size indicates number of cells that express a specific gene and color indicates the level of expression. More control 12-week neurons express AQP4 (astrocyte marker) than p53^{KD} neurons. (B) Heatmap of gene expression levels in different cells for various neuronal identity markers.

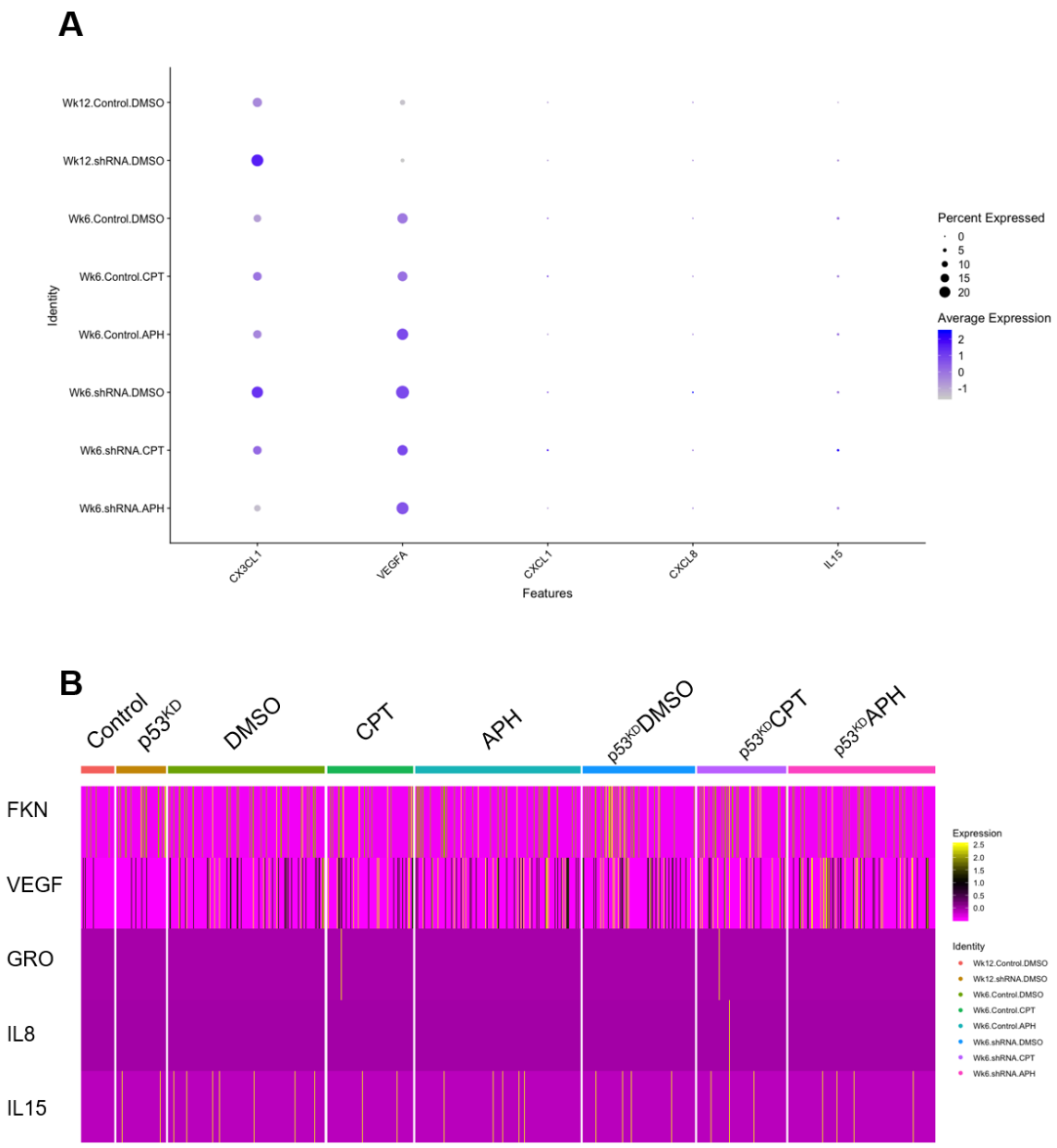

Figure 6. Increased Expression of Fractalkine and VEGF in p53^{KD} Neurons.

Figure 6. Increased Expression of Fractalkine and VEGF in p53^{KD} Neurons. Transcriptomic data from 6-week and 12-week control and p53^{KD} neurons. Genes listed are different cytokines and chemokines included in the Human Luminex Assay Experiments. (A) Dot plot of hiPSC-derived neurons. Size indicates number of cells that express a specific gene and color indicates the level of expression. More p53^{KD} neurons express CX3CL1 (Fractalkine) than control 12-week neurons. (B) Heatmap of gene expression levels in different cells for CX3CL1, VEFA, CXCL1, CXCL8, and IL-15.

Discussion

In these studies, we sought to examine whether p53 played a role in neuroinflammatory phenotypes observed in neurodegenerative disease (Becher, Spath, & Goverman, 2017). We first observed whether cytokine secretion profiles change in the absence of p53. The most striking result was a marked increase in VEGF, GRO, IFNα2 and FKN (Figure 1). Fractalkine expression has been observed in neurons, and it is shown to play a variety of roles by protecting neurons from inflammation by controlling microglial activation, and in other instances exacerbating the inflammatory response in neurodegeneration (Hatori, Nagai, Heisel, Ryu, & Kim, 2002; Sheridan & Murphy, 2013; Sokolowski, Chabanon-Hicks, Han, Heffron, & Mandell, 2014). Although previous studies have assessed FKN in the context of stroke and degeneration, we decided to further examine the role of FKN in response to genomic stress.

Our data led to two seemingly contradictory results. $p53^{KD}$ neurons secret more FKN and yet in genomic stress, particularly transcriptional stress when p53 is activated, we observed higher levels of FKN. It is very possible that the higher secretion levels of FKN in $p53^{KD}$ cultures does not actually indicate higher levels of expression. When plated at the same density, $p53^{KD}$ cultures generate at least twice as many neurons (Chapter III), which indicates that the $p53^{KD}$ cultures may be secreting less FKN if the secretion increases by two-fold but the cell number has increased by four-fold. To truly understand this mechanism, one would need to normalize cell number between cultures and investigate whether individual neurons could be secreting more chemokine or if the increase in cell number accounts for the increase in secretion.

A model in which p53 is activated in response to genomic stress, leading to more neuronal FKN secretion and potential induction of cell death by microglial is highly plausible as a mechanism of immunosurveillance. In order to investigate this hypothesis more thoroughly, microglial should be included in the neuronal cultures. With newly emerging protocols to create hiPSC-derived microglia (Abud *et al.*, 2017), this hypothesis can be tested.

Several studies have demonstrated that cytokine and chemokine signaling is highly active during early brain development (Meyer, Feldon, & Yee, 2009). IL-1β and IL-6 have been observed to increase during distinct neurodevelopmental stages (Bilbo & Schwarz, 2009; Dziegielewska *et al.*, 2000); cytokines are also linked to the development of autism and schizophrenia (Meyer, Feldon, & Dammann, 2011). Surprisingly, we observed little to no IL-1β and IL-6 secretion in our neurons, however it remains possible that the expression of these cytokines happens at discrete stages in development. Another possibility is that a lack of microglial and low percentages of astrocytes in the hiPSC-derived neuronal cultures led to minimal secretion of these cytokines. Microglial and astrocytes are two cell types that both secrete and respond to the vast majority of cytokines and chemokines in the brain (Jack *et al.*, 2005; Meeuwsen, Persoon-Deen, Bsibsi, Ravid, & van Noort, 2003).To investigate whether this was the case, we derived astrocytes from our NPCs and quantified their cytokine secretion. However, we still observed minimal levels of IL-1β, TGFβ and IL-6.

We did however, observe an inverse relationship between astrocytes and neurons for the following cytokines and chemokines: IL-8, GRO, VEGF, and FKN. Astrocytes secreted higher levels of IL-8 and GRO while neurons secreted more VEGF and FKN. Most of these cytokines have been observed to play a role in the pathogenesis of a variety of brain disorders: IL-8 levels are altered in schizophrenia (An *et al.*, 2015; Brown *et al.*, 2004), VEGF is associated with cognitive aging and Alzheimer's disease (Mahoney *et al.*, 2019), and FKN is linked to Alzheimer's disease and other neurodegenerative disorders (Finneran & Nash, 2019; Sheridan & Murphy, 2013). VEGF was increased in both of the neurotypic cell lines (Figure 3A, 3B). Given the connection between VEGF and cognitive aging, which is exacerbated by DNA damage accumulation (Chow & Herrup, 2015); VEGF is an ideal cytokine for follow up studies on neuroinflammation and genomic stress.

To examine the effect of genomic stress and p53 on neuronal diversity we used ssRNA-seq. Our preliminary data from the ssRNA-seq data demonstrate that p53 may decrease astrocyte differentiation and drive chemokine secretion. Follow up

studies will be needed to reiterate this finding and further examine the biological significance of these results. ssRNA-seq proved to be a challenging approach for a variety of reasons. Collecting a high viability single-cell suspension of older neurons is difficult due to the interconnectivity of the neurons. Unfortunately, the most viable samples (>95%) still contained a significant percent of mitochondrial RNA which indicates that the cells were dying during the first stage of capturing transcripts. This approach could be improved by preparing cells in methanol and fixing them before processing rather than processing live cells which are more unstable (Alles *et al.*, 2017). In our analysis of chemokines and cytokines it became clear that these small molecules are expressed in gene families and have high levels of post-translational modifications, complicating the transcript detection. This issue could be avoided if protein is quantified in lieu of transcripts. Mass cytometry, a high through-put flow cytometry approach in which up to 80 antigens can be detected at once, could be employed as an alternative means to answer the question of cell type diversity (Bandura *et al.*, 2009; Pruszak *et al.*, 2007; Zunder *et al.*, 2015).

Our study indicates many more studies will be necessary to truly dissect the role that genomic stress and p53 could play in neuroinflammation and consequent brain disease. Follow up experiments could include stressing NPCs (in p53 competent and deficient cells) and observing cytokine secretion immediately after treatment. It is possible the dynamics in cytokine release happen quickly and observing neurons several weeks after initial stress is too far along the process. While these studies do not concretely clarify a role for p53 and genomic stress in neuroinflammation, they suggest that neurons and astrocytes have distinct cytokine signatures. These experiments also provide insight into the challenges associated with studying neuroinflammation *in vitro* and highlight the barriers that must be addressed to do single-cell analysis of neuronal cultures.

Materials and Methods

Cell Culture

Fibroblasts from neurotypical individuals were reprogrammed to induced pluripotent stem cells using lentiviral vectors (9319, 9429). NPCs and neurons were generated following methods outlined by Brennand and Livesey (Brennand *et al.*, 2011; Y. Shi, Kirwan, & Livesey, 2012). Briefly, hiPSC-derived NPCs were plated on Matrigel and passaged 1:6 every four days. NPCs (<passage 14) were cultured in NPC medium (DMEM/F12 +Glutamax, 1x N2, 1X B27-Vitamin A, 1ug/ml Laminin, 20ng/ml FGF-2 and dissociated in Accutase for 5 min at 37°C. hiPSC-derived neurons were cultured on Matrigel in Neuron Medium (DMEM/F12 +Glutamax, 1x N2, 1X B27 with Vitamin A, 20ng/ml BDNF, 20ng/ml GDNF, 1mM dibutryl-cyclic AMP, and 200nM ascorbic acid. Neurons received half media changes once a week.

Astrocyte Differentiation

Astrocytes were derived using a protocol outlined by Brennand and colleagues (Tcw *et al.*, 2017) in which hiPSC-derived NPCs are differentiated into astrocytes in 30 days in commercially available astrocyte medium by ScienCell. NPCs were differentiated to astrocytes by seeding dissociated cells at 15,000 cells/cm^2 on Matrigel coated plates. After 24 hours the NPCs were permanently switched to astrocyte media. Astrocyte media contains 2% fetal bovine serum, astrocyte growth supplement, and 10U/ml penicillin/streptomycin solution. During the 30-day period of the hiPSC-NPCs growing in astrocyte media, they remain on Matrigel coated plates and get seeded at the same low density for every passage. After 30 days, the astrocytes are passaged 1:3 on gelatin coated plates.

p53 shRNA cell line confirmation

hiPSC-derived NPCs were transfected with a lentivirus containing a puromycin resistant plasmid containing a vector backbone control (pLKO.1) or p53 shRNA containing plasmid. After 24 hours of exposure to the lentivirus, NPCs were

changed to normal NPC media for 24 hours and puromycin selection for 4 days at 0.4µg/mL. Knockdown efficiency was confirmed with Western Blot.

Immunocytochemistry

NPCs were cultured for 24 hours with various drugs and rinsed with PBS. NPCs at ~80% confluency were fixed on 18mm glass coverslips with 4% PFA for 15 minutes at room temperature and rinsed (3 times for 5-minute washes) in PBS. Cells were permeabilized with .5% Triton-X 100 for 10 minutes and incubated in blocking buffer (2% BSA in PBS-T (.1% Triton-X 100)) for one hour at room temperature. The cells were probed overnight at 4°C with CX3CL1 (Fractalkine), DAPI, and γH2AX followed by labeling with secondary staining and incubated for one hour at room temperature. CX3CL1 positive cells were manually counted by a blinded researcher.

Flow Cytometry

NPCs were collected and processed for flow cytometry as described in Chapter III and IV (Michel *et al.*, 2019a). In short, samples were collected, fixed, and stained with antibodies for flow cytometry (Anti-γH2AX, Anti-CX3CL1, and Anti-Caspase-3). Samples were run through a CaliburA cytometer and analyzed using FCSExpress6 and Modfit for cell cycle analysis.

Human Luminex Assay

hiPSC-derived neurons and astrocytes were cultured for several weeks. Media from each cell type was collected and centrifuged at high speed to remove cellular debris. The supernatant was collected and stored at -80°C. Samples were tested for secreted cytokines and chemokines using the Human Luminex Assay kit (EMD Millipore). Both neurons and astrocytes were tested for the following molecules and peptides: EGF, Eotaxin, FGF-2, FLT-3L, IP-10, Fractalkine, GM-CSF, G-CSF, IFN-y, GRO, IL-1a, IFN-a-2, IL-10, IL-1ra, IL-12p40, IL-3, IL-12p70, IL-15, IL-13, MCP-1, IL-17a, MCP-1, IL-17a, MCP-3, IL-2, MDC, IL-4, MIP-1a, IL-5, MIP-1b, IL-

6, TNF-a, IL-7, sCD40L, IL-8, TGF-a, IL-9, TNF-b, VEGF, IL-1B. Technical replicates were pooled together.

Single-cell RNA Sequencing

NPCs were exposed to either 400nM APH, 5nM CPT, DMSO (control), or no treatment for 24 hours. High viability cell samples collected for scRNA-seq using the 10x Genomics V2 Kit for reverse transcription and library preparation. Sequencing was performed on the Next-seq 500. For each sequencing run, cellranger-count (Cell Ranger Version 3.1.0) was used to convert the raw BCL files from the Illumina run folders into FASTQ files. The FASTQ files were then aligned to the human genome assembly GRCh38.p12, and single-cell gene expression was quantified against the Gencode Human Release 31 primary assembly annotation set (Frankish *et al.*, 2019), using STAR-solo (Version 2.7.3a)(Dobin *et al.*, 2013). STAR-solo produced matrices of UMI counts per cell barcode per gene, which were loaded into R, and analyzed using Seurat (Butler, Hoffman, Smibert, Papalexi, & Satija, 2018). To evaluate cell viability, UMI counts per cell, detected genes per cell, and percentage of total UMIs mapping to mitochondrial genes were plotted, which showed a high level of mitochondrial gene expression in the majority of cells. To evaluate the distribution of cell identities across the sequencing runs, UMI counts were plotted for a collection of cell-type markers taken from the Allen Brain Atlas matrix of single-cell gene expression in the human cortex (Hodge *et al.*, 2019).

Chapter V

Conclusions, Perspectives, and Future Directions

As described throughout this dissertation, neurodevelopment is a complex process that lends itself to genomic stress and consequent DNA damage as evidenced by the presence of somatic mosaicism (McConnell *et al.*, 2017; Paquola *et al.*, 2017; Rohrback, Siddoway, *et al.*, 2018). The sheer number of neurons that need to be generated during early development creates an environment that demands rapid proliferation and transcription as progenitors differentiate into neurons. Mouse models have revealed the intricate process of cortical development and the necessity for DNA damage repair to ensure proper nervous system development (McKinnon, 2017). Somatic mosaicism in the form of CNVs and SNVs are present in the normal developing brain and point back to unique genomic stress during brain development (Abyzov *et al.*, 2017; Bae *et al.*, 2018). In this dissertation, hiPSC-derived neurogenesis was used to unravel some of the sources of that genomic stress and identify the role of p53 in responding to DNA DSBs that arise in neural cells.

Our first goal was to identify the dynamics of DNA DSBs during neural development (Chapter II). In order to quantify DNA DSBs, we developed an approach using imaging flow cytometry and γH2AX foci to detect DNA DSBs in neural cells. We successfully detected DNA DSBs in neural cells; identified whether the cell was an NPC, neuron, or transitioning NPC; and examined DNA DSBs and cell death in cell populations with different mitotic activity. From this study we discovered that:

1. Proliferating progenitors and post-mitotic neurons can accumulate DNA DSBs during neurogenesis, but more early differentiating NPCs die than progenitors

Next, we sought to uncouple the consequences of replication stress and transcriptional stress in hiPSC-NPCs by examining DNA DSBs, cell fate, and DDR protein activation (Chapter III). With the knowledge that p53 induces apoptosis of neural cells harboring DNA damage in rodent models of cortical development we also characterized its role in hiPSC-based neurogenesis. We conducted studies to

test the role of p53 during the first six weeks of hiPSC-based neurogenesis. This work culminated in data yielding the following major conclusions:

2. p53 is activated in response to transcriptionally mediated DNA DSBs in NPCs and prevents NPC proliferation during early neurogenesis
3. NPCs with low levels of p53 accumulate DNA DSBs in the transcription start site (TSS) of high-risk alleles for neurodevelopmental disorders regardless of gene length

We also piloted a study to determine whether exposure to genomic stress or a deficiency in p53 as an NPC would lead to changes in cell diversity or neuroinflammatory phenotypes in neurons or astrocytes (Chapter IV). While our initial findings suggest that genomic stress does not affect cytokine secretion in neural cells, our keys findings do indicate that:

4. Neurons and astrocytes derived from the same NPC lineage have unique cytokine and chemokine production

Proliferating progenitors and post-mitotic neurons can accumulate DNA DSBs during neurogenesis

In Chapter II we presented the advantage of analyzing DNA DSBs in NPCs using single-cell approaches (e.g. microscopy, flow cytometry) instead of bulk analyses (e.g. western blot). NPCs are very heterogeneous (Harbom *et al.*, 2018; Z. Shi *et al.*, 2018), thus to truly understand the dynamics of the cell population single-cell approaches are warranted. To provide high-throughput qualitative and quantitative data we used multi-spectral imaging flow cytometry (Bourton *et al.*, 2012). The combination of flow cytometry and microscopy provided information about the cell cycle, cell type (proliferating, dying, differentiating cells), and localization of proteins of interest (γH2AX foci). With this technique we observed DNA DSBs in NPCs at various time points from the first day to the 14^{th} day in neuronal differentiation medium. DNA DSBs were present in NPCs, lowered during the first week of differentiation but increased again during the second week. Mitotically active neural cells contained the highest percentage of breaks but interestingly the

highest level of cell death was observed in early differentiating neurons and not NPCs despite having equivalent percentages of cells with DNA DSBs. The major difference between the NPCs and early differentiating neurons is that NPCs remain proliferative (i.e. prone to replicative stress), while the neurons are post-mitotic and differentiating (i.e. prone to transcriptional stress). Therefore, our findings suggest that early differentiating neural cells may be more susceptible to transcriptional stress than replication stress.

p53 is activated in response to transcriptionally mediated DNA DSBs in NPCs and prevents NPC proliferation during early neurogenesis

If neural cells are more susceptible to transcriptional stress than replicative stress, what is mediating that response? Literature on DNA damage in the nervous system has consistently used models of DNA DSB repair knockout mice to observe the phenotype associated with neurons that harbor DNA damage. However, most of these models require concurrent *p53*$^{-/-}$ because the mice with p53 are embryonically lethal or develop a smaller cortex (Barnes *et al.*, 1998; Frank *et al.*, 2000). This made p53 the ideal protein responsible for the difference in cell death between neural cells with DNA DSBs from transcription versus replication stress.

In Chapter III we directly examined the role of p53 during early neuronal differentiation by applying IFC to p53^{KD} neurons. We strikingly observed a significant increase in p53^{KD} neurons compared to controls at six weeks in differentiation medium. To determine the cause of the increase in neurons we observed neurons after one week and observed less cell death in the p53^{KD} neurons in addition to a higher proportion of progenitors with actively cycling cells compared to controls. These phenotypes were rescued when NPCs were treated with Nutlin-3, a p53 agonist (Arva *et al.*, 2008; Shangary & Wang, 2009). This revealed that p53 was not only killing early differentiating NPCs with damage but also preventing the proliferation of those cells through cell cycle arrest. This finding is consistent with functions of p53 observed in other cell types and tissues in the body (Bieging *et al.*, 2014; Culmsee & Mattson, 2005; Dasika *et al.*, 1999).

However, our study is the first to investigate p53 in hiPSC-based neurogenesis using IFC technology.

To distinguish when p53 was becoming active in NPCs we exposed the progenitors to replication stress or transcriptional stress and discovered that p53 was only activated upon transcriptional stress. The pChk2-pATM pathway was also only activated in response to transcriptional stress despite significant cell cycle arrest in both forms of stress. Cell death was also markedly increased in transcription versus replication stress. Taken together these findings reveal that transcriptional stress is mostly likely the cause for p53 activation and consequent cell death in early differentiating neural cells.

In our studies of p53 activation, a more ideal approach would have been to use a p53 reporter to provide temporal information on how much DNA damage is necessary to induce cell death, differentiation, and temporary cell cycle arrest (Lahav, 2004; Lahav *et al.*, 2004). With a reporter or p53 antibody for flow cytometry it would be possible to discover at what time points p53 is active during neurogenesis. This approach has been used in other cell types but has yet to be applied to neural cells during differentiation (Hafner *et al.*, 2017; Reyes *et al.*, 2018).

Future studies should aim to further elucidate the role of p53 by dissecting whether p53 is activated in cells with a fate of cell death or whether it is also active in cells that continue on to become neurons. While the bulk of our data suggest that p53 is activated in transcriptional stress and it predominately kills NPCs with DNA DSBs, our ssRNA-seq data revealed a larger population of neurons in highly stressed NPCs (Chapter III, Figure 3). It is possible that in the CPT treated NPCs, p53 was activated in all of the NPCs, but in the subpopulation that differentiated into neurons the DNA damage was resolved and p53 levels went back down. Alternatively, it is also possible that p53 was simply not activated in the cluster of cells expressing neuronal genes so they differentiated while the other NPCs with high levels of p53 remained arrested in the cell cycle. Given the difficulties in reliably making high viability cell samples for ssRNA-seq, it could be useful to employ mass cytometry for cell lineage tracing (Bandura *et al.*, 2009; Zunder *et al.*,

2015). With this approach, cell fate could be mapped temporally and NPCs with and without p53 activation could be followed over time. *NPCs with low levels of p53 accumulate DNA DSBs in the TSS of high-risk alleles for neurodevelopmental disorders regardless of gene length*

In the past few years, several research groups have been working to understand the link between genomic stress and CNV formation during neurodevelopment (Arlt, Rajendran, *et al.*, 2012; Arlt, Wilson, *et al.*, 2012; Hastings *et al.*, 2009). In human fibroblasts, Wilson and colleagues determined common fragile sites, or regions with recurrent DNA DSBs from mild replication stress, co-localize with CNV hotspots due to large transcriptional units (Wilson *et al.*, 2015). Another study linked replication stress to de novo CNVs by showing the co-localization of DNA DSBs in mouse NPCs to genes that contain CNVs in humans (Wei *et al.*, 2016). The genes identified in the study overlapped with the Wilson study and another study by King *et al.* that observed an enrichment in DNA DSBs in long neural genes (>200kb)(King *et al.*, 2013). Many of the genes were high risk alleles for autism, schizophrenia, and various neuropsychiatric disorders. More recently, a study in hiPSCs derived from patients with macrocephalic autism revealed that excess replication stress leads to increased DNA DSBs in the same long neural genes that are high risk alleles for autism that encode genes for cell adhesion and migration (M. Wang *et al.*, 2020).

The mechanism behind replicative stress induced DNA DSBs and CNV formation is proposed from a model in which replication and transcription machinery collide due to stalled replication forks in long actively transcribed genes (Aguilera & Garcia-Muse, 2012; Aguilera & Gomez-Gonzalez, 2008; Wilson *et al.*, 2015). To test whether p53 deficient NPCs had increased breaks in long genes we analyzed the difference in DNA DSBs in $p53^{KD}$ and control NPCs at various gene lengths. We observed more DNA DSBs in $p53^{KD}$ neurons regardless of gene length, suggesting that p53 is not activated in response to transcription and replication collisions.

After observing an increase in p53 activation in response to transcriptional stress, we wanted to determine what genes were enriched for DNA DSBs near the TSS of highly transcribed genes. We observed an enrichment in DSBs in genes linked to neurodevelopmental disorders, intellectual disorders, demyelinating disorders, absence epilepsy, and early onset neurodegenerative disorders (Chapter III, Table 1). Many of the high risk alleles were associated with rare neurological disorders, which is markedly different from those observed in other studies observing DNA DSBs in NPCs (M. Wang *et al.*, 2020). Many of those studies found breaks in genes involved in autism and schizophrenia (Wei *et al.*, 2016). This could be due to several factors. First, our DNA DSB mapping approach is truly unbiased compared to high-throughput translocation sequencing. HTGS relies on a translocation to occur in order for the DNA DSB to be detected which results in less DNA DSBs being detected. It is also unknown if translocations happen in long genes more frequently, and since neural genes tend to be long this could introduce a potential bias.

The most highly expressed genes in our NPCs were not long neural genes as described in other studies (M. Wang *et al.*, 2020; Wei *et al.*, 2016; Wilson *et al.*, 2015). This discrepancy between our findings and those in published literature may also stem from differences in approaches used to detect highly transcribed genes. In the aforementioned studies, highly transcribed genes were examined using ssRNA-seq while others have used GRO-seq and Bru-seq. In addition, the conditions used to induce replication stress between different research groups have been inconsistent. Some employ the standard 400nM (or 0.4μM) Aphidicolin, commonly used in fragile site studies. Others use different doses for a range of different lengths of time (24-96 hours). All of these variables make it difficult to compare the DNA DSB data in NPCs from different groups and reach a consensus. Ideally, future studies should only employ unbiased techniques to detect DNA DSBs and transcription levels to ensure accurate detection of DNA DSBs and gene transcription. To this end, DNA DSB mapping combined with Bru-seq would be optimal for two reasons. First, DNA DSB mapping is single-nucleotide resolution, and unbiased. Second, Bru-seq reveals nascent transcription versus nascent

transcripts (e.g. GRO-seq). The effects of DNA DSBs on transcription, for instance whether it prevents transcription, induces transcription, or causes structural gene alterations are still unclear although several models have been proposed. Therefore, the most unbiased approach to determine which genes are being actively transcribed regardless of whether they finish transcription would be Bru-seq. Finally, the variations in drugs and treatment doses and times could be resolved by clarifying which mechanisms are being explored. In work assessing replication stress and somatic mosaicism, applying the standard drugs (i.e. aphidicolin) that induce common fragile sites and CNV hotspots are the most appropriate approach (Wilson et al., 2015).

One of the essential questions that still remains unanswered is whether p53 prevents the formation of CNVs in the human brain. Using single-cell whole genome amplification, this question can be answered by picking single control and $p53^{KD}$ neurons. In the appendix, we highlight an effective approach to the single-cell selection process and include data supporting the use of NeuO to detect viable neurons and DAPI/PI staining to exclude dying cells. This investigation will continue through future members of the lab but will be essential to answering whether CNVs exist at a higher rate in neurons without p53. Based on the findings that support replication stress as the mechanism of CNV formation (Arlt, Wilson, et al., 2012; Wilson et al., 2015), it is unlikely that there will be a difference in CNV levels between control and knockdown neurons. Our work shows that p53 is not activated in response to replication stress but transcriptional stress. This suggests that CNVs are formed in early neurogenesis when progenitors are going through final cell divisions and differentiating. However, the hypothesis that p53 does not protect against mega-base scale CNVs does not apply to other forms of somatic mutations (i.e aneuploidy, SNVs). In particular, SNVs increase with age (M. A. Lodato et al., 2018), making them susceptible to the genome maintenance mechanisms present in mammalian cells.

Neurons and astrocytes derived from the same NPC lineage have unique cytokine and chemokine production

We conducted initial studies to examine the role of genomic stress on neuroinflammatory phenotypes. While the majority of these pilot studies indicate that genomic stress does not have a long-term effect on neuroinflammatory phenotypes, studies that examine progenitors, neurons, and astrocytes immediately following stress would be helpful to deduce acute effects of genomic stress. These studies did reveal that hiPSC-derived astrocytes and neurons have distinct cytokine/chemokine secretion patterns. Consequent studies should include co-cultures between astrocytes and neurons in which stressed astrocytes are cultured with unstressed neurons. Preliminary experiments included in the appendix highlight the possibility that astrocytes are more resistant to genomic stress and therefore do not activate p53 in response to DNA DSBs compared to isogenic NPCs. This emphasizes the necessity to investigate the interaction between the two cell types if they respond differently to the same level of genomic stress. Due to the current limitations in neural hiPSC protocols, microglia are not generated with standard neural ectoderm induction of hiPSCs. However, protocols for hiPSC-based microglia are emerging (Abud et al., 2017), and co-cultures would provide insight into how surrounding cells react to stressed or $p53^{KD}$ neurons. Specifically, phagocytosis or synaptic pruning would be particularly of interest to examine as some of the cytokines and chemokines secreted by hiPSC-neurons have been indicated in those roles (e.g. Fractalkine) (Sheridan & Murphy, 2013; Sokolowski *et al.*, 2014).

Conclusion

In conclusion this study characterized the dynamics of genomic stress in the early developing cortex using an hiPSC model of neurogenesis and single-cell approaches. We developed an approach to examine cell fate, DNA DSBs, and cell type during neurogenesis using imaging flow cytometry. We determined that DNA DSBs, an indicator of genomic stress, are present in proliferative and post-mitotic neural cells undergoing neuronal differentiation. p53 is activated during hiPSC-based neurogenesis and induces apoptosis in NPCs harboring DNA DSBs due to transcriptional stress. Among the genes with DNA DSBs in the absence of p53, we identified high risk alleles for neurodevelopmental disorders.

Appendix

Selected Studies and Additional Protocol Information

Protocol to Generate p53 shRNA NPC Lines

The following protocol was used to generate p53 shRNA cells lines used for experiments in Chapter III, IV, and V.

Control (scramble) Plasmid Map: http://www.addgene.org/1864/

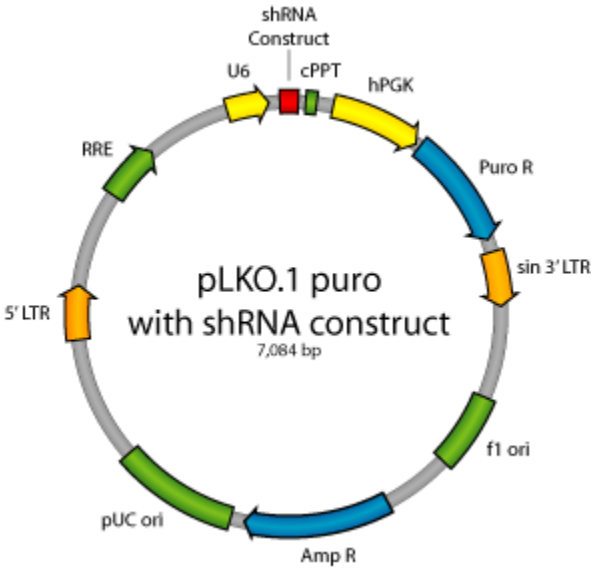

p53 shRNA Plasmid Map: http://www.addgene.org/19119/

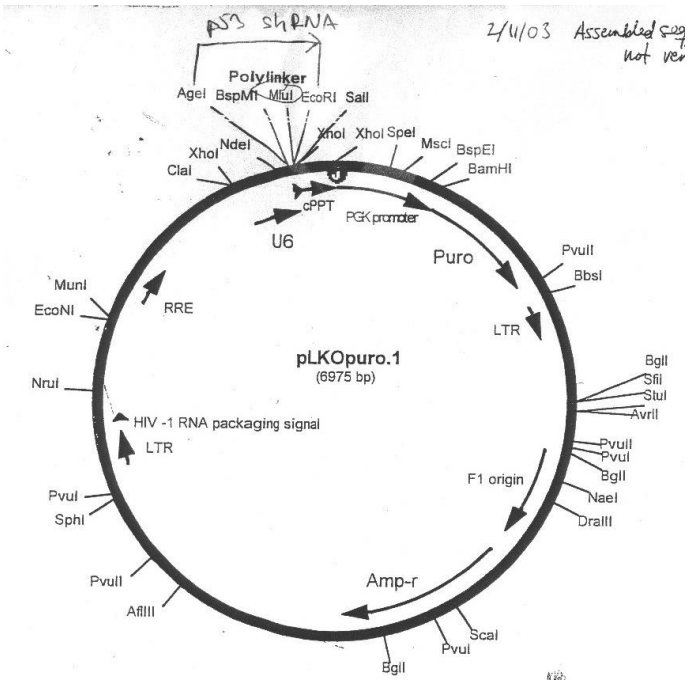

Processing Addgene Plasmid

Use the bacterial stab received from Addgene to streak bacteria onto a plate, grow overnight, and isolate single colonies. Select a single colony to inoculate in overnight culture (selecting a few colonies is ideal). Use a miniprep kit (e.g. Qiagen) to isolate the plasmid DNA. Once the plasmid concentration has been measured and the plasmid is verified, make glycerol stocks and store in -20°C.

Packaging Virus

Combine 2µg of pPAX2 and 4µg of pMD2.G with 6µg of DNA of interest (from steps). Add 15µL of Lip2000 and 12µg of DNA (made in previous step) to 500µL of Opti-Mem Media. Mix by inverting three times and incubate for 15-20 minutes at room temperature. Add 500µL of Opti-Mem.

Virus Production and Collection

Add packaged virus directly to HEK293T cells in a 10cm plate (when they are ~30% confluent). The next day, preferably first thing in the morning, replace media with fresh growth media. 48 hours later, collect media and store at 4°C. 24 hours after that, collect media. Filter all collected media through a SFCA 0.45µm filter, aliquot, and store virus containing media at -80°C. Virus could be concentrated at this point if desired.

Viral Transduction and Antibiotic Selection

Add various levels of virus directly to NPCs to determine lowest effective volume. Range from 20µL-150µL if virus is not concentrated. Range from 0.5µL-2µL if virus is concentrated. Change to fresh NPC media after 24-36 hours. After 24 hours in fresh growth media change to puromycin containing NPC media. Optimal concentration for NPCs is generally 0.4µg/mL but a negative control and kill curves should be generating for individual cell lines. NPCs will should be selected in puromycin for 4 days (media is still changed every other day). NPCs can then recover in fresh NPC media for whatever time is necessary to grow back to confluency and get passaged for further confirmation of knockdown and desired

experiments. Due to limitations on passage number of NPCs for experimental purposes (passage 15 NPCs cannot be used), NPCs should not be transduced at a passage number >p8 to allow sufficient time for passaging, growth, and expansion of cell lines.

hiPSC-derived Astrocytes and Genomic Stress

An unanswered question in the study of genomic stress in the developing brain is how glia are affected by stress and how they respond to DNA DSBs. To examine whether astrocytes respond to genomic stress similarly to NPCs (i.e. is p53 activated by transcriptional stress), we derived astrocytes from the same lineage of NPCs used in previous studies (Chapter II, III, and IV) and exposed them to the same dosage of replicative and transcriptional stress. We observed that astrocytes responded to transcriptional stress with more DNA DSBs per cell, more cell death, and greater cell cycle arrest compared to replicative stress. However, astrocytes did not activate p53 in response to either form of stress. Furthermore, in relation to isogenic NPCs, astrocytes have lower levels of cell cycle arrest, cell death, and DNA DSBs indicating that they are more resistant to genomic stress than their precursors.

For Astrocyte Differentiation see Chapter IV, for all other methods see Chapter III.

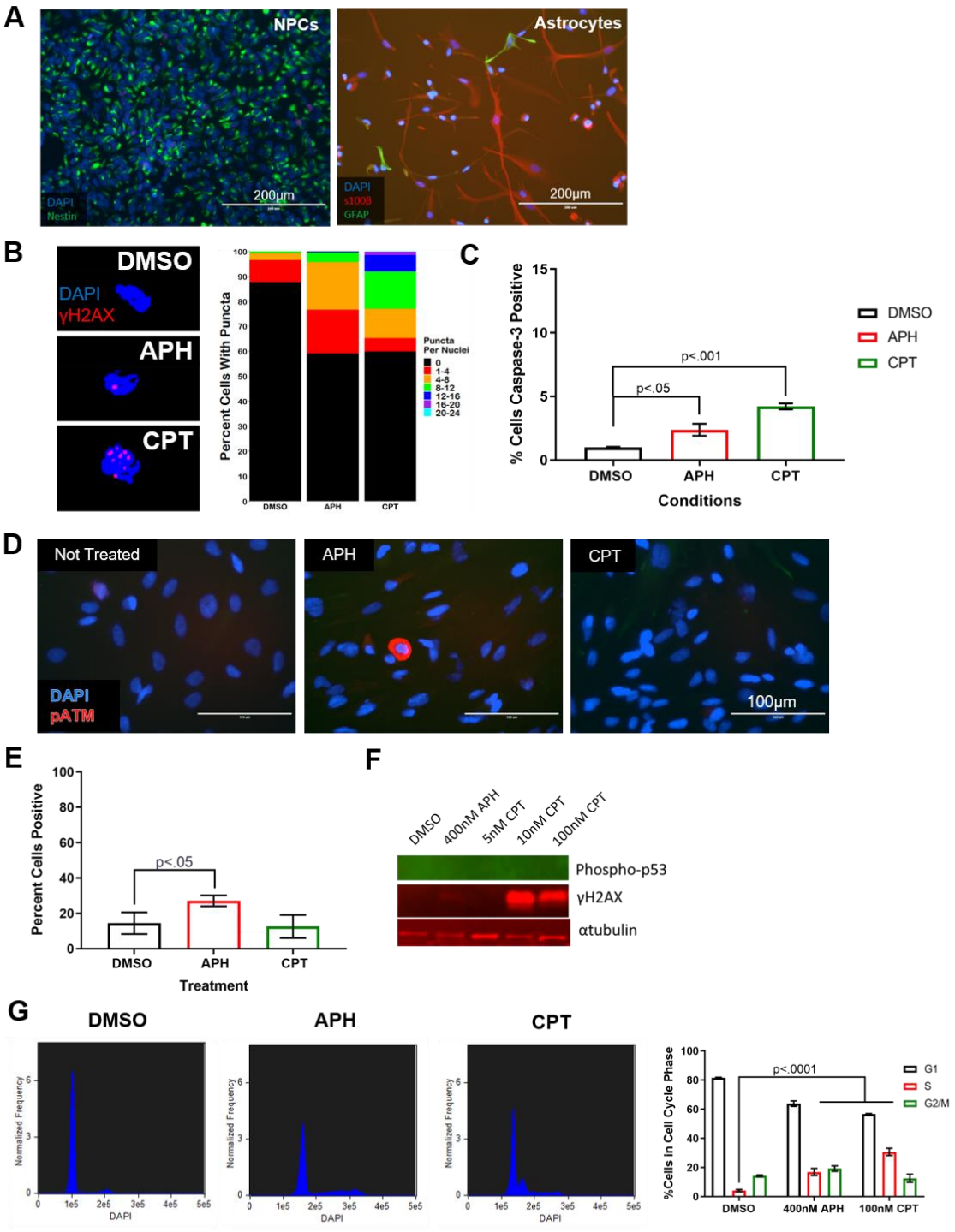

Appendix Figure 1. hiPSC-derived Astrocytes Respond to Genomic Stress without p53 activation.

Appendix Figure 1. hiPSC-derived Astrocytes Respond to Genomic Stress without p53 activation. (A) NPCs were differentiated to astrocytes using a protocol developed by the Brennand research group (Tcw *et al.*, 2017). For all of the following experiments, astrocytes were exposed to genomic stress or vehicle control for 24 hours and collected or fixed for analysis. (B) Imaging flow cytometry reveals that astrocytes acquire DNA DSBs in response to both replicative and transcriptional stress (Chi-square, $p<.0001$). (C) Flow cytometry studies show that astrocytes have slightly more cell death in response to replication stress (Two-way ANOVA, Tukey's Test, $p<.05$) and transcriptional stress (Two-way ANOVA, Tukey's Test, $p<.001$). (D, E) Astrocytes exposed to replicative stress have higher levels of pATM compared to controls (Unpaired t-test, $p<.05$). (F) Initial western blots reveal that p53 is not phosphorylated in astrocytes exposed to genomic stress. (G) More astrocytes are in s-phase in stressed conditions than control (Two-way ANOVA, Tukey's Test, $p<.0001$).

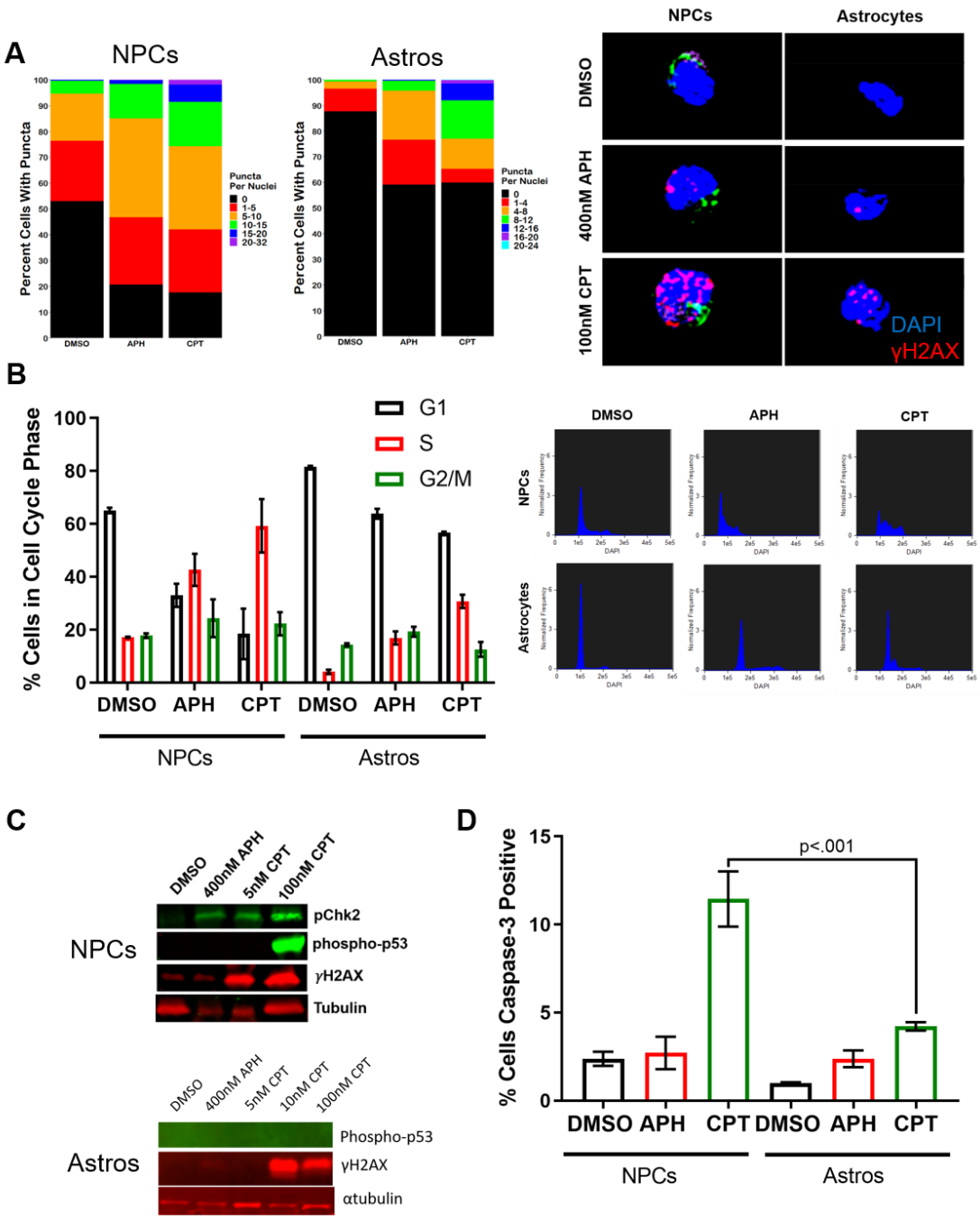

Appendix Figure 2. hiPSC-derived Astrocytes Are More Resistant to Genomic Stress compared to Isogenic NPCs.

Appendix Figure 2. hiPSC-derived Astrocytes Are More Resistant to Genomic Stress compared to Isogenic NPCs. 9429 NPCs were compared to 9429 astrocytes exposed to 24 hours of DMSO, 400nM APH, or 100nM CPT and collected for subsequent analysis. (A) NPCs have more DNA DSBs compared to astrocytes exposed to the same genomic stress (Chi-square, $p<.0001$). (B) NPCs have significantly more cells arrest in the cell cycle compared to astrocytes (Two-way ANOVA, Tukey's Test, $p<.0001$) (C) NPCs show p53 phosphorylation in response to CPT treatment while astrocytes do not. (D) NPCs have significantly more cell death after CPT treatment compared to astrocytes (Two-way ANOV, Tukey's Test, $p<.001$).

Protocol to Collect Single-Neurons for CNV Analysis

Papain Dissociation

hiPSC-derived neurons were detached from plates using an in-house developed papain dissociation protocol. To prepare papain solution, 5mL of neuron media was added to lyophilized papain (Worthington). 50µL DNAse I and 500µL 10x DNAse I Buffer (New England BioLabs) were added to the solution. To dissociate cells, 2mL of papain was added per ~500, 000 cells. Cells were kept in an incubator at 37° and triturated every 20minutes over the course of 40 mins to an hour. Once the cell clumps were broken down and a single cell suspension was obtained, the cells were spun down at 250xg and resuspended in neuron media using wide bore pipettes. Approximately 60,000 cells were seeded onto cell rafts and given 5-7 days to recover.

Single-cell Picking and Amplification

We verified the viability of the neurons by staining with propidium iodine (PI) and DAPI to exclude dead cells from consideration. We confirmed identity of neurons by staining with NeuO (Stem Cell Technologies) as per manufacturer instructions. We imaged cell rafts on the automated cell isolation AIR system (Cell Microsystems) in red, green and blue channels to exclude dead cells and positively identify live single neurons. We isolated 48 live single neurons from both the p53 KD and neurotypic hiPSC-derived neuron preparations. Single neurons were placed in 2 microliters of TE buffer in single wells of thin-wall PCR strips (8-weel, Grienger) on the AIR system. We immediately amplified the genomic contents of each individual well using the Picoplex kit according to manufacturer's instructions (Illumina). The amplified DNA in each well was purified from reaction components and enzymes using Qiaquick PCR clean-up columns (Qiagen) and eluted in 45 microliters of TE. We quantified yield of DNA synthesized in each reaction by measuring the DNA content in 2 microliters of sample using Picogreen reagent (Thermo) in 200 microliters and measuring fluorescence in a plate format using the Synergy plate reader (BioTek). We verified synthesis of high molecular weight

DNA products in each Picoplex reaction by resolving 1 microliter of samples in 1X TBE polyacrylamide gels at 35 mA for 20 minutes and stained for DNA using 1:10,000 dilution of SYBR gold in 1X TBE for five minutes. We imaged gels using 254 nm UV light and photographed.

We calculated DNA concentration of each amplified cell and pooled equimolar quantities of each of 48 cells into a single mixture and sized selected fragments with an average size of 650 bp using a double gel method as previously described (W. Chronister *et al.*, 2018).

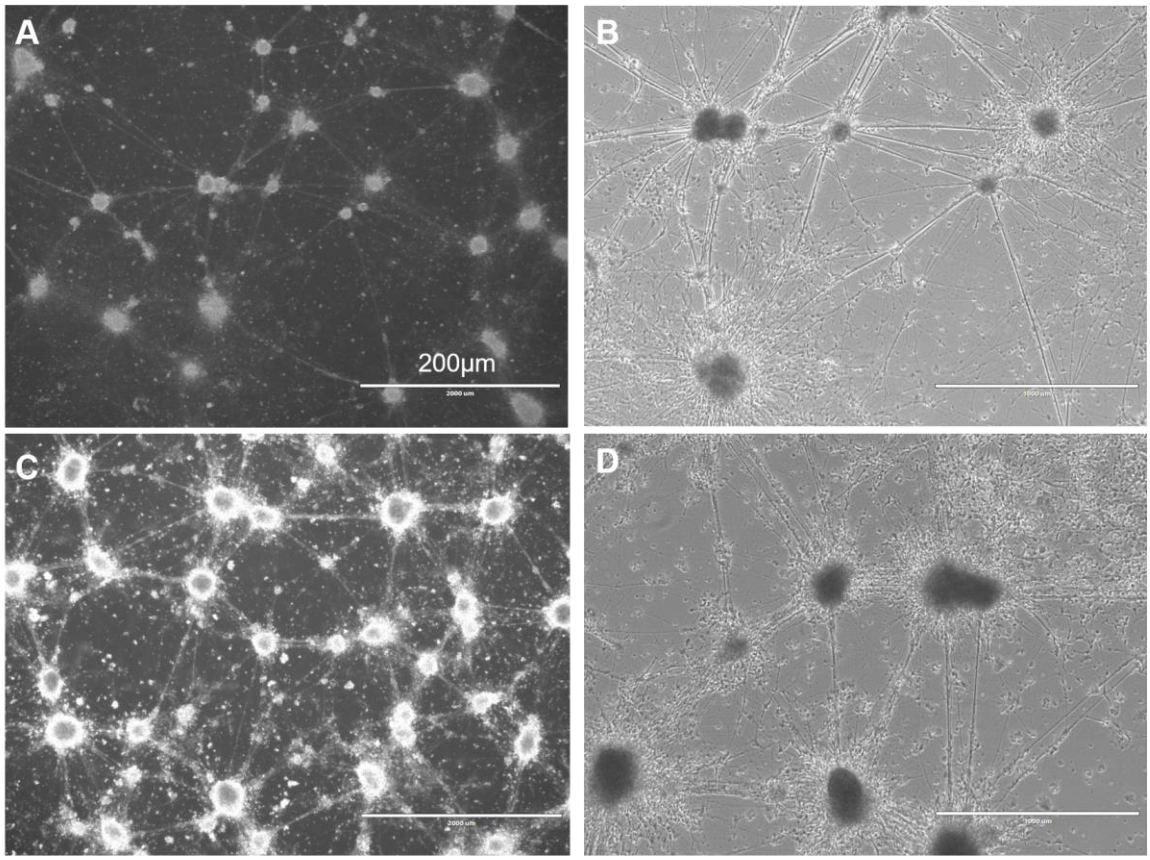

Appendix Figure 3. Brightfield Images of Control and p53 shRNA 8-week Neurons. 7545-5B Neurons were imaged at 8-weeks in neuron media in t75 cell culture flasks. (A) Control neurons imaged at 2x. (B) Control neurons imaged at 4x.(C) $p53^{KD}$ neurons imaged at 2x, (D) and 4x. $p53^{KD}$ neurons had an observable increase in “nodes and hubs”, which are often present in mature neuronal cultures that indicate neural network formation.

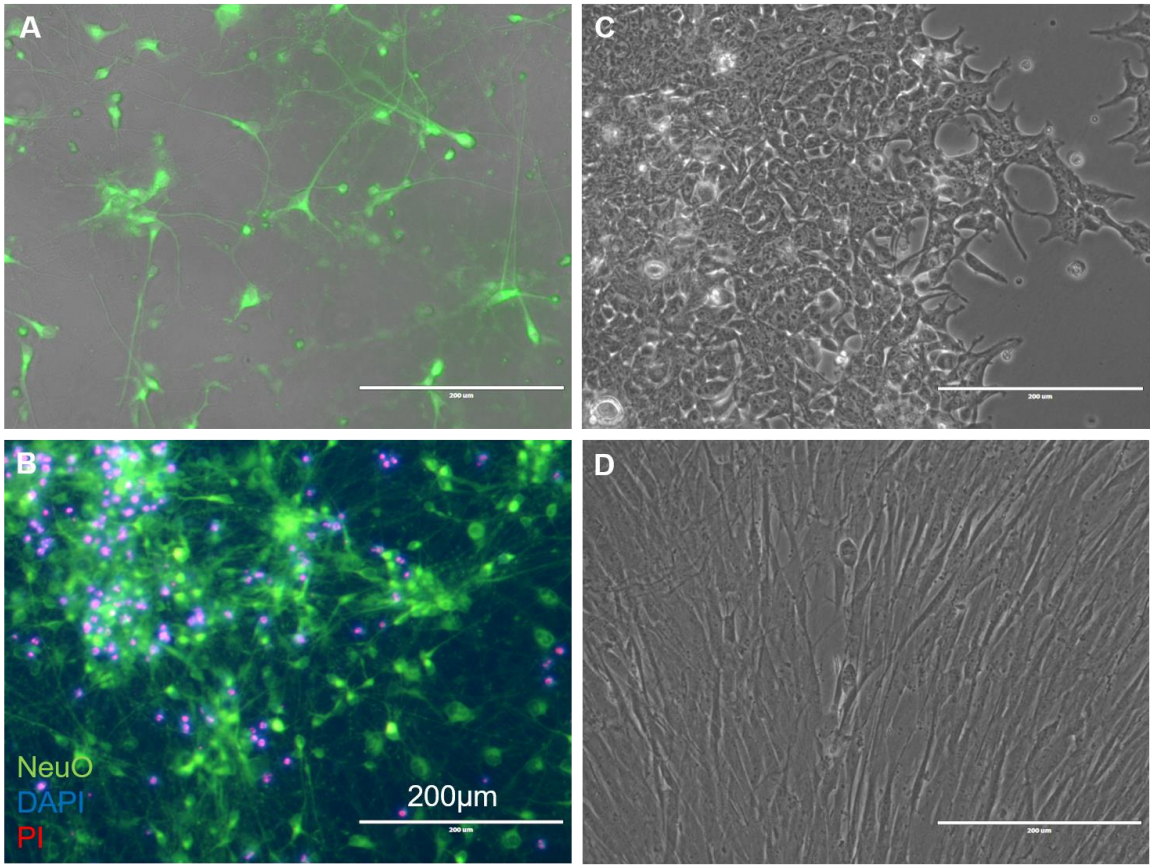

Appendix Figure 4. NeuO, DAPI, and PI staining of neurons, fibroblasts, and kidney cells. To validate the specificity of NeuO staining, several cell types were stained with NeuO and markers of cell viability (DAPI, PI). (A) NeuO stains 8-week hiPSC-derived neurons. (B) NeuO specifically stains neurons that are viable, while DAPI and PI stain dead cells. (C) NeuO does not stain HEK293T cells or (D) IMR-90 fibroblasts.

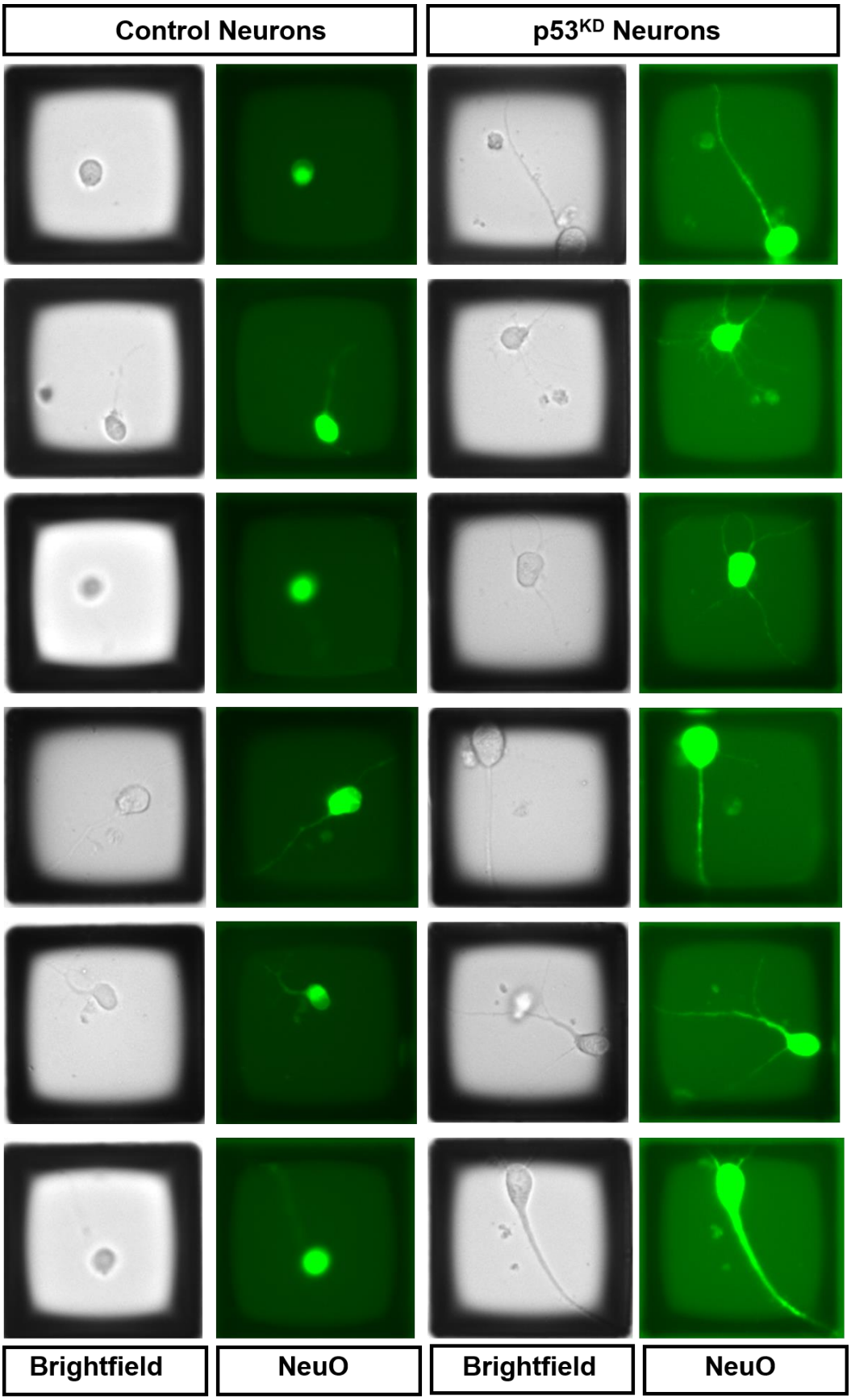
Control Neurons
p53KD Neurons
Brightfield
NeuO
Brightfield
NeuO

Appendix Figure 5. Cell Raft Images of Control and p53^{KD} Neurons. Images taken of single-neurons that were picked and collected for amplification using the AIR system. A few days after papain dissociation the neurons have re-grew neurites and axons. Picked cells were DAPI/Propidium Iodide negative and NeuO positive. Upon observations, the p53^{KD} neurons had more cells with more developed axons and neurites compared to control neurons.

References

Abud, E. M., Ramirez, R. N., Martinez, E. S., Healy, L. M., Nguyen, C. H. H., Newman, S. A., . . . Blurton-Jones, M. (2017). iPSC-Derived Human Microglia-like Cells to Study Neurological Diseases. *Neuron, 94*(2), 278-293 e279. doi:10.1016/j.neuron.2017.03.042

Abyzov, A., Tomasini, L., Zhou, B., Vasmatzis, N., Coppola, G., Amenduni, M., . . . Vaccarino, F. M. (2017). One thousand somatic SNVs per skin fibroblast cell set baseline of mosaic mutational load with patterns that suggest proliferative origin. *Genome Res, 27*(4), 512-523. doi:10.1101/gr.215517.116

Agirman, G., Broix, L., & Nguyen, L. (2017). Cerebral cortex development: an outside-in perspective. *FEBS Lett, 591*(24), 3978-3992. doi:10.1002/1873-3468.12924

Aguilera, A., & Garcia-Muse, T. (2012). R loops: from transcription byproducts to threats to genome stability. *Mol Cell, 46*(2), 115-124. doi:10.1016/j.molcel.2012.04.009

Aguilera, A., & Garcia-Muse, T. (2013). Causes of genome instability. *Annu Rev Genet, 47*, 1-32. doi:10.1146/annurev-genet-111212-133232

Aguilera, A., & Gomez-Gonzalez, B. (2008). Genome instability: a mechanistic view of its causes and consequences. *Nature Reviews Genetics, 9*, 204-217.

Alles, J., Karaiskos, N., Praktiknjo, S. D., Grosswendt, S., Wahle, P., Ruffault, P. L., . . . Rajewsky, N. (2017). Cell fixation and preservation for droplet-based single-cell transcriptomics. *BMC Biol, 15*(1), 44. doi:10.1186/s12915-017-0383-5

Alsina, F. C., & Silver, D. L. (2019). Damage Control in the Developing Brain: Tradeoffs and Consequences. *Trends Neurosci, 42*(10), 661-663. doi:10.1016/j.tins.2019.08.004

Altmann, T., & Gennery, A. R. (2016). DNA ligase IV syndrome; a review. *Orphanet J Rare Dis, 11*(1), 137. doi:10.1186/s13023-016-0520-1

Amit, M., Takahashi, H., Dragomir, M. P., Lindemann, A., Gleber-Netto, F. O., Pickering, C. R., . . . Myers, J. N. (2020). Loss of p53 drives neuron reprogramming in head and neck cancer. *Nature, 578*(7795), 449-454. doi:10.1038/s41586-020-1996-3

An, H. M., Tan, Y. L., Shi, J., Wang, Z. R., Soars, J. C., Wu, J. Q., . . . Zhang, X. Y. (2015). Altered IL-2, IL-6 and IL-8 serum levels in schizophrenia patients with tardive dyskinesia. *Schizophr Res, 162*(1-3), 261-268. doi:10.1016/j.schres.2014.12.037

Aranha, M. M., Sola, S., Low, W. C., Steer, C. J., & Rodrigues, C. M. (2009). Caspases and p53 modulate FOXO3A/Id1 signaling during mouse neural

stem cell differentiation. *J Cell Biochem, 107*(4), 748-758. doi:10.1002/jcb.22172

Ardhanareeswaran, K., Mariani, J., Coppola, G., Abyzov, A., & Vaccarino, F. M. (2017). Human induced pluripotent stem cells for modelling neurodevelopmental disorders. *Nat Rev Neurol, 13*(5), 265-278. doi:10.1038/nrneurol.2017.45

Arlt, M. F., Rajendran, S., Birkeland, S. R., Wilson, T. E., & Glover, T. W. (2012). De novo CNV formation in mouse embryonic stem cells occurs in the absence of Xrcc4-dependent nonhomologous end joining. *PLoS Genet, 8*(9), e1002981. doi:10.1371/journal.pgen.1002981

Arlt, M. F., Wilson, T. E., & Glover, T. W. (2012). Replication stress and mechanisms of CNV formation. *Curr Opin Genet Dev, 22*(3), 204-210. doi:10.1016/j.gde.2012.01.009

Armstrong, J. F., Kaufman, M. H., Harrison, D. J., & Clarke, A. R. (1995). High-frequency developmental abnormalities in p53-deficient mice. *Curr Biol, 5*(8), 931-936. doi:10.1016/s0960-9822(95)00183-7

Arva, N. C., Talbott, K. E., Okoro, D. R., Brekman, A., Qiu, W. G., & Bargonetti, J. (2008). Disruption of the p53-Mdm2 complex by Nutlin-3 reveals different cancer cell phenotypes. *Ethn Dis, 18*(2 Suppl 2), S2-1-8. Retrieved from https://www.ncbi.nlm.nih.gov/pubmed/18646312

Bae, T., Tomasini, L., Mariani, J., Zhou, B., Roychowdhury, T., Franjic, D., . . . Vaccarino, F. M. (2018). Different mutational rates and mechanisms in human cells at pregastrulation and neurogenesis. *Science, 359*(6375), 550-555. doi:10.1126/science.aan8690

Baillie, J. K., Barnett, M. W., Upton, K. R., Gerhardt, D. J., Richmond, T. A., De Sapio, F., . . . Faulkner, G. J. (2011). Somatic retrotransposition alters the genetic landscape of the human brain. *Nature, 479*(7374), 534-537. doi:10.1038/nature10531

Bandura, D. R., Baranov, V. I., Ornatsky, O. I., Antonov, A., Kinach, R., Lou, X., . . . Tanner, S. D. (2009). Mass cytometry: technique for real time single cell multitarget immunoassay based on inductively coupled plasma time-of-flight mass spectrometry. *Anal Chem, 81*(16), 6813-6822. doi:10.1021/ac901049w

Bardy, C., van den Hurk, M., Kakaradov, B., Erwin, J. A., Jaeger, B. N., Hernandez, R. V., . . . Gage, F. H. (2016). Predicting the functional states of human iPSC-derived neurons with single-cell RNA-seq and electrophysiology. *Mol Psychiatry, 21*(11), 1573-1588. doi:10.1038/mp.2016.158

Barnes, D. E., Stamp, G., Rosewell, I., Denzel, A., & Lindahl, T. (1998). Targeted disruption of the gene encoding DNA ligase IV leads to lethality in embryonic mice. *Curr Biol, 8*(25), 1395-1398. Retrieved from https://www.ncbi.nlm.nih.gov/pubmed/9889105

Baulac, S., Ishida, S., Marsan, E., Miquel, C., Biraben, A., Nguyen, D. K., . . . Picard, F. (2015). Familial focal epilepsy with focal cortical dysplasia due to DEPDC5 mutations. *Ann Neurol, 77*(4), 675-683. doi:10.1002/ana.24368

Becher, B., Spath, S., & Goverman, J. (2017). Cytokine networks in neuroinflammation. *Nat Rev Immunol, 17*(1), 49-59. doi:10.1038/nri.2016.123

Bendall, S. C., Davis, K. L., Amir el, A. D., Tadmor, M. D., Simonds, E. F., Chen, T. J., . . . Pe'er, D. (2014). Single-cell trajectory detection uncovers progression and regulatory coordination in human B cell development. *Cell, 157*(3), 714-725. doi:10.1016/j.cell.2014.04.005

Betermier, M., Bertrand, P., & Lopez, B. S. (2014). Is non-homologous end-joining really an inherently error-prone process? *PLoS Genet, 10*(1), e1004086. doi:10.1371/journal.pgen.1004086

Bhardwaj, R. D., Curtis, M. A., Spalding, K. L., Buchholz, B. A., Fink, D., Bjork-Eriksson, T., . . . Frisen, J. (2006). Neocortical neurogenesis in humans is restricted to development. *Proc Natl Acad Sci U S A, 103*(33), 12564-12568. doi:10.1073/pnas.0605177103

Bieging, K. T., Mello, S. S., & Attardi, L. D. (2014). Unravelling mechanisms of p53-mediated tumour suppression. *Nat Rev Cancer, 14*(5), 359-370. doi:10.1038/nrc3711

Bilbo, S. D., & Schwarz, J. M. (2009). Early-life programming of later-life brain and behavior: a critical role for the immune system. *Front Behav Neurosci, 3*, 14. doi:10.3389/neuro.08.014.2009

Blaschke, A. J., Staley, K., & Chun, J. (1996). Widespread programmed cell death in proliferative and postmitotic regions of the fetal cerebral cortex. *Development, 122*(4), 1165-1174. Retrieved from https://www.ncbi.nlm.nih.gov/pubmed/8620843

Bock, C., Farlik, M., & Sheffield, N. C. (2016). Multi-Omics of Single Cells: Strategies and Applications. *Trends Biotechnol, 34*(8), 605-608. doi:10.1016/j.tibtech.2016.04.004

Bourton, E. C., Plowman, P. N., Zahir, S. A., Senguloglu, G. U., Serrai, H., Bottley, G., & Parris, C. N. (2012). Multispectral imaging flow cytometry reveals distinct frequencies of gamma-H2AX foci induction in DNA double strand break repair defective human cell lines. *Cytometry A, 81*(2), 130-137. doi:10.1002/cyto.a.21171

Brennand, K., Savas, J. N., Kim, Y., Tran, N., Simone, A., Hashimoto-Torii, K., . . . Gage, F. H. (2015). Phenotypic differences in hiPSC NPCs derived from patients with schizophrenia. *Mol Psychiatry, 20*(3), 361-368. doi:10.1038/mp.2014.22

Brennand, K. J., Marchetto, M. C., Benvenisty, N., Brustle, O., Ebert, A., Izpisua Belmonte, J. C., . . . Jaenisch, R. (2015). Creating Patient-Specific Neural

Cells for the In Vitro Study of Brain Disorders. *Stem Cell Reports, 5*(6), 933-945. doi:10.1016/j.stemcr.2015.10.011

Brennand, K. J., Simone, A., Jou, J., Gelboin-Burkhart, C., Tran, N., Sangar, S., . . . Gage, F. H. (2011). Modelling schizophrenia using human induced pluripotent stem cells. *Nature, 473*(7346), 221-225. doi:10.1038/nature09915

Brown, A. S., Hooton, J., Schaefer, C. A., Zhang, H., Petkova, E., Babulas, V., . . . Susser, E. S. (2004). Elevated maternal interleukin-8 levels and risk of schizophrenia in adult offspring. *Am J Psychiatry, 161*(5), 889-895. doi:10.1176/appi.ajp.161.5.889

Budhram-Mahadeo, V. S., Bowen, S., Lee, S., Perez-Sanchez, C., Ensor, E., Morris, P. J., & Latchman, D. S. (2006). Brn-3b enhances the pro-apoptotic effects of p53 but not its induction of cell cycle arrest by cooperating in trans-activation of bax expression. *Nucleic Acids Res, 34*(22), 6640-6652. doi:10.1093/nar/gkl878

Budnik, B. L., E.; Slavov, N. (2017). Mass-spectrometry of single mammalian cells quantifies proteome heterogeneity during cell differentiation. *bioRxiv*. doi:https://doi.org/10.1101/102681

Bunting, S. F., & Nussenzweig, A. (2013). End-joining, translocations and cancer. *Nat Rev Cancer, 13*(7), 443-454. doi:10.1038/nrc3537

Bushman, D. M., Kaeser, G. E., Siddoway, B., Westra, J. W., Rivera, R. R., Rehen, S. K., . . . Chun, J. (2015). Genomic mosaicism with increased amyloid precursor protein (APP) gene copy number in single neurons from sporadic Alzheimer's disease brains. *Elife, 4*. doi:10.7554/eLife.05116

Butler, A., Hoffman, P., Smibert, P., Papalexi, E., & Satija, R. (2018). Integrating single-cell transcriptomic data across different conditions, technologies, and species. *Nat Biotechnol, 36*(5), 411-420. doi:10.1038/nbt.4096

Byers, B., Lee, H. L., & Reijo Pera, R. (2012). Modeling Parkinson's disease using induced pluripotent stem cells. *Curr Neurol Neurosci Rep, 12*(3), 237-242. doi:10.1007/s11910-012-0270-y

Caccamo, D. V., Herman, M. M., Frankfurter, A., Katsetos, C. D., Collins, V. P., & Rubinstein, L. J. (1989). An immunohistochemical study of neuropeptides and neuronal cytoskeletal proteins in the neuroepithelial component of a spontaneous murine ovarian teratoma. Primitive neuroepithelium displays immunoreactivity for neuropeptides and neuron-associated beta-tubulin isotype. *Am J Pathol, 135*(5), 801-813. Retrieved from https://www.ncbi.nlm.nih.gov/pubmed/2817080

Cai, X., Evrony, G. D., Lehmann, H. S., Elhosary, P. C., Mehta, B. K., Poduri, A., & Walsh, C. A. (2014). Single-cell, genome-wide sequencing identifies clonal somatic copy-number variation in the human brain. *Cell Rep, 8*(5), 1280-1289. doi:10.1016/j.celrep.2014.07.043

Cajal, S. (1890). Textura de las circunvoluticiones cerebrales de los mamiferos inferiores. *Gaceta Medica Catalana*, 22-31.

Cajal, S. (1891). Sur la structure de l'ecorce cerebrale de quelques mammiferes. *La Cellule*, 125-176.

Capranico, G., Ferri, F., Fogli, M. V., Russo, A., Lotito, L., & Baranello, L. (2007). The effects of camptothecin on RNA polymerase II transcription: roles of DNA topoisomerase I. *Biochimie, 89*(4), 482-489. doi:10.1016/j.biochi.2007.01.001

Casanova, M. F., Buxhoeveden, D., & Gomez, J. (2003). Disruption in the inhibitory architecture of the cell minicolumn: implications for autism. *Neuroscientist, 9*(6), 496-507. doi:10.1177/1073858403253552

Caviness, V. S., Jr., Takahashi, T., & Nowakowski, R. S. (1995). Numbers, time and neocortical neuronogenesis: a general developmental and evolutionary model. *Trends Neurosci, 18*(9), 379-383. doi:10.1016/0166-2236(95)93933-o

Chang, H. H. Y., Pannunzio, N. R., Adachi, N., & Lieber, M. R. (2017). Non-homologous DNA end joining and alternative pathways to double-strand break repair. *Nat Rev Mol Cell Biol, 18*(8), 495-506. doi:10.1038/nrm.2017.48

Chen, H. M., DeLong, C. J., Bame, M., Rajapakse, I., Herron, T. J., McInnis, M. G., & O'Shea, K. S. (2014). Transcripts involved in calcium signaling and telencephalic neuronal fate are altered in induced pluripotent stem cells from bipolar disorder patients. *Transl Psychiatry, 4*, e375. doi:10.1038/tp.2014.12

Chipuk, J. E., & Green, D. R. (2006). Dissecting p53-dependent apoptosis. *Cell Death Differ, 13*(6), 994-1002. doi:10.1038/sj.cdd.4401908

Choi, S. H., Kim, Y. H., Hebisch, M., Sliwinski, C., Lee, S., D'Avanzo, C., . . . Kim, D. Y. (2014). A three-dimensional human neural cell culture model of Alzheimer's disease. *Nature, 515*(7526), 274-278. doi:10.1038/nature13800

Chow, H. M., & Herrup, K. (2015). Genomic integrity and the ageing brain. *Nat Rev Neurosci, 16*(11), 672-684. doi:10.1038/nrn4020

Chronister, W., Wierman, M., Burbulis, I., Wolpert, M., Haakenson, M., Kleinman, J., . . . McConnell, M. (2018). CNV Neurons Are Rare in Aged Human Neocortex. *bioRxiv*.

Chronister, W. D., Burbulis, I. E., Wierman, M. B., Wolpert, M. J., Haakenson, M. F., Smith, A. C. B., . . . McConnell, M. J. (2019). Neurons with Complex Karyotypes Are Rare in Aged Human Neocortex. *Cell Rep, 26*(4), 825-835 e827. doi:10.1016/j.celrep.2018.12.107

Chun, J., & Schatz, D. G. (1999). Rearranging views on neurogenesis: neuronal death in the absence of DNA end-joining proteins. *Neuron, 22*(1), 7-10. doi:10.1016/s0896-6273(00)80671-6

Conforti, L., Adalbert, R., & Coleman, M. P. (2007). Neuronal death: where does the end begin? *Trends Neurosci, 30*(4), 159-166. doi:10.1016/j.tins.2007.02.004

Coppede, F. (2011). An overview of DNA repair in amyotrophic lateral sclerosis. *ScientificWorldJournal, 11*, 1679-1691. doi:10.1100/2011/853474

Coppede, F., & Migliore, L. (2009). DNA damage and repair in Alzheimer's disease. *Curr Alzheimer Res, 6*(1), 36-47. Retrieved from https://www.ncbi.nlm.nih.gov/pubmed/19199873

Coufal, N. G., Garcia-Perez, J. L., Peng, G. E., Yeo, G. W., Mu, Y., Lovci, M. T., . . . Gage, F. H. (2009). L1 retrotransposition in human neural progenitor cells. *Nature, 460*(7259), 1127-1131. doi:10.1038/nature08248

Culmsee, C., & Mattson, M. P. (2005). p53 in neuronal apoptosis. *Biochem Biophys Res Commun, 331*(3), 761-777. doi:10.1016/j.bbrc.2005.03.149

D'Gama, A. M., & Walsh, C. A. (2018). Somatic mosaicism and neurodevelopmental disease. *Nat Neurosci, 21*(11), 1504-1514. doi:10.1038/s41593-018-0257-3

Dasika, G. K., Lin, S. C., Zhao, S., Sung, P., Tomkinson, A., & Lee, E. Y. (1999). DNA damage-induced cell cycle checkpoints and DNA strand break repair in development and tumorigenesis. *Oncogene, 18*(55), 7883-7899. doi:10.1038/sj.onc.1203283

Davenport, C. M., Sevastou, I. G., Hooper, C., & Pocock, J. M. (2010). Inhibiting p53 pathways in microglia attenuates microglial-evoked neurotoxicity following exposure to Alzheimer peptides. *J Neurochem, 112*(2), 552-563. doi:10.1111/j.1471-4159.2009.06485.x

Di Giovanni, S., Knights, C. D., Rao, M., Yakovlev, A., Beers, J., Catania, J., . . . Faden, A. I. (2006). The tumor suppressor protein p53 is required for neurite outgrowth and axon regeneration. *EMBO J, 25*(17), 4084-4096. doi:10.1038/sj.emboj.7601292

Dobin, A., Davis, C. A., Schlesinger, F., Drenkow, J., Zaleski, C., Jha, S., . . . Gingeras, T. R. (2013). STAR: ultrafast universal RNA-seq aligner. *Bioinformatics, 29*(1), 15-21. doi:10.1093/bioinformatics/bts635

Dulken, B. W., Leeman, D. S., Boutet, S. C., Hebestreit, K., & Brunet, A. (2017). Single-Cell Transcriptomic Analysis Defines Heterogeneity and Transcriptional Dynamics in the Adult Neural Stem Cell Lineage. *Cell Rep, 18*(3), 777-790. doi:10.1016/j.celrep.2016.12.060

Dziegielewska, K. M., Moller, J. E., Potter, A. M., Ek, J., Lane, M. A., & Saunders, N. R. (2000). Acute-phase cytokines IL-1beta and TNF-alpha in

brain development. *Cell Tissue Res, 299*(3), 335-345. doi:10.1007/s004419900157

Eberwine, J., & Kim, J. (2015). Cellular Deconstruction: Finding Meaning in Individual Cell Variation. *Trends Cell Biol, 25*(10), 569-578. doi:10.1016/j.tcb.2015.07.004

Erwin, J. A., Paquola, A. C., Singer, T., Gallina, I., Novotny, M., Quayle, C., . . . Gage, F. H. (2016). L1-associated genomic regions are deleted in somatic cells of the healthy human brain. *Nat Neurosci, 19*(12), 1583-1591. doi:10.1038/nn.4388

Espuny-Camacho, I., Michelsen, K. A., Gall, D., Linaro, D., Hasche, A., Bonnefont, J., . . . Vanderhaeghen, P. (2013). Pyramidal neurons derived from human pluripotent stem cells integrate efficiently into mouse brain circuits in vivo. *Neuron, 77*(3), 440-456. doi:10.1016/j.neuron.2012.12.011

Evrony, G. D., Cai, X., Lee, E., Hills, L. B., Elhosary, P. C., Lehmann, H. S., . . . Walsh, C. A. (2012). Single-neuron sequencing analysis of L1 retrotransposition and somatic mutation in the human brain. *Cell, 151*(3), 483-496. doi:10.1016/j.cell.2012.09.035

Farkas, L. M., & Huttner, W. B. (2008). The cell biology of neural stem and progenitor cells and its significance for their proliferation versus differentiation during mammalian brain development. *Curr Opin Cell Biol, 20*(6), 707-715. doi:10.1016/j.ceb.2008.09.008

Farlik, M., Sheffield, N. C., Nuzzo, A., Datlinger, P., Schonegger, A., Klughammer, J., & Bock, C. (2015). Single-cell DNA methylome sequencing and bioinformatic inference of epigenomic cell-state dynamics. *Cell Rep, 10*(8), 1386-1397. doi:10.1016/j.celrep.2015.02.001

Ferguson, D. O., Sekiguchi, J. M., Chang, S., Frank, K. M., Gao, Y., DePinho, R. A., & Alt, F. W. (2000). The nonhomologous end-joining pathway of DNA repair is required for genomic stability and the suppression of translocations. *Proc Natl Acad Sci U S A, 97*(12), 6630-6633. doi:10.1073/pnas.110152897

Ferguson, D. O., Sekiguchi, J. M., Frank, K. M., Gao, Y., Sharpless, N. E., Gu, Y., . . . Alt, F. W. (2000). The interplay between nonhomologous end-joining and cell cycle checkpoint factors in development, genomic stability, and tumorigenesis. *Cold Spring Harb Symp Quant Biol, 65*, 395-403. doi:10.1101/sqb.2000.65.395

Finneran, D. J., & Nash, K. R. (2019). Neuroinflammation and fractalkine signaling in Alzheimer's disease. *J Neuroinflammation, 16*(1), 30. doi:10.1186/s12974-019-1412-9

Flaherty, E., Deranieh, R. M., Artimovich, E., Lee, I. S., Siegel, A. J., Levy, D. L., . . . Brennand, K. J. (2017). Patient-derived hiPSC neurons with heterozygous CNTNAP2 deletions display altered neuronal gene

expression and network activity. *NPJ Schizophr, 3*, 35. doi:10.1038/s41537-017-0033-5

Frank, K. M., Sharpless, N. E., Gao, Y., Sekiguchi, J. M., Ferguson, D. O., Zhu, C., . . . Alt, F. W. (2000). DNA ligase IV deficiency in mice leads to defective neurogenesis and embryonic lethality via the p53 pathway. *Mol Cell, 5*(6), 993-1002. Retrieved from https://www.ncbi.nlm.nih.gov/pubmed/10911993

Frankish, A., Diekhans, M., Ferreira, A. M., Johnson, R., Jungreis, I., Loveland, J., . . . Flicek, P. (2019). GENCODE reference annotation for the human and mouse genomes. *Nucleic Acids Res, 47*(D1), D766-D773. doi:10.1093/nar/gky955

Gao, Y., Ferguson, D. O., Xie, W., Manis, J. P., Sekiguchi, J., Frank, K. M., . . . Alt, F. W. (2000). Interplay of p53 and DNA-repair protein XRCC4 in tumorigenesis, genomic stability and development. *Nature, 404*(6780), 897-900. doi:10.1038/35009138

Genetic Modifiers of Huntington's Disease Consortium. Electronic address, g. h. m. h. e., & Genetic Modifiers of Huntington's Disease, C. (2019). CAG Repeat Not Polyglutamine Length Determines Timing of Huntington's Disease Onset. *Cell, 178*(4), 887-900 e814. doi:10.1016/j.cell.2019.06.036

Gerdes, J., Lemke, H., Baisch, H., Wacker, H. H., Schwab, U., & Stein, H. (1984). Cell cycle analysis of a cell proliferation-associated human nuclear antigen defined by the monoclonal antibody Ki-67. *J Immunol, 133*(4), 1710-1715. Retrieved from https://www.ncbi.nlm.nih.gov/pubmed/6206131

Geric, M., Gajski, G., & Garaj-Vrhovac, V. (2014). gamma-H2AX as a biomarker for DNA double-strand breaks in ecotoxicology. *Ecotoxicol Environ Saf, 105*, 13-21. doi:10.1016/j.ecoenv.2014.03.035

Golgi, C. (1886). Sulla Fina Anatomia degli Organi Centrali del Sistema Nervosa. *Milano: U. Hoepli*.

Gottlieb, E., Haffner, R., King, A., Asher, G., Gruss, P., Lonai, P., & Oren, M. (1997). Transgenic mouse model for studying the transcriptional activity of the p53 protein: age- and tissue-dependent changes in radiation-induced activation during embryogenesis. *EMBO J, 16*(6), 1381-1390. doi:10.1093/emboj/16.6.1381

Gotz, M., & Huttner, W. B. (2005). The cell biology of neurogenesis. *Nat Rev Mol Cell Biol, 6*(10), 777-788. doi:10.1038/nrm1739

Gravina, S., Dong, X., Yu, B., & Vijg, J. (2016). Single-cell genome-wide bisulfite sequencing uncovers extensive heterogeneity in the mouse liver methylome. *Genome Biol, 17*(1), 150. doi:10.1186/s13059-016-1011-3

Griesi-Oliveira, K., Acab, A., Gupta, A. R., Sunaga, D. Y., Chailangkarn, T., Nicol, X., . . . Muotri, A. R. (2015). Modeling non-syndromic autism and the impact of TRPC6 disruption in human neurons. *Mol Psychiatry, 20*(11), 1350-1365. doi:10.1038/mp.2014.141

Grindberg, R. V., Yee-Greenbaum, J. L., McConnell, M. J., Novotny, M., O'Shaughnessy, A. L., Lambert, G. M., . . . Lasken, R. S. (2013). RNA-sequencing from single nuclei. *Proc Natl Acad Sci U S A, 110*(49), 19802-19807. doi:10.1073/pnas.1319700110

Gu, Y., Sekiguchi, J., Gao, Y., Dikkes, P., Frank, K., Ferguson, D., . . . Alt, F. W. (2000). Defective embryonic neurogenesis in Ku-deficient but not DNA-dependent protein kinase catalytic subunit-deficient mice. *Proc Natl Acad Sci U S A, 97*(6), 2668-2673. doi:10.1073/pnas.97.6.2668

Guirouilh-Barbat, J., Lambert, S., Bertrand, P., & Lopez, B. S. (2014). Is homologous recombination really an error-free process? *Front Genet, 5*, 175. doi:10.3389/fgene.2014.00175

Gurdon, J. B. (1962). The developmental capacity of nuclei taken from intestinal epithelium cells of feeding tadpoles. *J Embryol Exp Morphol, 10*, 622-640. Retrieved from https://www.ncbi.nlm.nih.gov/pubmed/13951335

Hafner, A., Stewart-Ornstein, J., Purvis, J. E., Forrester, W. C., Bulyk, M. L., & Lahav, G. (2017). p53 pulses lead to distinct patterns of gene expression albeit similar DNA-binding dynamics. *Nat Struct Mol Biol, 24*(10), 840-847. doi:10.1038/nsmb.3452

Hancks, D. C., & Kazazian, H. H., Jr. (2012). Active human retrotransposons: variation and disease. *Curr Opin Genet Dev, 22*(3), 191-203. doi:10.1016/j.gde.2012.02.006

Handel, A. E., Chintawar, S., Lalic, T., Whiteley, E., Vowles, J., Giustacchini, A., . . . Cader, M. Z. (2016). Assessing similarity to primary tissue and cortical layer identity in induced pluripotent stem cell-derived cortical neurons through single-cell transcriptomics. *Hum Mol Genet, 25*(5), 989-1000. doi:10.1093/hmg/ddv637

Hansen, D. V., Rubenstein, J. L., & Kriegstein, A. R. (2011). Deriving excitatory neurons of the neocortex from pluripotent stem cells. *Neuron, 70*(4), 645-660. doi:10.1016/j.neuron.2011.05.006

Harbom, L. J., Michel, N., & McConnell, M. J. (2018). Single-cell analysis of diversity in human stem cell-derived neurons. *Cell Tissue Res, 371*(1), 171-179. doi:10.1007/s00441-017-2728-3

Hastings, P. J., Lupski, J. R., Rosenberg, S. M., & Ira, G. (2009). Mechanisms of change in gene copy number. *Nat Rev Genet, 10*(8), 551-564. doi:10.1038/nrg2593

Hatori, K., Nagai, A., Heisel, R., Ryu, J. K., & Kim, S. U. (2002). Fractalkine and fractalkine receptors in human neurons and glial cells. *J Neurosci Res, 69*(3), 418-426. doi:10.1002/jnr.10304

Haubensak, W., Attardo, A., Denk, W., & Huttner, W. B. (2004). Neurons arise in the basal neuroepithelium of the early mammalian telencephalon: a major site of neurogenesis. *Proc Natl Acad Sci U S A, 101*(9), 3196-3201. doi:10.1073/pnas.0308600100

Haupt, Y., Maya, R., Kazaz, A., & Oren, M. (1997). Mdm2 promotes the rapid degradation of p53. *Nature, 387*(6630), 296-299. doi:10.1038/387296a0

Hazen, J. L., Faust, G. G., Rodriguez, A. R., Ferguson, W. C., Shumilina, S., Clark, R. A., . . . Baldwin, K. K. (2016). The Complete Genome Sequences, Unique Mutational Spectra, and Developmental Potency of Adult Neurons Revealed by Cloning. *Neuron, 89*(6), 1223-1236. doi:10.1016/j.neuron.2016.02.004

Helton, E. S., & Chen, X. (2007). p53 modulation of the DNA damage response. *J Cell Biochem, 100*(4), 883-896. doi:10.1002/jcb.21091

Hodge, R. D., Bakken, T. E., Miller, J. A., Smith, K. A., Barkan, E. R., Graybuck, L. T., . . . Lein, E. S. (2019). Conserved cell types with divergent features in human versus mouse cortex. *Nature, 573*(7772), 61-68. doi:10.1038/s41586-019-1506-7

Hoffman, G. E., Hartley, B. J., Flaherty, E., Ladran, I., Gochman, P., Ruderfer, D. M., . . . Brennand, K. J. (2017). Transcriptional signatures of schizophrenia in hiPSC-derived NPCs and neurons are concordant with post-mortem adult brains. *Nat Commun, 8*(1), 2225. doi:10.1038/s41467-017-02330-5

Hunter, J. D. (2007). Matplotlib: A 2D graphics environment. *Computing in Science & Engineering, 9*(3), 90-95. doi:Doi 10.1109/Mcse.2007.55

Jack, C. S., Arbour, N., Manusow, J., Montgrain, V., Blain, M., McCrea, E., . . . Antel, J. P. (2005). TLR signaling tailors innate immune responses in human microglia and astrocytes. *J Immunol, 175*(7), 4320-4330. doi:10.4049/jimmunol.175.7.4320

Jayadev, S., Nesser, N. K., Hopkins, S., Myers, S. J., Case, A., Lee, R. J., . . . Garden, G. A. (2011). Transcription factor p53 influences microglial activation phenotype. *Glia, 59*(10), 1402-1413. doi:10.1002/glia.21178

Jebelli, J., Hooper, C., & Pocock, J. M. (2014). Microglial p53 activation is detrimental to neuronal synapses during activation-induced inflammation: Implications for neurodegeneration. *Neurosci Lett, 583*, 92-97. doi:10.1016/j.neulet.2014.08.049

Jin, Z., & El-Deiry, W. S. (2005). Overview of cell death signaling pathways. *Cancer Biol Ther, 4*(2), 139-163. doi:10.4161/cbt.4.2.1508

Johnson, M. B., Wang, P. P., Atabay, K. D., Murphy, E. A., Doan, R. N., Hecht, J. L., & Walsh, C. A. (2015). Single-cell analysis reveals transcriptional heterogeneity of neural progenitors in human cortex. *Nat Neurosci, 18*(5), 637-646. doi:10.1038/nn.3980

Kageyama, R., Ohtsuka, T., Shimojo, H., & Imayoshi, I. (2008). Dynamic Notch signaling in neural progenitor cells and a revised view of lateral inhibition. *Nat Neurosci, 11*(11), 1247-1251. doi:10.1038/nn.2208

Kaneshiro, K., Tsutsumi, S., Tsuji, S., Shirahige, K., & Aburatani, H. (2007). An integrated map of p53-binding sites and histone modification in the human

ENCODE regions. *Genomics, 89*(2), 178-188. doi:10.1016/j.ygeno.2006.09.001

Kawamura, T., Suzuki, J., Wang, Y. V., Menendez, S., Morera, L. B., Raya, A., . . . Izpisua Belmonte, J. C. (2009). Linking the p53 tumour suppressor pathway to somatic cell reprogramming. *Nature, 460*(7259), 1140-1144. doi:10.1038/nature08311

Kim, Y. H., Choi, S. H., D'Avanzo, C., Hebisch, M., Sliwinski, C., Bylykbashi, E., . . . Kim, D. Y. (2015). A 3D human neural cell culture system for modeling Alzheimer's disease. *Nat Protoc, 10*(7), 985-1006. doi:10.1038/nprot.2015.065

King, I. F., Yandava, C. N., Mabb, A. M., Hsiao, J. S., Huang, H. S., Pearson, B. L., . . . Zylka, M. J. (2013). Topoisomerases facilitate transcription of long genes linked to autism. *Nature, 501*(7465), 58-62. doi:10.1038/nature12504

Knouse, K. A., Wu, J., & Amon, A. (2016). Assessment of megabase-scale somatic copy number variation using single-cell sequencing. *Genome Res, 26*(3), 376-384. doi:10.1101/gr.198937.115

Kurek, K. C., Luks, V. L., Ayturk, U. M., Alomari, A. I., Fishman, S. J., Spencer, S. A., . . . Warman, M. L. (2012). Somatic mosaic activating mutations in PIK3CA cause CLOVES syndrome. *Am J Hum Genet, 90*(6), 1108-1115. doi:10.1016/j.ajhg.2012.05.006

Kuwabara, T., Hsieh, J., Muotri, A., Yeo, G., Warashina, M., Lie, D. C., . . . Gage, F. H. (2009). Wnt-mediated activation of NeuroD1 and retro-elements during adult neurogenesis. *Nat Neurosci, 12*(9), 1097-1105. doi:10.1038/nn.2360

Kwan, K. Y., Sestan, N., & Anton, E. S. (2012). Transcriptional co-regulation of neuronal migration and laminar identity in the neocortex. *Development, 139*(9), 1535-1546. doi:10.1242/dev.069963

Lacar, B., Linker, S. B., Jaeger, B. N., Krishnaswami, S., Barron, J., Kelder, M., . . . Gage, F. H. (2016). Nuclear RNA-seq of single neurons reveals molecular signatures of activation. *Nat Commun, 7*, 11022. doi:10.1038/ncomms11022

Lahav, G. (2004). The strength of indecisiveness: oscillatory behavior for better cell fate determination. *Sci STKE, 2004*(264), pe55. doi:10.1126/stke.2642004pe55

Lahav, G., Rosenfeld, N., Sigal, A., Geva-Zatorsky, N., Levine, A. J., Elowitz, M. B., & Alon, U. (2004). Dynamics of the p53-Mdm2 feedback loop in individual cells. *Nat Genet, 36*(2), 147-150. doi:10.1038/ng1293

Lake, B. B., Ai, R., Kaeser, G. E., Salathia, N. S., Yung, Y. C., Liu, R., . . . Zhang, K. (2016). Neuronal subtypes and diversity revealed by single-nucleus RNA sequencing of the human brain. *Science, 352*(6293), 1586-1590. doi:10.1126/science.aaf1204

Lancaster, M. A., Renner, M., Martin, C. A., Wenzel, D., Bicknell, L. S., Hurles, M. E., . . . Knoblich, J. A. (2013). Cerebral organoids model human brain development and microcephaly. *Nature, 501*(7467), 373-379. doi:10.1038/nature12517

Langmead, B., & Salzberg, S. L. (2012). Fast gapped-read alignment with Bowtie 2. *Nat Methods, 9*(4), 357-359. doi:10.1038/nmeth.1923

Lee, J. H., Huynh, M., Silhavy, J. L., Kim, S., Dixon-Salazar, T., Heiberg, A., . . . Gleeson, J. G. (2012). De novo somatic mutations in components of the PI3K-AKT3-mTOR pathway cause hemimegalencephaly. *Nat Genet, 44*(8), 941-945. doi:10.1038/ng.2329

Lensing, S. V., Marsico, G., Hansel-Hertsch, R., Lam, E. Y., Tannahill, D., & Balasubramanian, S. (2016). DSBCapture: in situ capture and sequencing of DNA breaks. *Nat Methods, 13*(10), 855-857. doi:10.1038/nmeth.3960

Levine, A. J. (1997). p53, the cellular gatekeeper for growth and division. *Cell, 88*(3), 323-331. doi:10.1016/s0092-8674(00)81871-1

Levine, A. J., & Oren, M. (2009). The first 30 years of p53: growing ever more complex. *Nat Rev Cancer, 9*(10), 749-758. doi:10.1038/nrc2723

Li, H., Handsaker, B., Wysoker, A., Fennell, T., Ruan, J., Homer, N., . . . Genome Project Data Processing, S. (2009). The Sequence Alignment/Map format and SAMtools. *Bioinformatics, 25*(16), 2078-2079. doi:10.1093/bioinformatics/btp352

Liao, M. C., Muratore, C. R., Gierahn, T. M., Sullivan, S. E., Srikanth, P., De Jager, P. L., . . . Young-Pearse, T. L. (2016). Single-Cell Detection of Secreted Abeta and sAPPalpha from Human IPSC-Derived Neurons and Astrocytes. *J Neurosci, 36*(5), 1730-1746. doi:10.1523/JNEUROSCI.2735-15.2016

Lin, T., Chao, C., Saito, S., Mazur, S. J., Murphy, M. E., Appella, E., & Xu, Y. (2005). p53 induces differentiation of mouse embryonic stem cells by suppressing Nanog expression. *Nat Cell Biol, 7*(2), 165-171. doi:10.1038/ncb1211

Liu, C., Zhong, Y., Apostolou, A., & Fang, S. (2013). Neural differentiation of human embryonic stem cells as an in vitro tool for the study of the expression patterns of the neuronal cytoskeleton during neurogenesis. *Biochem Biophys Res Commun, 439*(1), 154-159. doi:10.1016/j.bbrc.2013.07.130

Liu, D., & Xu, Y. (2011). p53, oxidative stress, and aging. *Antioxid Redox Signal, 15*(6), 1669-1678. doi:10.1089/ars.2010.3644

Liu, S. J., Nowakowski, T. J., Pollen, A. A., Lui, J. H., Horlbeck, M. A., Attenello, F. J., . . . Lim, D. A. (2016). Single-cell analysis of long non-coding RNAs in the developing human neocortex. *Genome Biol, 17*, 67. doi:10.1186/s13059-016-0932-1

Liu, Y., Lopez-Santiago, L. F., Yuan, Y., Jones, J. M., Zhang, H., O'Malley, H. A., . . . Parent, J. M. (2013). Dravet syndrome patient-derived neurons suggest a novel epilepsy mechanism. *Ann Neurol, 74*(1), 128-139. doi:10.1002/ana.23897

Lodato, M. A., Rodin, R. E., Bohrson, C. L., Coulter, M. E., Barton, A. R., Kwon, M., . . . Walsh, C. A. (2018). Aging and neurodegeneration are associated with increased mutations in single human neurons. *Science, 359*(6375), 555-559. doi:10.1126/science.aao4426

Lodato, M. A., Woodworth, M. B., Lee, S., Evrony, G. D., Mehta, B. K., Karger, A., . . . Walsh, C. A. (2015). Somatic mutation in single human neurons tracks developmental and transcriptional history. *Science, 350*(6256), 94-98. doi:10.1126/science.aab1785

Lodato, S., & Arlotta, P. (2015). Generating neuronal diversity in the mammalian cerebral cortex. *Annu Rev Cell Dev Biol, 31*, 699-720. doi:10.1146/annurev-cellbio-100814-125353

Lovell, M. A., & Markesbery, W. R. (2007). Oxidative damage in mild cognitive impairment and early Alzheimer's disease. *J Neurosci Res, 85*(14), 3036-3040. doi:10.1002/jnr.21346

Lui, J. H., Hansen, D. V., & Kriegstein, A. R. (2011). Development and evolution of the human neocortex. *Cell, 146*(1), 18-36. doi:10.1016/j.cell.2011.06.030

Lynch, M. (2010). Rate, molecular spectrum, and consequences of human mutation. *Proc Natl Acad Sci U S A, 107*(3), 961-968. doi:10.1073/pnas.0912629107

Macaulay, I. C., Ponting, C. P., & Voet, T. (2017). Single-Cell Multiomics: Multiple Measurements from Single Cells. *Trends Genet, 33*(2), 155-168. doi:10.1016/j.tig.2016.12.003

Madabhushi, R., Gao, F., Pfenning, A. R., Pan, L., Yamakawa, S., Seo, J., . . . Tsai, L. H. (2015). Activity-Induced DNA Breaks Govern the Expression of Neuronal Early-Response Genes. *Cell, 161*(7), 1592-1605. doi:10.1016/j.cell.2015.05.032

Mahoney, E. R., Dumitrescu, L., Moore, A. M., Cambronero, F. E., De Jager, P. L., Koran, M. E. I., . . . Hohman, T. J. (2019). Brain expression of the vascular endothelial growth factor gene family in cognitive aging and alzheimer's disease. *Mol Psychiatry*. doi:10.1038/s41380-019-0458-5

Manzini, M. C., & Walsh, C. A. (2011). What disorders of cortical development tell us about the cortex: one plus one does not always make two. *Curr Opin Genet Dev, 21*(3), 333-339. doi:10.1016/j.gde.2011.01.006

Marchetto, M. C., Belinson, H., Tian, Y., Freitas, B. C., Fu, C., Vadodaria, K., . . . Muotri, A. R. (2017). Altered proliferation and networks in neural cells derived from idiopathic autistic individuals. *Mol Psychiatry, 22*(6), 820-835. doi:10.1038/mp.2016.95

Marchetto, M. C., Carromeu, C., Acab, A., Yu, D., Yeo, G. W., Mu, Y., . . . Muotri, A. R. (2010). A model for neural development and treatment of Rett syndrome using human induced pluripotent stem cells. *Cell, 143*(4), 527-539. doi:10.1016/j.cell.2010.10.016

Marechal, A., & Zou, L. (2013). DNA damage sensing by the ATM and ATR kinases. *Cold Spring Harb Perspect Biol, 5*(9). doi:10.1101/cshperspect.a012716

Martin, L. J. (2008). DNA damage and repair: relevance to mechanisms of neurodegeneration. *J Neuropathol Exp Neurol, 67*(5), 377-387. doi:10.1097/NEN.0b013e31816ff780

Masland, R. H. (2004). Neuronal cell types. *Curr Biol, 14*(13), R497-500. doi:10.1016/j.cub.2004.06.035

Matsuoka, S., Ballif, B. A., Smogorzewska, A., McDonald Iii, E. R., Hurov, K. E., Luo, J., . . . Elledge, S. J. (2007). ATM and ATR substrate analysis reveals extensive protein networks responsive to DNA damage. *Science, 316*, 1160-1166.

McConnell, M. J., Kaushal, D., Yang, A. H., Kingsbury, M. A., Rehen, S. K., Treuner, K., . . . Barlow, C. (2004). Failed clearance of aneuploid embryonic neural progenitor cells leads to excess aneuploidy in the Atm-deficient but not the Trp53-deficient adult cerebral cortex. *J Neurosci, 24*(37), 8090-8096. doi:10.1523/JNEUROSCI.2263-04.2004

McConnell, M. J., Lindberg, M. R., Brennand, K. J., Piper, J. C., Voet, T., Cowing-Zitron, C., . . . Gage, F. H. (2013). Mosaic copy number variation in human neurons. *Science, 342*(6158), 632-637. doi:10.1126/science.1243472

McConnell, M. J., Moran, J. V., Abyzov, A., Akbarian, S., Bae, T., Cortes-Ciriano, I., . . . Brain Somatic Mosaicism, N. (2017). Intersection of diverse neuronal genomes and neuropsychiatric disease: The Brain Somatic Mosaicism Network. *Science, 356*(6336). doi:10.1126/science.aal1641

McKinnon, P. J. (2017). Genome integrity and disease prevention in the nervous system. *Genes Dev, 31*(12), 1180-1194. doi:10.1101/gad.301325.117

McVey, M., & Lee, S. E. (2008). MMEJ repair of double-strand breaks (director's cut): deleted sequences and alternative endings. *Trends Genet, 24*(11), 529-538. doi:10.1016/j.tig.2008.08.007

Meek, D. W., & Anderson, C. W. (2009). Posttranslational modification of p53: cooperative integrators of function. *Cold Spring Harb Perspect Biol, 1*(6), a000950. doi:10.1101/cshperspect.a000950

Meeuwsen, S., Persoon-Deen, C., Bsibsi, M., Ravid, R., & van Noort, J. M. (2003). Cytokine, chemokine and growth factor gene profiling of cultured human astrocytes after exposure to proinflammatory stimuli. *Glia, 43*(3), 243-253. doi:10.1002/glia.10259

Meyer, U., Feldon, J., & Dammann, O. (2011). Schizophrenia and autism: both shared and disorder-specific pathogenesis via perinatal inflammation? *Pediatr Res, 69*(5 Pt 2), 26R-33R. doi:10.1203/PDR.0b013e318212c196

Meyer, U., Feldon, J., & Yee, B. K. (2009). A review of the fetal brain cytokine imbalance hypothesis of schizophrenia. *Schizophr Bull, 35*(5), 959-972. doi:10.1093/schbul/sbn022

Michel, N., Majumdar, U. B., Lannigan, J., & McConnell, M. J. (2019a). Imaging Flow Cytometry Quantifies Neural Genome Dynamics. *Cytometry A*. doi:10.1002/cyto.a.23783

Michel, N., Majumdar, U. B., Lannigan, J., & McConnell, M. J. (2019b). Imaging Flow Cytometry Quantifies Neural Genome Dynamics. *Cytometry A, 95*(8), 825-835. doi:10.1002/cyto.a.23783

Miller, F. D., & Kaplan, D. R. (2007). To die or not to die: neurons and p63. *Cell Cycle, 6*(3), 312-317. doi:10.4161/cc.6.3.3795

Miller, I., Min, M., Yang, C., Tian, C., Gookin, S., Carter, D., & Spencer, S. L. (2018). Ki67 is a Graded Rather than a Binary Marker of Proliferation versus Quiescence. *Cell Rep, 24*(5), 1105-1112 e1105. doi:10.1016/j.celrep.2018.06.110

Miyata, T., Kawaguchi, A., Saito, K., Kawano, M., Muto, T., & Ogawa, M. (2004). Asymmetric production of surface-dividing and non-surface-dividing cortical progenitor cells. *Development, 131*(13), 3133-3145. doi:10.1242/dev.01173

Mou, X., Wu, Y., Cao, H., Meng, Q., Wang, Q., Sun, C., . . . Zhang, H. (2012). Generation of disease-specific induced pluripotent stem cells from patients with different karyotypes of Down syndrome. *Stem Cell Res Ther, 3*(2), 14. doi:10.1186/scrt105

Muller, F. J., Schuldt, B. M., Williams, R., Mason, D., Altun, G., Papapetrou, E. P., . . . Loring, J. F. (2011). A bioinformatic assay for pluripotency in human cells. *Nat Methods, 8*(4), 315-317. doi:10.1038/nmeth.1580

Muotri, A. R., Chu, V. T., Marchetto, M. C., Deng, W., Moran, J. V., & Gage, F. H. (2005). Somatic mosaicism in neuronal precursor cells mediated by L1 retrotransposition. *Nature, 435*(7044), 903-910. doi:10.1038/nature03663

Muotri, A. R., Zhao, C., Marchetto, M. C., & Gage, F. H. (2009). Environmental influence on L1 retrotransposons in the adult hippocampus. *Hippocampus, 19*(10), 1002-1007. doi:10.1002/hipo.20564

Namba, T., & Huttner, W. B. (2017). Neural progenitor cells and their role in the development and evolutionary expansion of the neocortex. *Wiley Interdiscip Rev Dev Biol, 6*(1). doi:10.1002/wdev.256

Nguyen, H. N., Byers, B., Cord, B., Shcheglovitov, A., Byrne, J., Gujar, P., . . . Pera, R. R. (2011). LRRK2 mutant iPSC-derived DA neurons demonstrate

increased susceptibility to oxidative stress. *Cell Stem Cell, 8*(3), 267-280. doi:10.1016/j.stem.2011.01.013

Ni, X., Trakalo, J., Valente, J., Azevedo, M. H., Pato, M. T., Pato, C. N., & Kennedy, J. L. (2005). Human p53 tumor suppressor gene (TP53) and schizophrenia: case-control and family studies. *Neurosci Lett, 388*(3), 173-178. doi:10.1016/j.neulet.2005.06.050

Noctor, S. C., Flint, A. C., Weissman, T. A., Dammerman, R. S., & Kriegstein, A. R. (2001). Neurons derived from radial glial cells establish radial units in neocortex. *Nature, 409*(6821), 714-720. doi:10.1038/35055553

Noctor, S. C., Martinez-Cerdeno, V., Ivic, L., & Kriegstein, A. R. (2004). Cortical neurons arise in symmetric and asymmetric division zones and migrate through specific phases. *Nat Neurosci, 7*(2), 136-144. doi:10.1038/nn1172

Noctor, S. C., Martinez-Cerdeno, V., & Kriegstein, A. R. (2008). Distinct behaviors of neural stem and progenitor cells underlie cortical neurogenesis. *J Comp Neurol, 508*(1), 28-44. doi:10.1002/cne.21669

Ogino, M., Ichimura, M., Nakano, N., Minami, A., Kitagishi, Y., & Matsuda, S. (2016). Roles of PTEN with DNA Repair in Parkinson's Disease. *Int J Mol Sci, 17*(6). doi:10.3390/ijms17060954

Orre, L. M., Stenerlow, B., Dhar, S., Larsson, R., Lewensohn, R., & Lehtio, J. (2006). p53 is involved in clearance of ionizing radiation-induced RAD51 foci in a human colon cancer cell line. *Biochem Biophys Res Commun, 342*(4), 1211-1217. doi:10.1016/j.bbrc.2006.02.085

Ortyn, W. E., Perry, D. J., Venkatachalam, V., Liang, L., Hall, B. E., Frost, K., & Basiji, D. A. (2007). Extended depth of field imaging for high speed cell analysis. *Cytometry A, 71*(4), 215-231. doi:10.1002/cyto.a.20370

Paquola, A. C. M., Erwin, J. A., & Gage, F. H. (2017). Insights into the role of somatic mosaicism in the brain. *Curr Opin Syst Biol, 1*, 90-94. doi:10.1016/j.coisb.2016.12.004

Park, D., Xiang, A. P., Mao, F. F., Zhang, L., Di, C. G., Liu, X. M., . . . Lahn, B. T. (2010). Nestin is required for the proper self-renewal of neural stem cells. *Stem Cells, 28*(12), 2162-2171. doi:10.1002/stem.541

Polleux, F., & Ghosh, A. (2002). The slice overlay assay: a versatile tool to study the influence of extracellular signals on neuronal development. *Sci STKE, 2002*(136), pl9. doi:10.1126/stke.2002.136.pl9

Pruszak, J., Sonntag, K. C., Aung, M. H., Sanchez-Pernaute, R., & Isacson, O. (2007). Markers and methods for cell sorting of human embryonic stem cell-derived neural cell populations. *Stem Cells, 25*(9), 2257-2268. doi:10.1634/stemcells.2006-0744

Qi, Y., Zhang, X. J., Renier, N., Wu, Z., Atkin, T., Sun, Z., . . . Studer, L. (2017). Combined small-molecule inhibition accelerates the derivation of

functional cortical neurons from human pluripotent stem cells. *Nat Biotechnol, 35*(2), 154-163. doi:10.1038/nbt.3777

Quinlan, A. R., & Hall, I. M. (2010). BEDTools: a flexible suite of utilities for comparing genomic features. *Bioinformatics, 26*(6), 841-842. doi:10.1093/bioinformatics/btq033

Rakic, P. (2006). Neuroscience. No more cortical neurons for you. *Science, 313*(5789), 928-929. doi:10.1126/science.1131713

Rash, B. G., Lim, H. D., Breunig, J. J., & Vaccarino, F. M. (2011). FGF signaling expands embryonic cortical surface area by regulating Notch-dependent neurogenesis. *J Neurosci, 31*(43), 15604-15617. doi:10.1523/JNEUROSCI.4439-11.2011

Rehen, S. K., McConnell, M. J., Kaushal, D., Kingsbury, M. A., Yang, A. H., & Chun, J. (2001). Chromosomal variation in neurons of the developing and adult mammalian nervous system. *Proc Natl Acad Sci U S A, 98*(23), 13361-13366. doi:10.1073/pnas.231487398

Rehen, S. K., Yung, Y. C., McCreight, M. P., Kaushal, D., Yang, A. H., Almeida, B. S., . . . Chun, J. (2005). Constitutional aneuploidy in the normal human brain. *J Neurosci, 25*(9), 2176-2180. doi:10.1523/JNEUROSCI.4560-04.2005

Reyes, J., Chen, J. Y., Stewart-Ornstein, J., Karhohs, K. W., Mock, C. S., & Lahav, G. (2018). Fluctuations in p53 Signaling Allow Escape from Cell-Cycle Arrest. *Mol Cell, 71*(4), 581-591 e585. doi:10.1016/j.molcel.2018.06.031

Rodriguez-Acebes, S., Mouron, S., & Mendez, J. (2018). Uncoupling fork speed and origin activity to identify the primary cause of replicative stress phenotypes. *J Biol Chem, 293*(33), 12855-12861. doi:10.1074/jbc.RA118.003740

Roederer, M. (2002). Compensation in flow cytometry. *Curr Protoc Cytom, Chapter 1*, Unit 1 14. doi:10.1002/0471142956.cy0114s22

Rogakou, E. P., Pilch, D. R., Orr, A. H., Ivanova, V. S., & Bonner, W. M. (1998). DNA double-stranded breaks induce histone H2AX phosphorylation on serine 139. *J Biol Chem, 273*(10), 5858-5868. Retrieved from https://www.ncbi.nlm.nih.gov/pubmed/9488723

Rogel, A., Popliker, M., Webb, C. G., & Oren, M. (1985). p53 cellular tumor antigen: analysis of mRNA levels in normal adult tissues, embryos, and tumors. *Mol Cell Biol, 5*(10), 2851-2855. doi:10.1128/mcb.5.10.2851

Rohrback, S., April, C., Kaper, F., Rivera, R. R., Liu, C. S., Siddoway, B., & Chun, J. (2018). Submegabase copy number variations arise during cerebral cortical neurogenesis as revealed by single-cell whole-genome sequencing. *Proc Natl Acad Sci U S A, 115*(42), 10804-10809. doi:10.1073/pnas.1812702115

Rohrback, S., Siddoway, B., Liu, C. S., & Chun, J. (2018). Genomic mosaicism in the developing and adult brain. *Dev Neurobiol, 78*(11), 1026-1048. doi:10.1002/dneu.22626

Romanova, L. Y., Willers, H., Blagosklonny, M. V., & Powell, S. N. (2004). The interaction of p53 with replication protein A mediates suppression of homologous recombination. *Oncogene, 23*(56), 9025-9033. doi:10.1038/sj.onc.1207982

Roos, W. P., & Kaina, B. (2006). DNA damage-induced cell death by apoptosis. *Trends Mol Med, 12*(9), 440-450. doi:10.1016/j.molmed.2006.07.007

Rothblum-Oviatt, C., Wright, J., Lefton-Greif, M. A., McGrath-Morrow, S. A., Crawford, T. O., & Lederman, H. M. (2016). Ataxia telangiectasia: a review. *Orphanet J Rare Dis, 11*(1), 159. doi:10.1186/s13023-016-0543-7

Sancar, A., Lindsey-Boltz, L. A., Unsal-Kacmaz, K., & Linn, S. (2004). Molecular mechanisms of mammalian DNA repair and the DNA damage checkpoints. *Annu Rev Biochem, 73*, 39-85. doi:10.1146/annurev.biochem.73.011303.073723

Schmid, P., Lorenz, A., Hameister, H., & Montenarh, M. (1991). Expression of p53 during mouse embryogenesis. *Development, 113*(3), 857-865. Retrieved from https://www.ncbi.nlm.nih.gov/pubmed/1821855

Schwer, B., Wei, P. C., Chang, A. N., Kao, J., Du, Z., Meyers, R. M., & Alt, F. W. (2016). Transcription-associated processes cause DNA double-strand breaks and translocations in neural stem/progenitor cells. *Proc Natl Acad Sci U S A, 113*(8), 2258-2263. doi:10.1073/pnas.1525564113

Sepe, S., Milanese, C., Gabriels, S., Derks, K. W., Payan-Gomez, C., van, I. W. F., . . . Mastroberardino, P. G. (2016). Inefficient DNA Repair Is an Aging-Related Modifier of Parkinson's Disease. *Cell Rep, 15*(9), 1866-1875. doi:10.1016/j.celrep.2016.04.071

Seward, M. E., Swanson, E., Norambuena, A., Reimann, A., Cochran, J. N., Li, R., . . . Bloom, G. S. (2013). Amyloid-beta signals through tau to drive ectopic neuronal cell cycle re-entry in Alzheimer's disease. *J Cell Sci, 126*(Pt 5), 1278-1286. doi:10.1242/jcs.1125880

Shangary, S., & Wang, S. (2009). Small-molecule inhibitors of the MDM2-p53 protein-protein interaction to reactivate p53 function: a novel approach for cancer therapy. *Annu Rev Pharmacol Toxicol, 49*, 223-241. doi:10.1146/annurev.pharmtox.48.113006.094723

Sheridan, G. K., & Murphy, K. J. (2013). Neuron-glia crosstalk in health and disease: fractalkine and CX3CR1 take centre stage. *Open Biol, 3*(12), 130181. doi:10.1098/rsob.130181

Shi, Y., Kirwan, P., & Livesey, F. J. (2012). Directed differentiation of human pluripotent stem cells to cerebral cortex neurons and neural networks. *Nat Protoc, 7*(10), 1836-1846. doi:10.1038/nprot.2012.116

Shi, Y., Kirwan, P., Smith, J., Robinson, H. P., & Livesey, F. J. (2012). Human cerebral cortex development from pluripotent stem cells to functional excitatory synapses. *Nat Neurosci, 15*(3), 477-486, S471. doi:10.1038/nn.3041

Shi, Z., Geng, Y., Liu, J., Zhang, H., Zhou, L., Lin, Q., . . . Sun, Y. E. (2018). Single-cell transcriptomics reveals gene signatures and alterations associated with aging in distinct neural stem/progenitor cell subpopulations. *Protein Cell, 9*(4), 351-364. doi:10.1007/s13238-017-0450-2

Shiraishi, K., Fukuda, S., Mori, T., Matsuda, K., Yamaguchi, T., Tanikawa, C., . . . Arakawa, H. (2000). Identification of fractalkine, a CX3C-type chemokine, as a direct target of p53. *Cancer Res, 60*(14), 3722-3726. Retrieved from https://www.ncbi.nlm.nih.gov/pubmed/10919640

Shirley, M. D., Tang, H., Gallione, C. J., Baugher, J. D., Frelin, L. P., Cohen, B., . . . Pevsner, J. (2013). Sturge-Weber syndrome and port-wine stains caused by somatic mutation in GNAQ. *N Engl J Med, 368*(21), 1971-1979. doi:10.1056/NEJMoa1213507

Shrivastav, M., De Haro, L. P., & Nickoloff, J. A. (2008). Regulation of DNA double-strand break repair pathway choice. *Cell Res, 18*(1), 134-147. doi:cr2007111 [pii]

10.1038/cr.2007.111

So, A., Le Guen, T., Lopez, B. S., & Guirouilh-Barbat, J. (2017). Genomic rearrangements induced by unscheduled DNA double strand breaks in somatic mammalian cells. *FEBS J, 284*(15), 2324-2344. doi:10.1111/febs.14053

Sokolowski, J. D., Chabanon-Hicks, C. N., Han, C. Z., Heffron, D. S., & Mandell, J. W. (2014). Fractalkine is a "find-me" signal released by neurons undergoing ethanol-induced apoptosis. *Front Cell Neurosci, 8*, 360. doi:10.3389/fncel.2014.00360

Soliman, M. A., Aboharb, F., Zeltner, N., & Studer, L. (2017). Pluripotent stem cells in neuropsychiatric disorders. *Mol Psychiatry, 22*(9), 1241-1249. doi:10.1038/mp.2017.40

Sommer, A., Maxreiter, F., Krach, F., Fadler, T., Grosch, J., Maroni, M., . . . Winner, B. (2018). Th17 Lymphocytes Induce Neuronal Cell Death in a Human iPSC-Based Model of Parkinson's Disease. *Cell Stem Cell, 23*(1), 123-131 e126. doi:10.1016/j.stem.2018.06.015

Soutoglou, E., Dorn, J. F., Sengupta, K., Jasin, M., Nussenzweig, A., Ried, T., . . . Misteli, T. (2007). Positional stability of single double-strand breaks in mammalian cells. *Nat Cell Biol, 9*(6), 675-682. doi:10.1038/ncb1591

Srikanth, P., Han, K., Callahan, D. G., Makovkina, E., Muratore, C. R., Lalli, M. A., . . . Young-Pearse, T. L. (2015). Genomic DISC1 Disruption in hiPSCs

Alters Wnt Signaling and Neural Cell Fate. *Cell Rep, 12*(9), 1414-1429. doi:10.1016/j.celrep.2015.07.061

Sturzbecher, H. W., Donzelmann, B., Henning, W., Knippschild, U., & Buchhop, S. (1996). p53 is linked directly to homologous recombination processes via RAD51/RecA protein interaction. *EMBO J, 15*(8), 1992-2002. Retrieved from https://www.ncbi.nlm.nih.gov/pubmed/8617246

Sung, P., & Klein, H. (2006). Mechanism of homologous recombination: mediators and helicases take on regulatory functions. *Nat Rev Mol Cell Biol, 7*(10), 739-750. doi:10.1038/nrm2008

Takahashi, K., Tanabe, K., Ohnuki, M., Narita, M., Ichisaka, T., Tomoda, K., & Yamanaka, S. (2007). Induction of pluripotent stem cells from adult human fibroblasts by defined factors. *Cell, 131*(5), 861-872. doi:10.1016/j.cell.2007.11.019

Takahashi, K., & Yamanaka, S. (2006). Induction of pluripotent stem cells from mouse embryonic and adult fibroblast cultures by defined factors. *Cell, 126*(4), 663-676. doi:10.1016/j.cell.2006.07.024

Tasic, B., Menon, V., Nguyen, T. N., Kim, T. K., Jarsky, T., Yao, Z., . . . Zeng, H. (2016). Adult mouse cortical cell taxonomy revealed by single cell transcriptomics. *Nat Neurosci, 19*(2), 335-346. doi:10.1038/nn.4216

Taylor, W. R., & Stark, G. R. (2001). Regulation of the G2/M transition by p53. *Oncogene, 20*(15), 1803-1815. doi:10.1038/sj.onc.1204252

Tcw, J., Wang, M., Pimenova, A. A., Bowles, K. R., Hartley, B. J., Lacin, E., . . . Brennand, K. J. (2017). An Efficient Platform for Astrocyte Differentiation from Human Induced Pluripotent Stem Cells. *Stem Cell Reports, 9*(2), 600-614. doi:10.1016/j.stemcr.2017.06.018

Thomaidou, D., Mione, M. C., Cavanagh, J. F., & Parnavelas, J. G. (1997). Apoptosis and its relation to the cell cycle in the developing cerebral cortex. *J Neurosci, 17*(3), 1075-1085. Retrieved from https://www.ncbi.nlm.nih.gov/pubmed/8994062

Thomson, J. A., Itskovitz-Eldor, J., Shapiro, S. S., Waknitz, M. A., Swiergiel, J. J., Marshall, V. S., & Jones, J. M. (1998). Embryonic stem cell lines derived from human blastocysts. *Science, 282*(5391), 1145-1147. doi:10.1126/science.282.5391.1145

Tsankov, A. M., Akopian, V., Pop, R., Chetty, S., Gifford, C. A., Daheron, L., . . . Meissner, A. (2015). A qPCR ScoreCard quantifies the differentiation potential of human pluripotent stem cells. *Nat Biotechnol, 33*(11), 1182-1192. doi:10.1038/nbt.3387

Upton, K. R., Gerhardt, D. J., Jesuadian, J. S., Richardson, S. R., Sanchez-Luque, F. J., Bodea, G. O., . . . Faulkner, G. J. (2015). Ubiquitous L1 mosaicism in hippocampal neurons. *Cell, 161*(2), 228-239. doi:10.1016/j.cell.2015.03.026

van der Walt, S., Colbert, S. C., & Varoquaux, G. (2011). The NumPy Array: A Structure for Efficient Numerical Computation. *Computing in Science & Engineering, 13*(2), 22-30. doi:Doi 10.1109/Mcse.2011.37

van Os, J., & Kapur, S. (2009). Schizophrenia. *Lancet, 374*(9690), 635-645. doi:10.1016/S0140-6736(09)60995-8

Vassilev, L. T., Vu, B. T., Graves, B., Carvajal, D., Podlaski, F., Filipovic, Z., . . . Liu, E. A. (2004). In vivo activation of the p53 pathway by small-molecule antagonists of MDM2. *Science, 303*(5659), 844-848. doi:10.1126/science.1092472

Viollet, S., Monot, C., & Cristofari, G. (2014). L1 retrotransposition: The snap-velcro model and its consequences. *Mob Genet Elements, 4*(1), e28907. doi:10.4161/mge.28907

Wang, M., Wei, P. C., Lim, C. K., Gallina, I. S., Marshall, S., Marchetto, M. C., . . . Gage, F. H. (2020). Increased Neural Progenitor Proliferation in a hiPSC Model of Autism Induces Replication Stress-Associated Genome Instability. *Cell Stem Cell, 26*(2), 221-233 e226. doi:10.1016/j.stem.2019.12.013

Wang, Q., Zou, Y., Nowotschin, S., Kim, S. Y., Li, Q. V., Soh, C. L., . . . Massague, J. (2017). The p53 Family Coordinates Wnt and Nodal Inputs in Mesendodermal Differentiation of Embryonic Stem Cells. *Cell Stem Cell, 20*(1), 70-86. doi:10.1016/j.stem.2016.10.002

Wei, P. C., Chang, A. N., Kao, J., Du, Z., Meyers, R. M., Alt, F. W., & Schwer, B. (2016). Long Neural Genes Harbor Recurrent DNA Break Clusters in Neural Stem/Progenitor Cells. *Cell, 164*(4), 644-655. doi:10.1016/j.cell.2015.12.039

Weissman, I. L., & Gage, F. H. (2016). A Mechanism for Somatic Brain Mosaicism. *Cell, 164*(4), 593-595. doi:10.1016/j.cell.2016.01.048

Williams, R. W., & Herrup, K. (1988). The control of neuron number. *Annu Rev Neurosci, 11*, 423-453. doi:10.1146/annurev.ne.11.030188.002231

Wilson, T. E., Arlt, M. F., Park, S. H., Rajendran, S., Paulsen, M., Ljungman, M., & Glover, T. W. (2015). Large transcription units unify copy number variants and common fragile sites arising under replication stress. *Genome Res, 25*(2), 189-200. doi:10.1101/gr.177121.114

Wong, F. K., & Marin, O. (2019). Developmental Cell Death in the Cerebral Cortex. *Annu Rev Cell Dev Biol, 35*, 523-542. doi:10.1146/annurev-cellbio-100818-125204

Wong, K., Zhang, J., Awasthi, S., Sharma, A., Rogers, L., Matlock, E. F., . . . Harrod, R. (2004). Nerve growth factor receptor signaling induces histone acetyltransferase domain-dependent nuclear translocation of p300/CREB-binding protein-associated factor and hGCN5 acetyltransferases. *J Biol Chem, 279*(53), 55667-55674. doi:10.1074/jbc.M408174200

Yan, C. T., Kaushal, D., Murphy, M., Zhang, Y., Datta, A., Chen, C., . . . Alt, F. W. (2006). XRCC4 suppresses medulloblastomas with recurrent translocations in p53-deficient mice. *Proc Natl Acad Sci U S A, 103*(19), 7378-7383. doi:10.1073/pnas.0601938103

Yang, A. H., Kaushal, D., Rehen, S. K., Kriedt, K., Kingsbury, M. A., McConnell, M. J., & Chun, J. (2003). Chromosome segregation defects contribute to aneuploidy in normal neural progenitor cells. *J Neurosci, 23*(32), 10454-10462. Retrieved from https://www.ncbi.nlm.nih.gov/pubmed/14614104

Yu, J., Vodyanik, M. A., Smuga-Otto, K., Antosiewicz-Bourget, J., Frane, J. L., Tian, S., . . . Thomson, J. A. (2007). Induced pluripotent stem cell lines derived from human somatic cells. *Science, 318*(5858), 1917-1920. doi:10.1126/science.1151526

Yu, Y. C., Bultje, R. S., Wang, X., & Shi, S. H. (2009). Specific synapses develop preferentially among sister excitatory neurons in the neocortex. *Nature, 458*(7237), 501-504. doi:10.1038/nature07722

Yurov, Y. B., Iourov, I. Y., Monakhov, V. V., Soloviev, I. V., Vostrikov, V. M., & Vorsanova, S. G. (2005). The variation of aneuploidy frequency in the developing and adult human brain revealed by an interphase FISH study. *J Histochem Cytochem, 53*(3), 385-390. doi:10.1369/jhc.4A6430.2005

Yurov, Y. B., Iourov, I. Y., Vorsanova, S. G., Liehr, T., Kolotii, A. D., Kutsev, S. I., . . . Soloviev, I. V. (2007). Aneuploidy and confined chromosomal mosaicism in the developing human brain. *PLoS One, 2*(6), e558. doi:10.1371/journal.pone.0000558

Yurov, Y. B., Vorsanova, S. G., Iourov, I. Y., Demidova, I. A., Beresheva, A. K., Kravetz, V. S., . . . Gorbachevskaya, N. L. (2007). Unexplained autism is frequently associated with low-level mosaic aneuploidy. *J Med Genet, 44*(8), 521-525. doi:10.1136/jmg.2007.049312

Zeisel, A., Munoz-Manchado, A. B., Codeluppi, S., Lonnerberg, P., La Manno, G., Jureus, A., . . . Linnarsson, S. (2015). Brain structure. Cell types in the mouse cortex and hippocampus revealed by single-cell RNA-seq. *Science, 347*(6226), 1138-1142. doi:10.1126/science.aaa1934

Zhang, J., & Jiao, J. (2015). Molecular Biomarkers for Embryonic and Adult Neural Stem Cell and Neurogenesis. *Biomed Res Int, 2015*, 727542. doi:10.1155/2015/727542

Zunder, E. R., Lujan, E., Goltsev, Y., Wernig, M., & Nolan, G. P. (2015). A continuous molecular roadmap to iPSC reprogramming through progression analysis of single-cell mass cytometry. *Cell Stem Cell, 16*(3), 323-337. doi:10.1016/j.stem.2015.01.015

Zylka, M. J., Simon, J. M., & Philpot, B. D. (2015). Gene length matters in neurons. *Neuron, 86*(2), 353-355. doi:10.1016/j.neuron.2015.03.059